FRACTOGRAPHY OF RIM POLYCARBAMATE MATERIALS

Thesis

Submitted to

The School of Engineering of the

UNIVERSITY OF DAYTON

In Partial Fulfillment of the Requirements for

The Degree

Master of Science in Mechanical Engineering

by

Rafael Gonzalez Garcia

UNIVERSITY OF DAYTON

Dayton, Ohio

December 1987

Fractography of RIM Polycarbamate Materials

APPROVED BY:

James A. Snide, Ph.D.
Professor/Director of Graduate
Materials Engineering
Advisory Committee, Chairman

Gary A. Thiele, Ph.D.
Associate Dean/Director
Graduate Engineering and Research
School of Engineering

Gordon A. Sargent, Ph.D.
Dean, School of Engineering

ABSTRACT

The purpose of this investigation was to evaluate the failure modes of a fiber glass reinforced RIM polycarbamate composite material used or considered for use in automotive applications. The following tasks were completed: (1) preparation and characterization of the sample, (2) environmental conditioning and mechanical testing, and (3) fractographic evaluation of the failed samples. The samples were characterized with respect to fiber, resin, filler and void contents, specific gravity, and glass transition temperature. The mechanical tests included thermal aging at 180°F or 250°F and hot-humid aging at 120°F and 100% relative humidity. The failed samples were examined with a stereo optical microscope and a scanning electron microscope. Various topographical features on the fracture surfaces for the various test conditions were identified and cataloged. These topographical features were in some cases unique to the environmental conditioning and testing mode. Thermal aging appeared to improve the mechanical properties and the bonding of the matrix resin to the glass fibers. However, hot-humid aging seemed to degrade considerably the mechanical properties and fiber-matrix interfaces.

AKNOWLEDGEMENTS

The author would like to express his appreciation to the Chemical and Materials Engineering Department at the University of Dayton, as well as the Chrysler Corporation Challenge Fund, and the State of Ohio Research Grant for providing the opportunity and facilities to perform the work described in this thesis. The author wishes to extend his deepest gratitude to Dr. J. A. Snide whose academic help and guidance were very valuable. Also, special thanks are given to Drs. J. Gallagher, J. M. Whitney, and V. K. Jain for reviewing this thesis, and to S. E. Saliba and to Dr. R.P. Chartoff for their useful advice and guidance. In addition, the author would like to thank J. D. Wolf and T. N. Wittberg for their advise in SEM and XPS analyses, and to the staff at the University of Dayton Research Institute for their help with the mechanical testing and optical examination. I especially want to thank my friends and family for their moral support.

TABLE OF CONTENTS

LIST OF FIGURES

LIST OF TABLES

Table Page

CHAPTER I

INTRODUCTION

The use of new structural materials, such as composites, requires the ability to be able to determine the modes of failure in post-failure analysis. Failure analysis of metallic structures by examination of the fracture surfaces is a well established technology. The application of fractography for failure analysis of composites is relatively new and is much less well developed, but is an area of active research. Characterization of the failure modes of fiber reinforced composite materials is of crucial importance. It provides the tools and supporting documentation to conduct failure analysis of these materials. Failure analysis procedures include addressing the following issues [1]:

(1) Determining the appropiate history of the failed part, such as, (a) material specification, (b) fabrication procedure, (c) physical properties, and (d) load history.

(2) Conduct fracture mechanic analyses based on load conditions, load location, fracture modes etc.

(3) Conducting macroscopic and microscopic examinations using both optical and scanning electron microscopy (SEM).

(4) Employ chemical analyses techniques such as X-ray photoelectron spectroscopy (XPS), Fourier-Transform infrared (FTIR) spectrometry, Dynamic Mechanical Analysis (DMA), Rheometrics, and liquid chromatography.

Several of these techniques have been used in this investigation, with a major emphasis in the area of fractography.

Through optical and SEM examination, initiation sites, as well as direction of crack propagation can be determined. In addition, the type or types of failure may be determined by comparing the photomicrographs with previously documented failure characteristics for the specific material being investigated. The purpose of this investigation is to provide the documentation needed to conduct post-failure analysis of failed parts of glass reinforced reaction injection molded polycarbamate composites.

Composite materials have a long history of usage. Their beginnings are unknown, but all recorded history contains references to some form of composite material. For example, straw was used by the Israelites to strengthen mud bricks. Plywood was used by the ancient Egyptians when they realized that wood could be rearranged to achieve superior strength and resistance to thermal expansion, as well as to swelling due to the presence of moisture. Medieval armors were constructed with layers of different materials. More recently, starting in the 1950's, fiber-reinforced resin composites that have high strength-to-weight and stiffness-to-weight ratios have become very important in weight-sensitive applications such as aircraft and space vehicles. The aerospace industry has been interested in composites for the past thirty years developing active lines of research. During the last decade, composite materials have become very important for more common applications. For example, the automotive industry has already qualified some types of composites as materials for their production lines, and they have been used in many of the cars of the 80's.

The word "composite" signifies that two or more materials are

combined on a macroscopic scale to form a useful material. Different materials can be combined microscopically, such as alloys, but the resulting material is macroscopically homogeneous, while composites are not. The advantage of composites is that they usually exhibit the best qualities of their constituents, and often some qualities that none of the constituents possess [2].

The following properties can be improved by using composite materials:

* strength
* stiffness
* corrosion resistance
* wear resistance
* attractiveness
* cost
* weight
* fatigue life
* temperature-dependent behavior
* thermal conductivity
* acoustical & thermal insulation

Naturally, not all of the above properties are improved at the same time, nor is there usually any requirement to do so.

There are three commonly accepted types of resin-matrix composite materials:

1. Fibrous composites, which consist of fibers in a matrix
2. Laminated composites, which consist of layers of various materials
3. Particulate composites, which are composed of particles in a matrix

The composite materials investigated in this study belong to the first class [2]. They consist of continuous fibers in various orientations.

During the last decade, researchers developed advanced composite

materials by using new polymeric type resins, which were primarily formed of advanced fibers such as graphite and Kevlar embedded in the matrix material. This was based on the idea that polymeric materials perform best as fibers, due mainly to their long chain atomic structure, usually of a carbonic nature joined by covalent bonds. Under most conditions, the chains are either loosely tangled or crystallized in complex patterns. They can be pulled apart fairly easily, and the bulk material is flexible and weak as a result. If the chains are all oriented in the direction of stress, however, the polymer can be very stiff and strong. The matrix acts as an adhesive, binding the fibers and lending solidity to the material. It also protects the fibers from environmental stress and physical damage that could initiate a failure. The stress and stiffness of the composite remain very much a function of the reinforcing material (fibers), but the matrix makes its own contribution to the composite properties [2]. The binding between matrix and fibers, which is an area of research interest, is also of importance to the performance of the material.

Composite materials have many characteristics that are different from more conventional engineering materials. Some characteristics are merely modifications of conventional behavior; others are totally new, such as tailorability, the ability to tailor the properties of the material in the direction of stresses by orienting the fibers as necessary.

The need to develop a comprehensive post-failure analysis capability for composite materials has become apparent in recent years. With the increasing use of these materials in aerospace applications, and their introduction in the automotive industry,

unanticipated failures under full-scale test conditions as well as in-service are more likely to occur. This likelihood makes it necessary to develop the capability to identify the causes and understand the modes of such failures, thus, improvements to future designs can be made or appropriate corrective actions can be taken. Fractography can provide a basic tool required to successfully carrying out a composites post-failure investigation [2]. Fractography is a relatively new tool used to investigate the failure characteristics of materials. The use of fractogrphy has been widely demonstrated in metals failure analysis, and recently, during the last decade is starting to be used in analyzing the fracture surfaces of composite materials. Fractography is basically divided into two areas: (1) macrofractography and (2) microfractography. Macrofractography involves the use of both visual examinations as well as a optical microscopy for low magnification viewing of the fracture surface. Microfractography employs the higher magnification of the electron microscope (scanning and/or transmission) [3].

Locating the fracture origin and modes of failure are primary goals of fractography and is vital to successful failure analysis. The fracture markings formed during the event compare to a fingerprint that the analyst uses to identify the mode of failure. Fracture initiation and propagation produce certain characteristic marks on the fracture face, such as river patterns, radial lines, chevron patterns, that indicate the direction or orientation of crack propagation. The analyst traces these features backward to find the origin. The appearance of these marks on the fracture surface is a function of the nature of the stress system; its magnitude and orientation;

environmental factors; material factors;and the type of loading such as: tension, shear, bending, fatigue, or torsion. Macroscopic interpretation should normally precede microscopic examination for a good fracture interpretation. Macroscopy will yield a useful overall view of the entire fracture surface. When interesting features are found, higher magnification microscopy are used [3].

Literature Review

A literature survey on the subject of fractography and failure analysis of composite materials is presented. The majority of the research completed on composite materials is focused on advanced composites, with advanced reinforcement such as graphite and Kevlar fibers to form laminated composites. Some of the failure modes found in advanced composites can be extrapolated to other less refined composites that are becoming very important in today's industry, such as sheet molding compounds (SMC), bulk molding compounds (BMC), or reaction injection molding compounds (RIM). The majority of the reported research in composite fractography deals with graphite/epoxy laminated composites. A detailed summary of fracture surface characteristics of graphite/epoxy composites for specific failure modes was developed by Stumpff and Snide [4] and is listed in Appendix A. The literature survey addresses mainly the fractographic and failure features observed on the molding compounds (SMC, BMC, RIM) mentioned previously, focusing on glass fiber type reinforcement. Different modes of failure and conditioning have been reviewed. Also, a review of the chemical structure of the resin (polycarbamate), and its binding energies with the fibers is presented, to better understand the material structure and mechanical behavior.

Klein [5], presents a review of how reaction injection molding systems are produced. Basically, he indicates that

reaction injection molding (RIM) is a process in which two reactive liquid components are blended together via a high-pressure impingement mixing. The blend is then injected at low pressure into a mold. The material is left to cool in the mold. First the outside walls of the mold solidify, allowing unreacted material to go through the center of the part. Then the whole part cools to room temperature. At that point, it can be released from the mold and ready to use. He also reviews different materials suitable for this technique, including a large variety of polycarbamates and polyesters. He includes the mechanical and thermal properties to be of major importance for the different applications. He mentioned that RIM materials provide substantial energy savings during molding, and efficient low cost equipment for reaction molding. Strong and rigid parts can be obtained at very high production rates with excellent cost effectiveness.

Kropscott [6], from Dow Chemical Corporation reported a new rigid plastic material, which at that time was being introduced into the industry, but today is widely used. Chemically, this material is an instant-set polymer (ISP) but is referred to as a polycarbamate since it has recurring carbamate groups. The chemistry of the new resin system centers around urethane raw materials: isocynate and a polyol, which along with the proper catalyst, will polymerize rapidly and exothermally. The new liquid-reaction molding is done with lighter less costly molds and machines.

Nelson [7], evaluated the mechanical performance of two

different reaction injection molding systems. The materials he investigated were reaction molded glass reinforced structural polymers. One of the composites is formed using a continuous random glass mat, and the other an oriented glass mat. The high-temperature advantages of a polyisocyanurate resin and the random glass mat are demonstrated on the basis of static physical property testing and creep testing. In addition, a polycarbamate type of resin showed improved impact properties with the same random mat, while unidirectional glass fibers appeared not to offer any significant advantage within the limits of the study.

Interlaminar shear and interlaminar shear tests have been studied by J.M. Whitney and C.E. Browning [8]. They applied interlaminar beam tests in the form of three-point and four-point flexure, correlating both the analytical and the experimental results. Experimental data were obtained on unidirectional composites. Photomicrographs of actual failure modes and the results of the stress analysis based on classical theory of elasticity are used to supplement the experimental data. Complex failure modes in the presence of extremely high combined stress gradients were observed. Serious doubts were raised on the usefulness of testing standards for composites. J.M. Whitney and R.S. Short [9] also questioned the validity of short beam shear methods for characterizing interlaminar shear failure of composite materials. They indicated there is evidence that compression stresses in regions where high shear-stress components exist tend to suppress interlaminar shear failure modes. Thus, initial damage in the form of vertical cracks appears to be necessary in order to induce horizontal

interlaminar failures. Examination of the fracture surfaces, however, reveals a mixed-mode type of failure. For specimens without initial damage, the failure mode is often compressive buckling, or yielding in the upper portion of the beam under combined compression and shear.

S.S. Wang, et al. [10], studied the fracture of random short-fiber sheet molding compound (SMC) composites under shear loading (mode II, with a starting crack) using SMC-R50 material (random 50 weight % glass fiber reinforcement), which is a widely-used formulation in the automotive industry. The matrix material also contained calcium carbonate as a filler material, resin inhibitor, catalyst, alkaline earth oxide thickening agent, and mold release agent. The fracture specimens revealed that the macroscopic shear failure usually occurred along the original crack plane with a rough crack extension path that generally contained significant matrix cracking, trans-fiber fracture, fiber pullout, and some delamination. The authors point out that the mode II fracture toughness was only about one-half the mode I fracture toughness. They suggest that this lower mode II energy may result from the matrix-dominated fracture mechanisms. Matrix-dominated failure generally requires lower energy than the fiber-dominated mode I fracture. They indicated the low fracture toughness of the SMC material in resisting mode II shear loading appears to be unique, and it may be of importance in the safe design and failure analysis of structural components and parts made of the random short-fiber composite.

Wang, Suemasn, and Zahlan [11] studied mode I fracture toughness of SMC-R50 using the pre-cracked double-cantilever beam specimen. They reported an order of magnitude of higher toughness of the

composite compared to the unreinforced neat resin. The significant increase in the interlaminar fracture toughness of the SMC composite results from several unusual damage and fracture mechanisms during crack growth, including fiber bridging across crack surfaces, extensive matrix damage, fiber-bundle pullout at the crack tip, and formation of subcritical cracks ahead of the crack tip.

Compression failure mechanisms of composite materials were investigated by Hahn, et al. [12]. He included seven graphite/epoxy composites, two graphite/thermoplastic resin composites, one kevlar 49/epoxy composite, and an S-glass epoxy composite. The main modes of failure were the initiation and propagation of kink bands. These kink bands showed that, fiber failure can only be of the following two types: intrinsic or microbuckling-induced. The intrinsic compressive failure is the result of the fiber stress exceeding the fiber strength, and the microbuckling-induced failure is, in fact, a bending failure as a consequence of buckling. In most composites, the composite failure is the result of the microbuckling-induced failure of fibers. Fiber microbuckling is enhanced by the failure of yielding of the matrix, fiber-matrix debonding, or the presence of voids. Kinking was the mode of failure in all the unidirectional composites studied. Fiber microbuckling caused the kinking failure in graphite/epoxy, graphite/thermoplastic resin, and glass/epoxy composites. Whatever the incipient mode of failure, slip occurred on a plane oblique to the loading direction, because of the presence of a resolved shear stress on this plane. In glass/epoxy specimens tested at room temperature,

the kink band is broad, and no definite kink band boundaries can be identified due to the very gradual change of curvature in fibers leading into the failure zone. Whenever specimens are submitted to elevated temperatures, softening of the matrix is observed, and a well-defined kink band is formed.

Wang, Chim, and Zahlan [13] studied mode I of fatigue crack propagation in notched SMC-R50 subject to uniaxial tensile and mixed mode fatigue loading. Areas near the notch tip and further away within the propagation region were studied. In each case, fatigue crack growth characteristics associated with matrix-rich, fiber-rich, and fiber-matrix interface regions were studied in detail. SEM examination near the notch tip revealed that initiation of crack growth was closely related to the arrangement of local fiber strands. Rougher fracture surfaces in the notch-root area were observed than in the propagation area. The initial crack growth mechanism may be controlled by fiber pullout and separation between chopped fiber strands of different orientations in the fiber-rich regions. In the matrix-rich areas near the notch tip, separation of calcium carbonate filler from polyester resin matrix and debris due to cracking was observed. In the region away from the notch tip, fatigue crack propagation was dominated by the macroscopic crack rather than local heterogeneity. Relatively smooth fatigue fracture surfaces in both resin-rich and fiber-rich areas were observed. In the matrix-rich areas, significant damage in the forms of matrix cracking, debonding between fibers and separation between the matrix and filler had occurred. Owens [14] pointed out that

detailed description of damage would be of assistance in failure analysis and that identification of fundamental fracture processes should assist in the development of improved materials. Fatigue fracture surfaces are usually covered with relatively large amounts of debris not present on the static failure surface. In addition, it was also observed that in the matrix-rich areas, significant damage in the form of matrix cracking and debonding between fibers and filler occurred. Newman and Fesko [15] attributed the matrix cracking to (1) residual stresses caused by the rapid cooling of the polymer, and (2) thermal stresses.

In the fiber-rich areas, most of the damage occurred where fibers were oriented in unfavorable directions, e.g., normal to the loading direction. A small amount of fiber pullout was also observed in this region. Additional fatigue damage studies using random short fiber reinforced SMC were conducted by Wang and Chim [16]. They suggested that microscopic stress concentrators such as fiber ends, fiber-matrix interfaces, filler material particles and process-induced defects inherent in sheet molding compounds contribute to fatigue damage. This damage is seen in various forms, such as fiber-end cracking, fiber-matrix interface debonding, and separation of filler particles from the matrix. The state of homogeneous damage is generally affected by loading variables (maximum fatigue stress, cyclic stress amplitude and loading frequency, etc.), material variables (filler and filler volume fractions, fiber orientation distribution, dispersion of fibers and fillers, etc.), geometric parameters (notches, holes, boundaries and other cutouts, etc.), and environmental conditions

(temperature, moisture, etc.). Scanning electron microscopy was used to examine the fundamental damage mechanisms at different stages of fatigue degradation. In a fiber-rich area with fibers oriented parallel to the loading direction, microcracks developed mainly in the matrix, but had rather small crack lengths limited by interfiber spacing. In addition, in a chopped fiber strand oriented at an angle to the loading direction, microcracks propagate along the fiber-matrix interface. Fiber bundle fracture was rarely observed in the SMC material.

Jefferey, et al. [17] performed tension-tension fatigue tests on SMC-R50. Based on these tests, the damage process in SMC-50 proceeded as follows. In the first 5000 cycles of the fatigue test, the major damage consisted of small cracks at the edges of the test area. Other cracks ran along the tips of fiber bundles. After 10,000 and 15,000 cycles, further cracking along fibers and along tips of fiber bundles plus a small degree of matrix cracking was observed. It was determined that the surface of SMC-50 was matrix-rich and therefore the nature of the fracture path obscure.

At 20,000 cycles, a significant increase in the amount of matrix cracking was noted. At 25,000 cycles, cracking damage on the edges continued to go deeper into the sample. Micrographs showed that four layers of fiber bundles had been damaged. In general, it was found that in severely cracked areas, the matrix no longer adhered to the fiber.

To summarize, in SMC-50 material different types of damage occur throughout the fatigue life. A combination of cracks along fibers and fiber/matrix/filler interface is the major damaging

factor in the early part of fatigue life. Next, a combination of the above plus filler debonding contribute to the failure. Finally, the above contributions plus the weakening of the matrix around the filler particles which causes matrix cracking leads to the catastrophic failure of the composite.

The sequence of events in high-cycle fatigue failure was suggested to be as follows:

(1) Initiation and propagation of matrix cracks,

(2) Local fragmentation of the matrix,

(3) Local permanent tensile deformation causing specific fibers to be loaded in compression during the return stroke,

(4) Buckling and fracture of fibers which are both exposed due to matrix failure and put into compression due to local permanent tensile deformation, and

(5) At a late stage, when the overall stress is sufficiently high, general fiber-matrix interface failure and fiber pullout.

A study was conducted by Khetan and Chang [18] to determine the damage of SMC-35 panels (SMC with 35 wt. % chopped glass fiber reinforcement) when subjected to a point impact loading simulating flying stone damage. The SMC panels were impacted with a steel ball 22.2 mm in diameter with a mass of 45.4 grams which is fired by an air gun at speeds ranging from 45 to 100 km/hr. Three techniques, radiographic, ultrasonic C-scan and crack enhancement were used to measure the extent of the damaged area. Results generated by the crack enhancement technique proved to be the most informative. The surface damage area measurements were made on both the front and rear

side of the panel. The damage on the rear side included matrix cracking and fiber matrix debonding. On the impacted side, the enhancement resulted in a small central zone of surface cracks. At all impact speeds, the central zone of surface cracks that were obtained after enhancement on the front side were smaller than the visible damage on the rear side.

The effects of environment on glass fiber reinforced polyester and vinyl ester composites immersed in various industrial fluids and in humid air were investigated by Springer [19]. Tests were performed at temperatures of 23° and 90°C with the materials exposed to humid air at 50 to 100% relative humidity and to the following five industrial fluids: saturated salt water, No. 2 diesel fuel, lubricating oil, antifreeze, and indolene. Changes in weight, tensile strength, tensile modulus, short beam shear strength, and shear modulus were measured over a six month period and effects of the environment on these parameters were assessed.

The ultimate tensile strength, shear strength, and the tensile and shear modulus were determined at room temperature for the as-received materials. The results of these measurements were considered as baseline data and compared with the strengths and modulus of specimens after environment reduces both the strength, and modulus of the materials. The change in strength depends on the material, temperature, and environment (relative humidity of air, or type of liquid used). The temperature and the environment seemed to be the more significant factors. Exposure to saturated salt water, antifreeze, and indolene at 93 °C had the most pronounced effects on the mechanical properties.

As a complementary issue, a survey on adhesion between the fibers and matrix has been considered of importance. Adhesion mechanisms and adhesion promoters have been studied by Edwin P. Plueddemann [20] for organic polymers. Simple screening tests were conducted to compare potential coupling agents as adhesion promoters for the many polymers now available. Results of screening tests for a number of proposed coupling agents with common thermosetting and thermoplastic polymers were presented in the paper as a guide for selecting candidates for more complete evaluation using more sophisticated tests. A coupling agent is defined as a material that provides a water-resistant bond across the interface between an inorganic substrate and an organic matrix resin. The same material may at times promote adhesion between organic polymers. Other effects at the interface, such as modification of rheology, protection of surfaces against fracture, and modifying resin-cure at the interface may be very important in practical production of composites, but should not be classed as "coupling". Many organofunctional silanes have been prepared and evaluated as coupling agents in polymer matrix composites.

Kubel [21] considered the fiber/matrix as the heart of the composites reinforcement and stated that efficiency depends on the adhesion of the system at the fiber/matrix interface. Basically, materials will not support loads in compression or shear if the fiber/matrix interface is too weak; and if the bond is too strong the material will be brittle. He mentioned that the only reason why a brittle matrix and a brittle fiber bound together have any toughness is because cracks are diverted up to the fiber/matrix interface, much like fractures in wood. He explains how silane finishes are applied

to glass fibers to prevent surface degradation and to increase surface adhesion to the matrix. Also, he comments about a qualitative evaluation of composite damage tolerance done by Ak20 Research, that shows fiber/matrix debonding, which produces low interlaminar fracture toughness, and improves composite damage tolerance. Reasons for the beneficial effects are: decreasing stress concentration in debonded fibers, and possible occurrence of secondary energy-dissipating mechanisms, such as fiber pullout.

Whitaker, et al. [22] reported on some characterization and adhesive bonding studies of poly(etheretherketone) (PEEK). These studies were conducted in relation to its use in wire coatings and in fiberglass-filled molding compounds. Thermal analyses showed several peek resins with essentially the same glass transition and melting temperatures values indicating that the same starting PEEK polymer was used. X-ray diffraction was used to analyze thebinding energies between the PEEK resins and fiberglass. XPS analyses support the predominant structural repeat unit of PEEK as being O-phi-O-phi-CO-phi (where phi=benzene). Also, the crystallinity of the PEEK polymer was studied by differential scanning calorimetry (DSC) and XPS techniques. The data obtained indicates that the crystallinity of PEEK-fiberglass was found to be low.

CHAPTER II

EXPERIMENTAL PROCEDURE

Two panels of the material for evaluation and testing were supplied by the Chrysler Corporation. The material supplied was "Spectrim MM 353", which is a trademark of the Dow Chemical Company. It is a polyisocyanurate structural polymer system based on a specially formulated methylene diphenyl diisocyanate A-side and a fully formulated B-side. The chemical composition of the samples supplied were 22% Polyol and 78% Isocyanate by weight. As a reinforcement, a 57% by weight Owens Corning Fiberglass Mat (M-8610) was used. A final density for the composite was found to be 1.17 g/cc. Once the composite was identified, the experimental procedure consisted of the following principle tasks: (1) sample preparation and characterization, (2) environmental conditioning and mechanical testing of the samples, and (3) fractographic analysis of the fracture surfaces [1].

Sample Preparation and Characterization

Preparation and characterization of the test coupons prior to testing was conducted on the composite panels (12" x 12" x 1/8") supplied by the Chrysler Corporation. The panels were cut into test coupons and characterized to determine the quality of the material. Specimens from each panel were set aside for measurement of the physical properties [1].

The quality of the panels received was verified to ensure the reliability of the testing results. Four different physical properties have been included, such as specific gravity, resin content, fiber content and void content. A thermal property was also analyzed: the glass transition temperature, which was determined using a DuPont Dynamic Mechanical Analyzer (DMA). Surface energy analyses of clean fibers and fibers coated with the coupling agent were done by X-ray photoelectron spectroscopy (XPS), so interface problems between fibers and matrix could be better understood.

Sample Preparation

Machine diagrams were sketched on the panel surfaces and individual specimens were cut out of the panels for the different testing modes with a diamond cut-off wheel, according to the dimensions recommended in the ASTM standards for each mode. Specimens were machined to the required dimensions on a high speed router employing a sanding drum.

Physical Properties

The physical properties were experimentally measured included: specific gravity, resin, fiber and void contents. The experimental techniques used to measure each property will be discussed below.

Specific Gravity

The specific gravity of a material is the ratio of the weight in air of a unit volume of the impermeable portion of the material at 23°C (73.4°F), to the weight in air of equal density of an equal volume of gas-free distilled water at the same temperature. The specific gravity of the material was determined using the weight-in-air/weight-in-water technique according to ASTM D792 for specimens taken from various locations on the material panels [23].

Resin and Fiber Content

The resin and fiber content determinations were completed using the same specimens which were used for specific gravity measurements. For this type of material, the ignition loss method was used according to ASTM D2584. The specimen was weighed and placed in a crucible, then was ignited, where the specimen burned until only ash and carbon remained. The carbonaceous residue was reduced to an ash by heating it in an electric muffle furnace at 565°C (1050°F), and was then cooled in a desiccator and weighed again [23].

Void Content

The values calculated for specific gravity, resin, and fiber contents were used to calculate the void content of the composite

according to the computational procedure presented in ASTM D2734. The densities of the resin, the reinforcement, and the composite were measured. Then the resin content was measured, and a theoretical composite density calculated; this was compared to the measured composite density. The difference in densities was the void content. This method sometimes yields negative void contents because minor errors in the values used for resin, fiber and composite specific gravities may become significant at low void contents [23].

Environmental Conditioning and Mechanical Testing

Several samples exposed to various conditions were prepared for mechanical testing. The intention was to expose the samples to different environmental situations, so that their mechanical behavior could be compared and analyzed, and later on, to provide samples for fracture surface examination utilizing a stereo microscope and scanning electron microscope (SEM).

The exposure conditions were selected to simulate the possible operating conditions the material might be exposed to during service, and some extreme conditions that the component to which might be exposed to occasionally.

The first condition consisted of a dry dessicated storage of machined specimens at ambient temperature to simulate regular operating conditions. This set of room temperature specimens provided baseline data to compare with the specimens under other types of environmental conditioning.

Additional specimens were exposed to elevated temperatures.

Samples were placed into the ovens for one day, one week, and one month at two different temperatures, 180°F and 250°F, prior testing. In addition, specimens were exposed to humidity aging conditions. The specimens were placed in an environmental chamber at a temperature of 120°F and 100% relative humidity until saturation was reached. Saturation was determined by weighing the specimens every week until there was no appreciable weight gain. Once a constant weight was read for the samples, they were assumed to be ready for mechanical testing together with the other conditioned samples.

The mechanical testing conducted after environmental conditioning of the samples was based on standardized ASTM procedures for tension, flexure, compression, interlaminar shear, impact and tensile and flexural fatigue [23].

The tensile test applied to the samples was the standard test method for tensile properties of plastics ASTM D638-82a. The material was assumed to behave closer to a plastic than to a composite laminate; therefore, this standard was chosen for the determination of the tensile properties of this material. The method could be used for testing sheet or plate materials of any thickness up to 14mm. The tensile test was conducted at an extension rate of 0.05 in/min on an Instron Universal Testing machine. The tensile strains of the dried, dessicated, ambient temperature samples were monitored with extensometers [23].

The ASTM D695 standard was used to conduct the compression tests. These were performed in an Instron Universal Testing machine as the tensile specimens, since it was considered a suitable testing machine capable of controlling constant-rate of cross-head movement. A

compression fixture was used for applying the load to the test specimen. The fixture was constructed so the loading was axial within 1:1000 and applied through surfaces that were flat within 0.025 mm and parallel to each other in a plane normal to the vertical axis [23]. All flexural testing was conducted in accordance with ASTM method D790 using the three point loading system, utilizing center loading on a simply supported beam. The specimen consisted of a bar of rectangular cross section resting on two supports and loaded by means of a loading nose midway between the points. It was expected that the material would undergo large deflections, so the fixture was set up according to procedure B on the ASTM standard. A properly calibrated Instron Universal testing machine could be operated at constant rates of cross-head motion over the range required [23].

In-plane shear has been investigated by using ASTM D3846 double notch method with side supports. This type of testing has been widely used because of the simplicity of the sample design. However, it should be noted that there is a large controversy about interlaminar shear tests on composite materials as was pointed out before in the literature survey. An Instron Universal testing machine similar to the one used for tension, compression, and flexure was used for the in-plane shear tests [23].

Impact testing was done by a weight drop type of testing. Composite panels were impacted with a hemispherical tipped projectile weighing 6 lbs. was dropped over a 3.5" x 3.5" specimen, from both 3 and 6 ft. A picture of the set-up used for the impact test and projectile used are shown in Figures 1, 2, and 3. It was found that this material showed little surface indication of damage. Therefore,

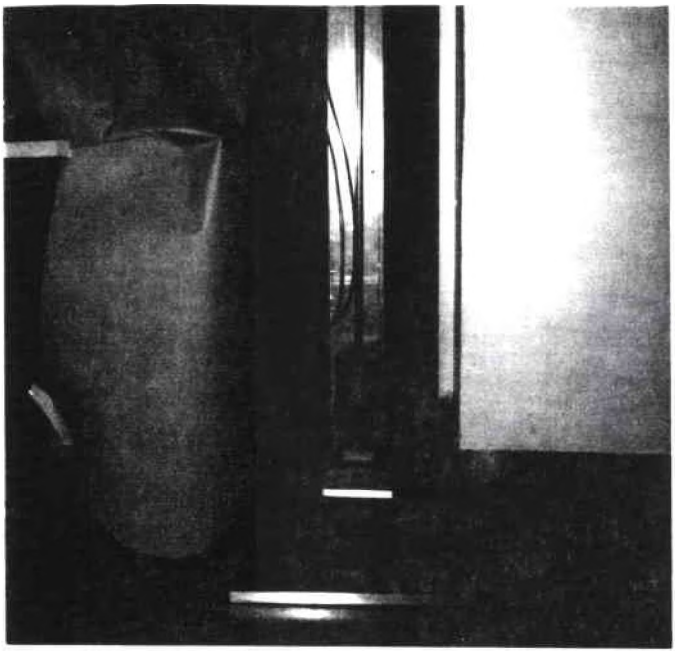

Figure 1. Experimental impact test fixture.

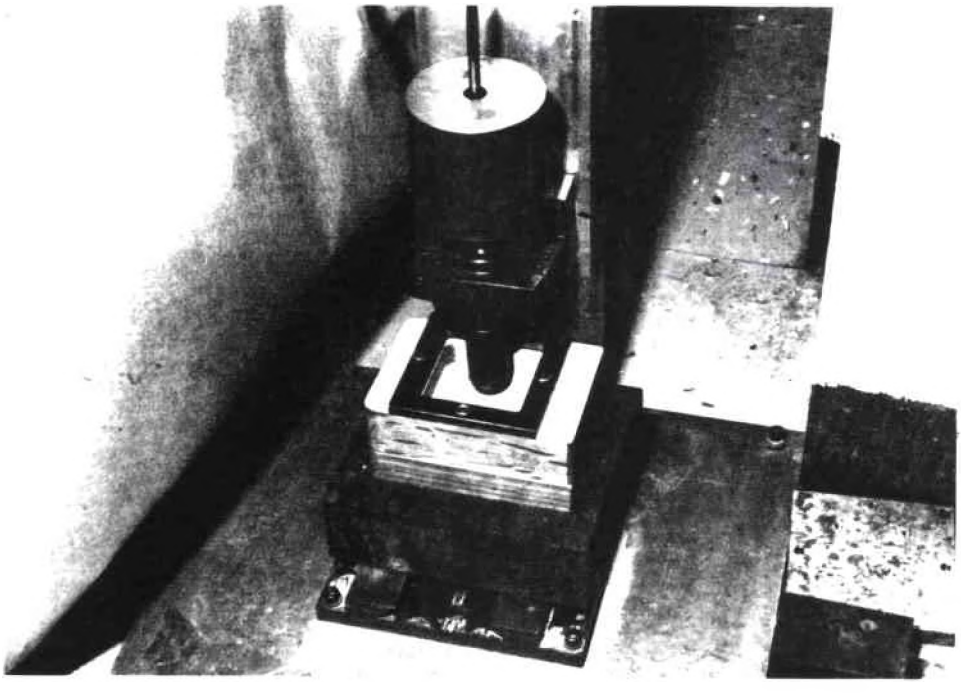

Figure 2. Impact test weight and projectile.

ultrasonic inspection was considered to be a convenient technique to assess the damage which occurred during impact [1].

Surface Analysis

X-Ray Photoelectron Spectroscopy (XPS)

XPS is a relatively new technique to the field of surface analysis, however the earliest measurements of the electron kinetic energy distribution resulting from X-ray irradiation for solid materials were reported in the early part of this century. The basic XPS experiment consists of X-ray photons, from a nearly monoenergetic beam directed onto a sample. The photon is observed by sample atoms with each absorption event resulting in the prompt emission of an electron. Electrons from all the orbitals of the atom with a binding energy, Eb, less than the X-ray energy are excited, though not with equal probability. Thus, some peaks are more intense in the spectra than others. Since energy is conserved, the kinetic energy of the electron plus the energy required to remove it from its orbital to the spectrometer vacuum must equal the X-ray energy. If the X-ray energy is measured with the electron spectrometer, the binding energy of the electron in the atomic orbital can be obtained. Since the atomic structure of each element in the periodic table is distinct from all the others, measurement of the positions of one or more of the electron lines allows the ready identification of an element present at a sample surface. The equipment used to do the surface energy analysis consisted of an X-ray source, an energy analyzer, and a detector enclosed in a vacuum chamber. A data display was used to plot the results obtained by this technique [24].

Fractography

The examination of the fracture surfaces was of crucial importance for this investigation. A Nikon optical stereo microscope, and a JEOL JSM 35 scanning electron microscope (SEM) were used for this purpose. Figure 4 shows the SEM system set up where photomicrographs were taken. Macrophotos of the broken specimens were also taken with a Nikon 35 mm SLR camera set up allowing for full documentation of the fractured specimens.

Figure 4. Scanning Electron Microscope (SEM) system.

CHAPTER III

RESULTS AND DISCUSSIONS

The fiber glass RIM material is a polyisocyanurate structural polymer system based on a specially formulated methylene diphenyl diisocyanate A-side, and a fully formulated B-side. The chemical composition of the samples supplied were 22 % polyol and 78 % isocyanate by weight. A 57 % by weight fiber glass mat was used as the reinforcement. Typical characteristics of the composite and individual components are given in Tables 1, 2, 3, and 4.

Physical Properties

Experiments were conducted to determine important physical properties of the material for characterization purposes. Results of these properties are presented in Table 5. The standard test method for the ignition loss of cure reinforced resins was used. Densities for E-glass and the isocyanate/polyol resin were required to calculate the fiber content (vol%) and the void content (vol%). The density used for the glass was the value widely published in the fiber glass literature. The density used for the resin was assumed, based on known density ranges for similar resins, and using the manufacturer information. The void content was determined in accordance with ASTM D2734-70. For comparison purposes, photomicrographs of typical crossections of the material were taken (Figure 5), so the determination of the void content could be made using a grid point

Table 1. TYPICAL PROCESSING INFORMATION OF RIM POLYCARBAMATE[1]

A/B ratio	2.28/1.00
Reactivity	
Handmix 77°F, sec	24
Machine free pour, sec	15
Closed molds (mats @ 200°F), sec	8
Mold temp, °F	210 - 230
Component temp, °F	
Isocyanate	75
Polyol	85
Demold time, sec	45
Injection rate, lbs/sec	0.5 - 2.5
Mold release, base coat (wax)	Chem Trend 2044
Mold release, top coat (wax)	Chem Trend 2007

[1] Dow Corning Product Information

Table 2. TYPICAL PROPERTIES OF COMPONENTS OF RIM POLYCARBAMATE[1]

PROPERTY	Spectrim MM 353-A	Spectrim MM 353-B
Specific Gravity, 25/25°C	1.21	1.04
Viscosity, cp @ 25°C	46.0	90.0
@ 66°C	9.9	16.6
@ 100°C	4.4	7.2

[1] Dow Corning Product Information

Table 3. TYPICAL MECHANICAL PROPERTIES OF RIM POLYCARBAMATE[1]

REINFORCEMENT, WT% [1]	ASTM METHOD	57
Specific Gravity, 25/25°C	D-792	1.74
Flexural Modulus, psi x 10^3	D-790	1816
Flexural Strength, psi x 10^3	D-790	55.2
Tensile Strength, psi x 10^3	D-638	28.8
Elongation, %	D-638	7.4
Notched Izod Impact, ft-lb/in	D-256	13.7
Heat Distortion Temp @ 264 psi, °C	D-648	251
Heat Sag, (6 in, 204°C, 30 min), in		0
Shrinkage, mils/in		0.25

[1] Dow Corning Product Information

Table 4. EFFECT OF POSTCURE (350°F/30 MIN) OF RIM POLYCARBAMATE

	NON-POSTCURED	POSTCURED
Reinforcement, wt % [1]	37.8	39.1
Specific Gravity, 25/25°C	1.54	1.46
Flexural Modulus, psi x 10^3	1181	1177
Flexural Strength, psi x 10^3	36.1	37.0
Tensile Strength, psi x 10^3	22.2	19.0
Elongation, %	7.3	6.2
Notched Izod Impact, ft-lb/in	9.5	9.3
Heat Distortion Temp @ 264 psi, °C	184	202

[1] Owens Corning Fiberglass Mat; M-8610

TABLE 5.

PHYSICAL PROPERTIES OF RIM POLYCARBAMATE

panel	Density (g/cc)	Resin Content (% wt.)	Fiber Content[1] (% vol.)	Void Content[2] (% vol.)
651-352-1	1.66	47.6	34.3	2.01
651-352-2	1.73	43.7	38.4	3.03

[1] Based on a density of E-glass = 2.54g/cc (literature).

[2] Based on a density of isocyanate/polyol resin = 1.17g/cc (assumed).

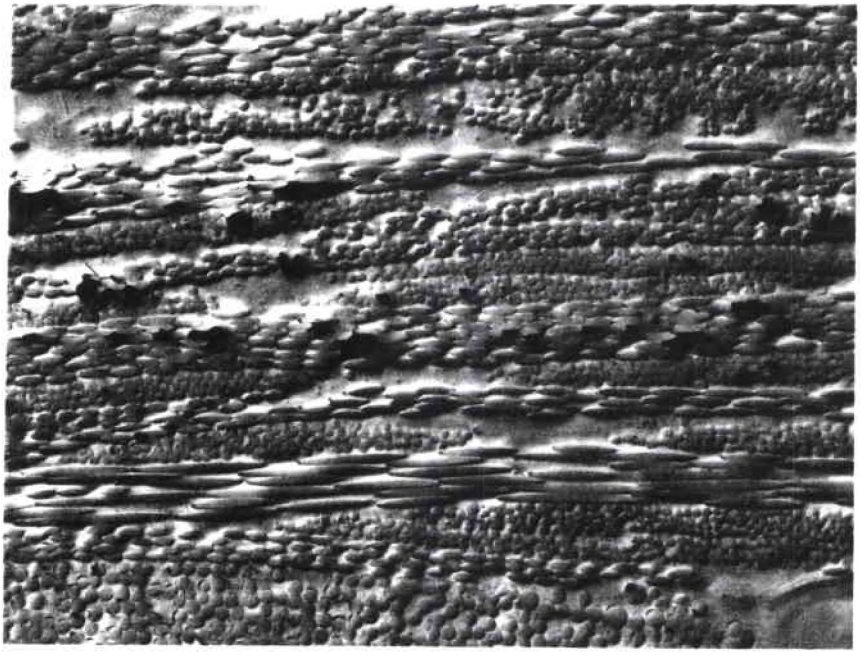

Figure 5. Cross-section photomicrograph (x 100).

determination technique. By the use of this technique, determination of the void content is made by placing a transparent grid over a photomicrograph (100X) of a crossection of the material. The number of intersecting grid points which fall on void areas of the material are noted, as well as the total number of intersecting grid points. The void content is then computed as follows:

$$\text{void content (vol\%)} = \frac{\text{Grid intersections with voids}}{\text{Total Grid Intersections}} \times 100$$

The average void contents determined using the grid point determination technique matches the value determined in accordance with ASTM D2734-70, and is the result presented in Table 5 [4].

Glass Transition Temperature

The glass transition temperature (T_g) has been determined by Dynamic Mechanical Analysis (DMA). Figure 6 illustrates the loss modulus curve used to determine the T_g of the RIM material. The peak of the loss modulus (E") is found to be approximately 116 °C, which is designated as the glass transition temperature [25], [26].

Thermal Aging Effects

Some interesting characteristics were found in all thermally-aged specimens. Yellow and brown discolorations were observed on specimens aged at both 180 °F and 250 °F for one month. It was assumed that oxidation of the material took place when the specimens were exposed to higher than normal temperatures. Similar discolorations have been reported in literature on similar compounds.

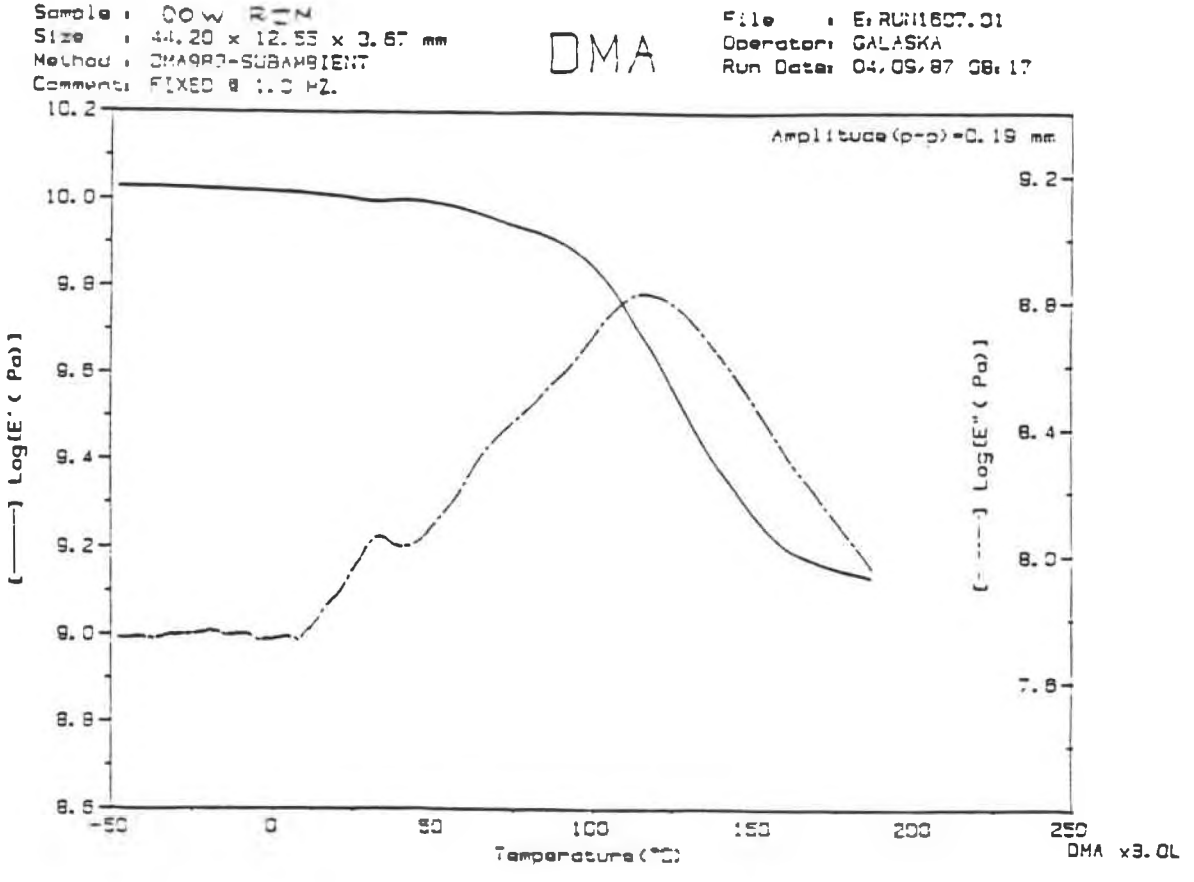

Figure 6. Dynamic Mechanical Analysis (DMA)

Polycarbamates tend to get a yellow discoloration under U.V. light and increased temperature. In order to determine a viable reason for this occurrence, a small piece of material was placed in an oven in an environment free of oxygen so that oxidation could not take place. The temperature of the oven was set at 250 °F, the same temperature at which the specimens turned brown. The results showed that, the tested specimen was only slightly discolored. This indicated that oxidation played a major role in the discoloration process. Typical discolorations observed in aged samples are presented in Figures 7 through 10. Note that, for longer aging temperature and time the material became darker. The increase in mechanical properties encountered on all of the thermally-aged specimens was attributed to a postcuring effect. Although polycarbamates are highly crosslinked polymers, some crosslinking due to postcuring must have taken place, increasing the mechanical properties. A second DMA analysis was conducted on one of the aged specimens to determine if the T_g of the polymer had shifted to a higher value. This would indicate that the material had crosslinked further. Results of this DMA are shown in Figure 11. An increase in the T_g of about 50 degrees was found with respect to the prior analysis confirming the assumption.

Mechanical Testing Properties

The various mechanical properties were measured for the composite under various environmental conditions and different layout orientations. The average strengths for the various specimens are sumarized in Table 6. Specific data for each sample is included in Appendix C.

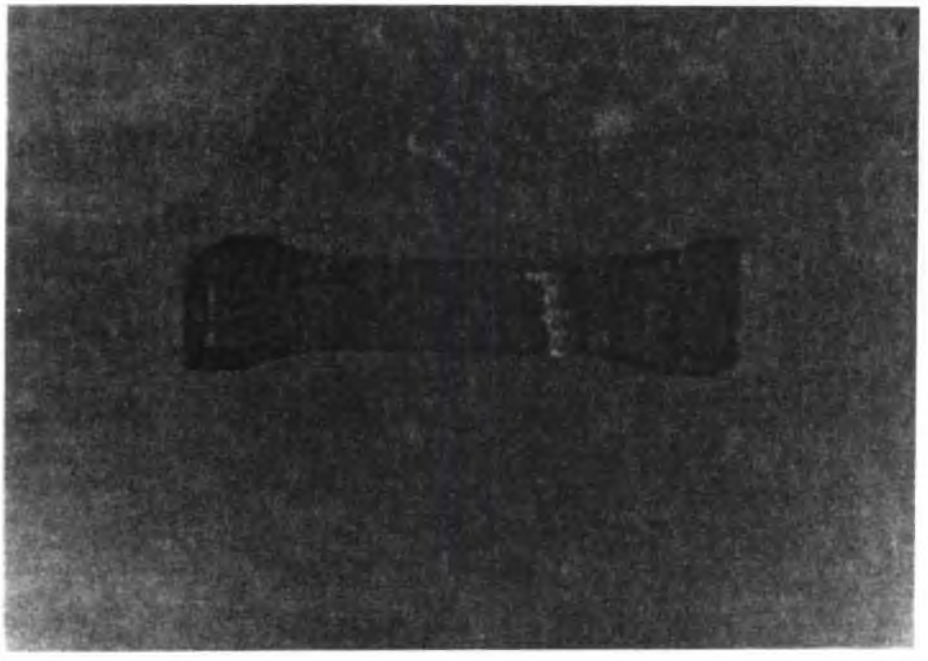

Figure 7. Thermally-aged compression specimen, (180°F for 1 month).

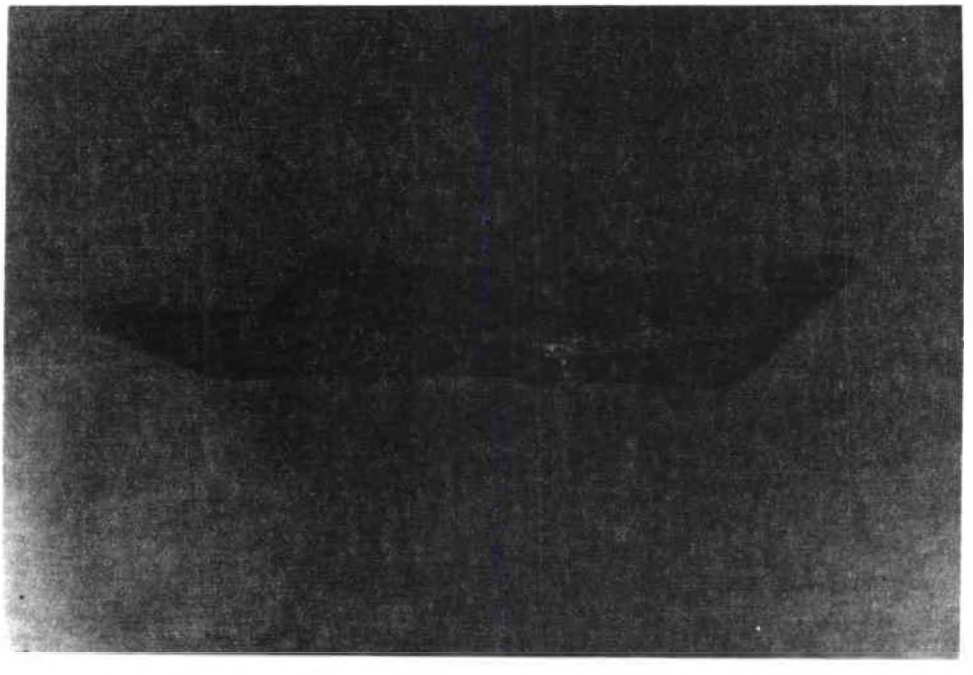

Figure 8. Thermally-aged compression specimen, (180°F for 1 month).

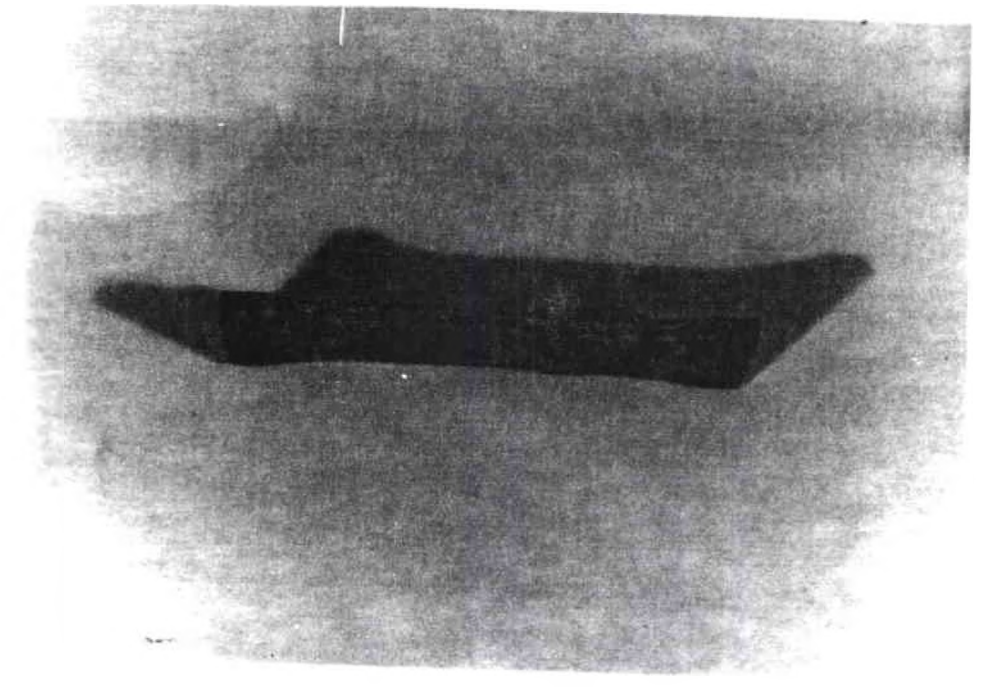

Figure 9. Thermally-aged compression specimen, (250°F for 1 month).

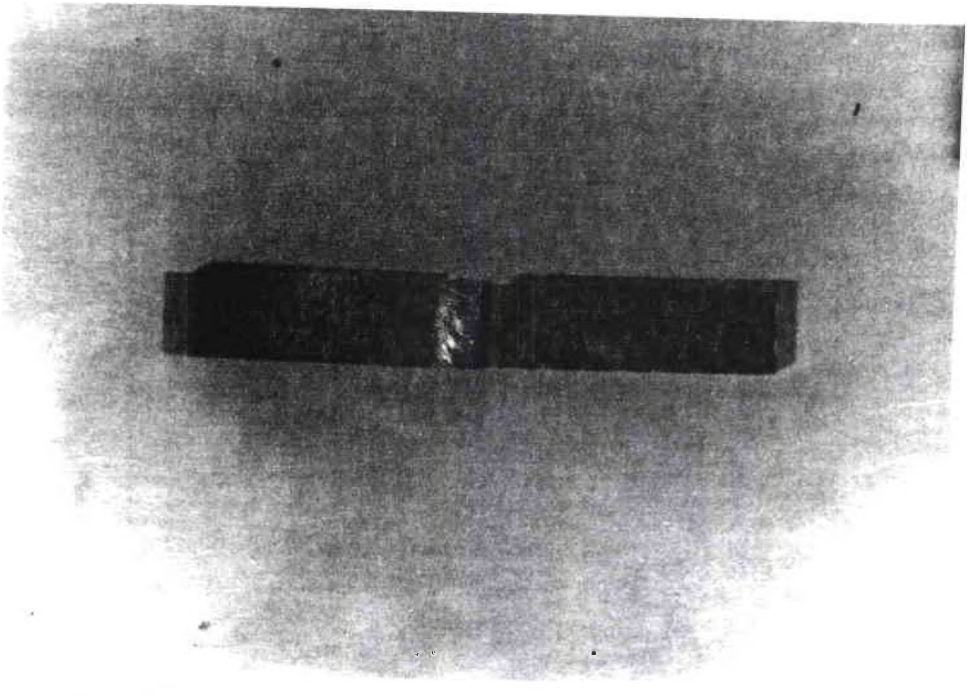

Figure 10. Thermally-aged in-plane shear specimen, (250°F for 1 month).

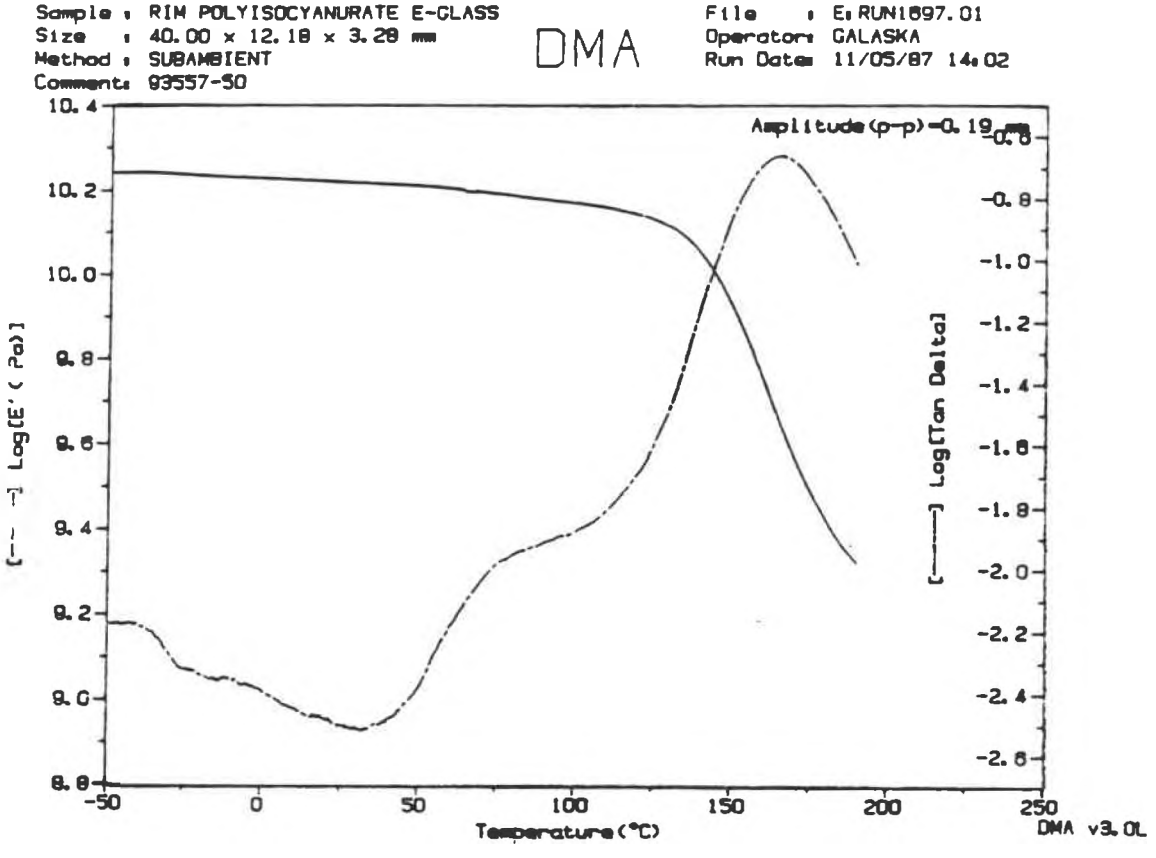

Figure 11. Dynamic Mechanical Analysis (DMA).

TABLE 6.

ULTIMATE STRENGTHS OF RIM POLYCARBAMATE (KSI)

ORIENTATION	UNAGED	THERMALLY AGED	(%) DIFF	HUMIDITY AGED	(%) DIFF
		TENSION.			
0° - 90°	44.2	47.7	7 up	39.2	12 down
45°	16.8	17.8	6 up		
		FLEXURE.			
0° - 90°	61.6	66.0	7 up	44.3	30 down
45°	38.5	44.3	15 up	34.5	22 down
		COMPRESSION.			
0° - 90 °	52.6	52.0	None	23.4	50 down
45°	18.8	22.2	18 up		
		IN-PLANE SHEAR.			
0° - 90°	6.5	5.6	16 down		
45°	5.0	5.2	None		

It has been noted that, in general, the ultimate strengths are lower for the 45° oriented specimens when compared with the 0° or 90° oriented speciemns. No difference in strength was noted between the 0° and the 90° specimens. The fact that the 45° oriented coupons have lower mechanical properties is due to the reinforcement distribution, which is primaraly in the 0° and 90° directions. Various, changes in properties for specimens that underwent environmental conditioning have been observed. In general, thermally-aged specimens showed an increase in mechanical strengths of approximately 7 % for tension and up to approximately 18% for some of the compression specimens. In contrast, humidity-aged specimens showed a significant decrease in mechanical properties. The most significant decrease was noted for the compression specimens (50%).

Microstructural Evaluation

A general overview of the internal geometrical structure of fiber orientation and matrix was considered the first step in the fractography analysis of the RIM material. Sectional views of failed specimens aided in the understanding of the material construction, and consequently how this material might fracture when exposed to specific testing modes. Specimens were placed in an oven to burn-off the polymeric matrix, so the skeleton of the material formed of glass fibers could be observed. It was found that the material was formed by distinct layers of fiber glass reinforcement symmetrical about the centerline. A random thin mat was placed at the outer surface, as can be observed in Figure 12, probably to prevent superficial cracking. Underneath this first random mat, woven uniform fibers oriented at

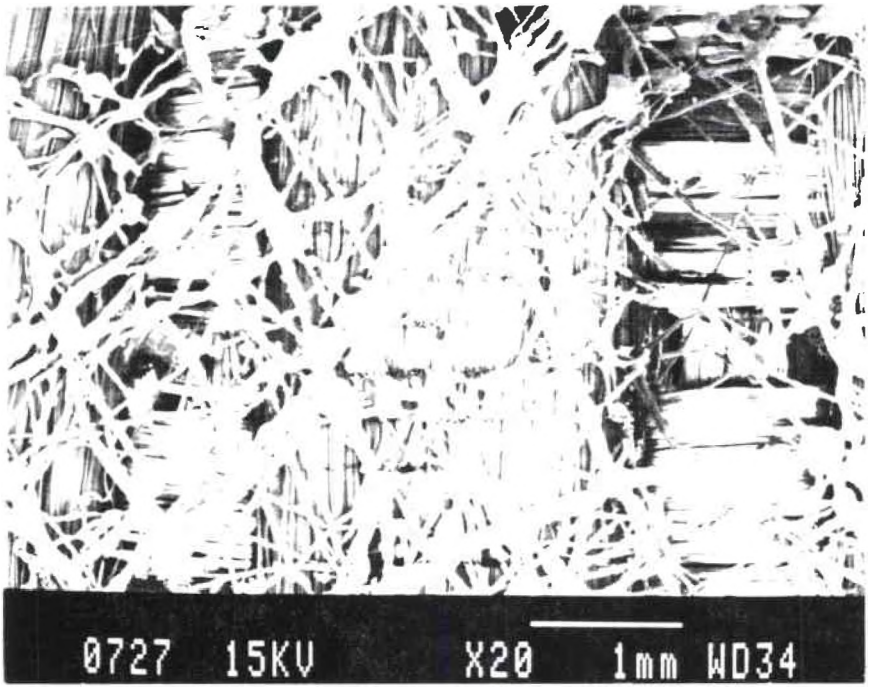

Figure 12. Random mat and general structure of RIM material, (x 20).

both 0° and 90° were observed. Figure 13 shows a view of the material where the 0° and 90° woven fibers can are shown. The same characteristics are illustrated in Figure 14. The next layer towards the center of the specimen was found to be formed by fibers aligned at 45° with respect to the 0° and 90° woven fibers. At the centerline of the composite a thick random fiber mat was encountered, providing reinforcement in all directions. Figure 15 illustrates a top view of a polished specimen from the outer surface towards the center showing the various orientations and symmetry of the material.A cross section of the composite is illustrated in Figure 16, note the various orientations of fibers and matrix areas.

Fractography

Once the general structure of the material was understood, the fracture surfaces provided by mechanical testing specimens exposed to various conditions were observed. Representative failed samples were examined using both the optical microscope and the SEM to identify the various fracture features of the fiber and the matrix. Comparisons were made between the typical morphologies of thermally-aged and humidity-aged specimens with those observed in the unaged specimens.

Unaged Tension

Typical macrographs of tensile failures are illustrated in Figures 17 and 18. Specimens oriented 0° and 90° failed normal to the load direction. In the 45° oriented specimens failure was located at 45 degrees to the loading direction. In both cases, delaminations and matrix cracking were observed. It should be noted that delamination

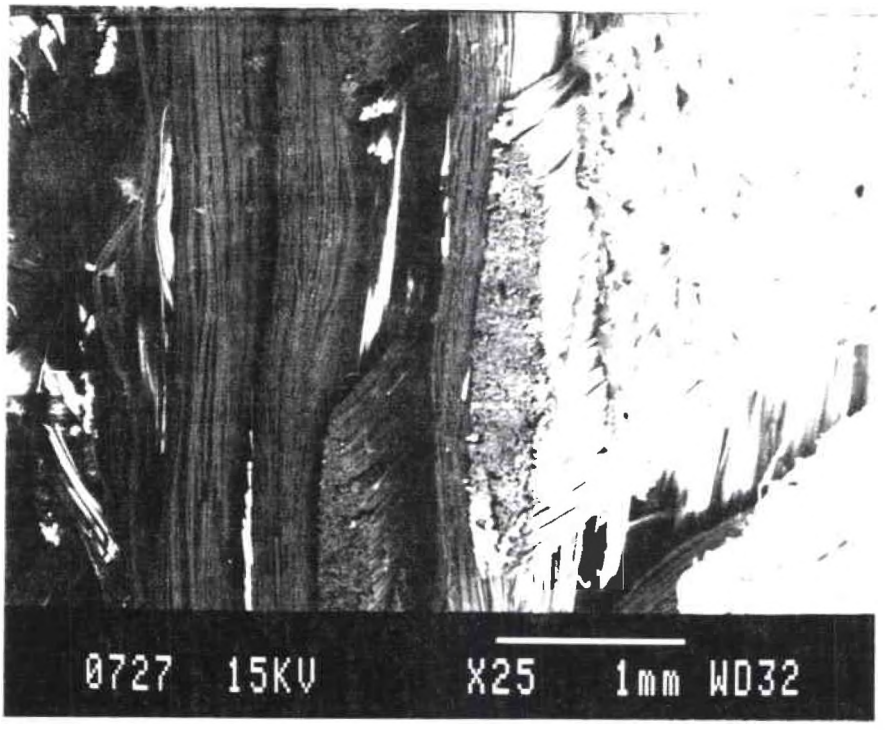

Figure 13. Woven 0°,90°,45° fibers on RIM material, (x 25).

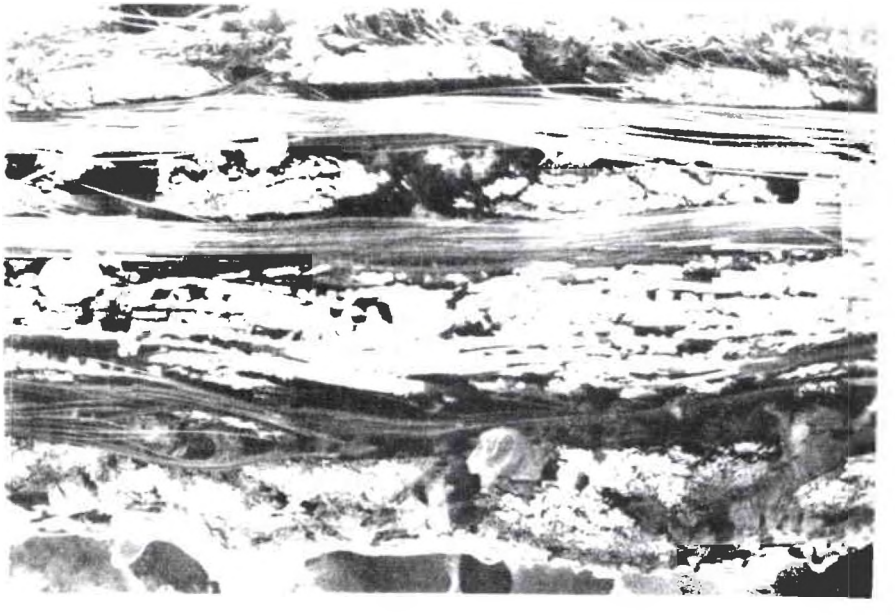

Figure 14. Various fiber orientations on RIM composite material, (x 10).

Figure 15. Top view of polished sample from outer surface, (x 50).

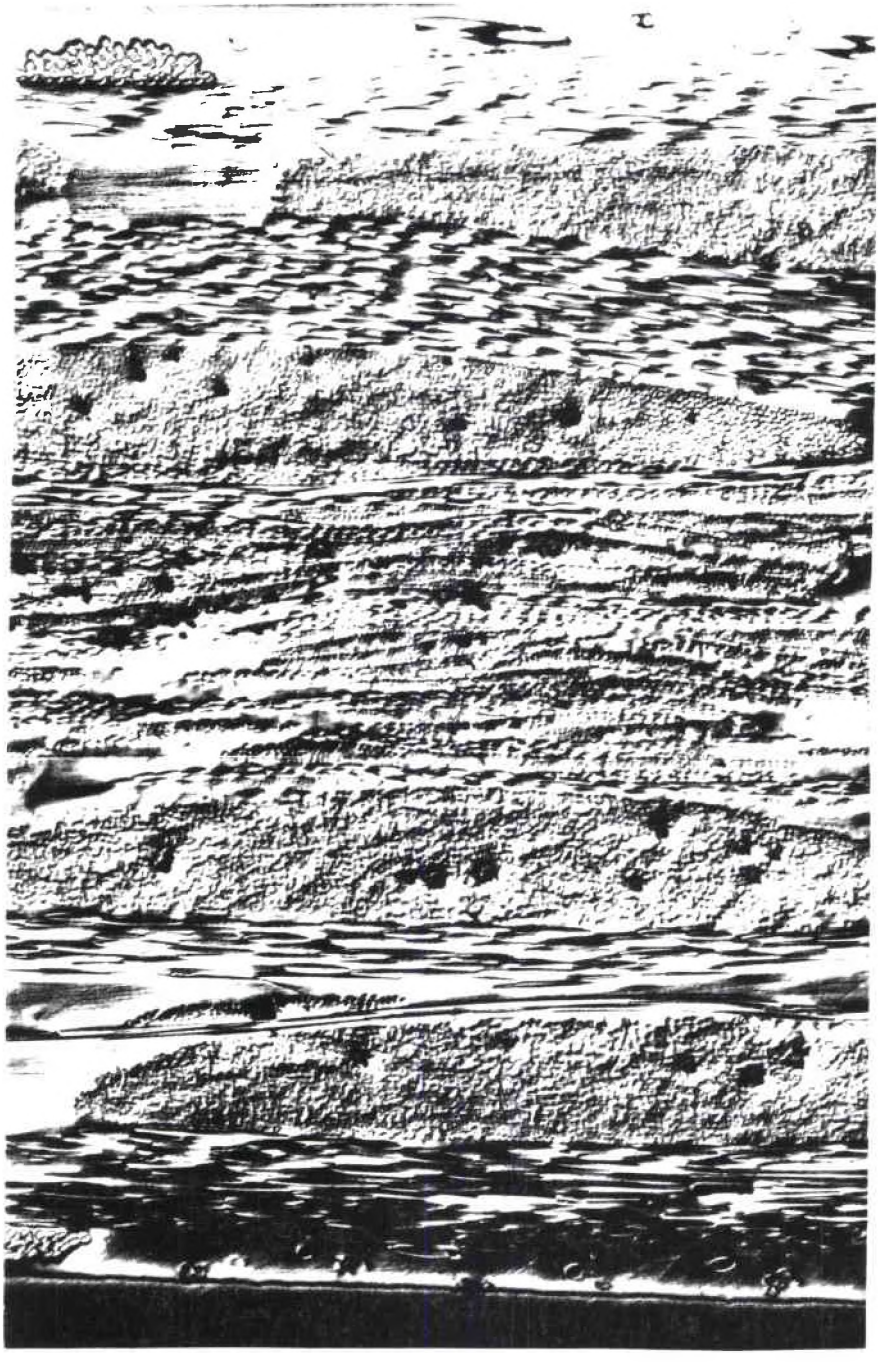

Figure 16. Side view of RIM composite material, (x 50).

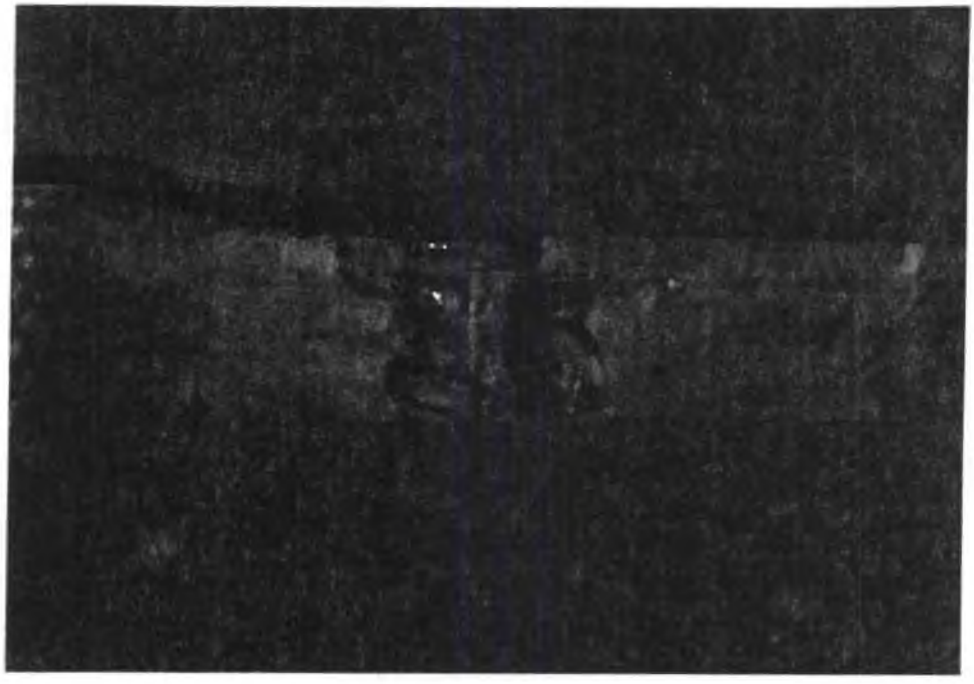

Figure 17. Fractured tension specimen, (90°layout orientation).

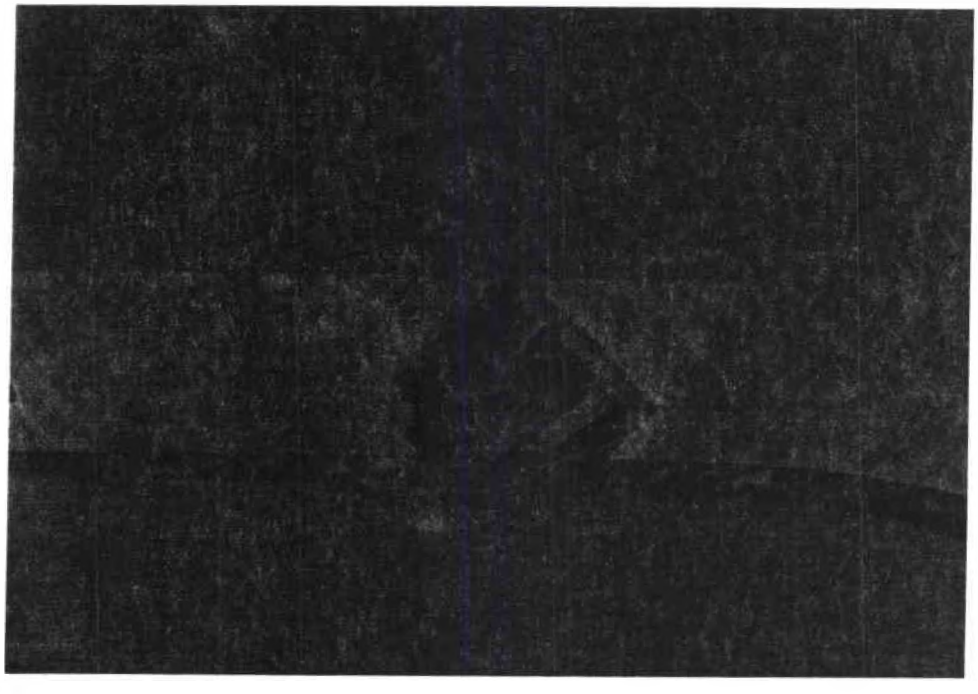

Figure 18. Fractured tension specimen, (45 layout orientation)

effects were more significant in the 45° oriented specimens.

Figure 19 illustrates fiber pullout due to the overloading condition. Fiber pullout is also illustrated in Figure 20. It should be noted from this figure that matrix areas where fibers have been pulled out left both a very smooth channel and/or a clean hole in the matrix. No matrix adhesion was observed on the fibers. Figures 21 illustrate river patterns in the matrix areas, which is a characteristic of brittle fractures. Another characteristic of the surfaces are the radial patterns noted on the fractured fiber tips. This feature have been illustrated in Figure 22. The propagation of the crack in the tension specimens was in the plane normal to the direction of the tensile load. No plastic deformation has been observed in either the fibers or the matrix. In summary, the following fracture surface characteristics have been observed on the unaged tension specimens:

(1) Fiber pullout (holes in the resin as well as matrix channels),
(2) Matrix cracking,
(3) River patterns in the matrix,
(4) Broken fibers, and
(5) Radial patterns on fractured fiber surface.

Thermally-aged Tension

A characteristic of the aged tensile specimens was some increase in fiber-matrix adhesion when compared with the unaged specimens. Figure 23 illustrates fiber bundles with matrix adhering to them. This effect was observed more in the specimens that underwent longer aging times, but no difference in adhesion was noted due to the different aging temperatures. After aging of one week, the increase

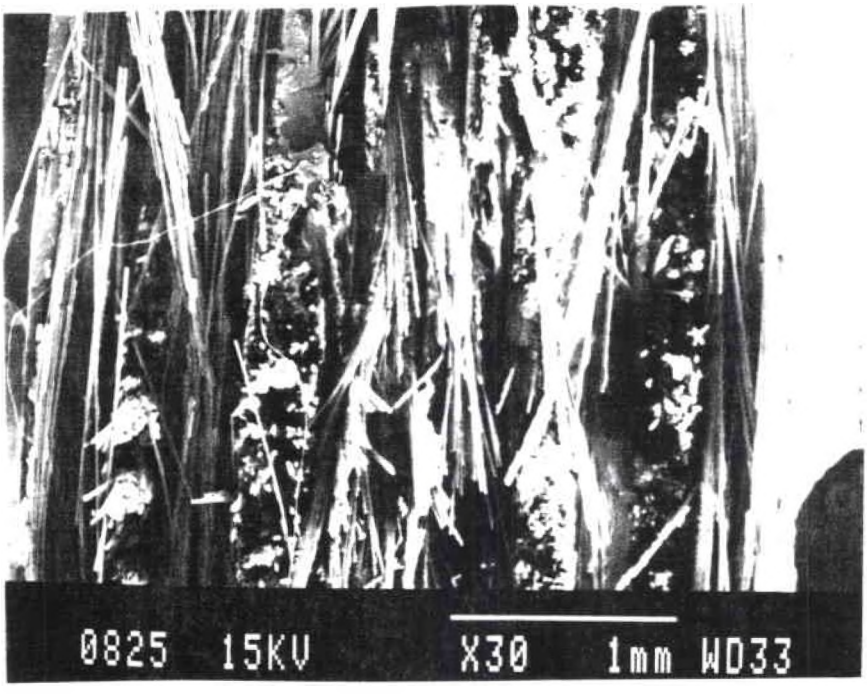

Figure 19. Fiber pullout, RIM tension specimen, (x 30).

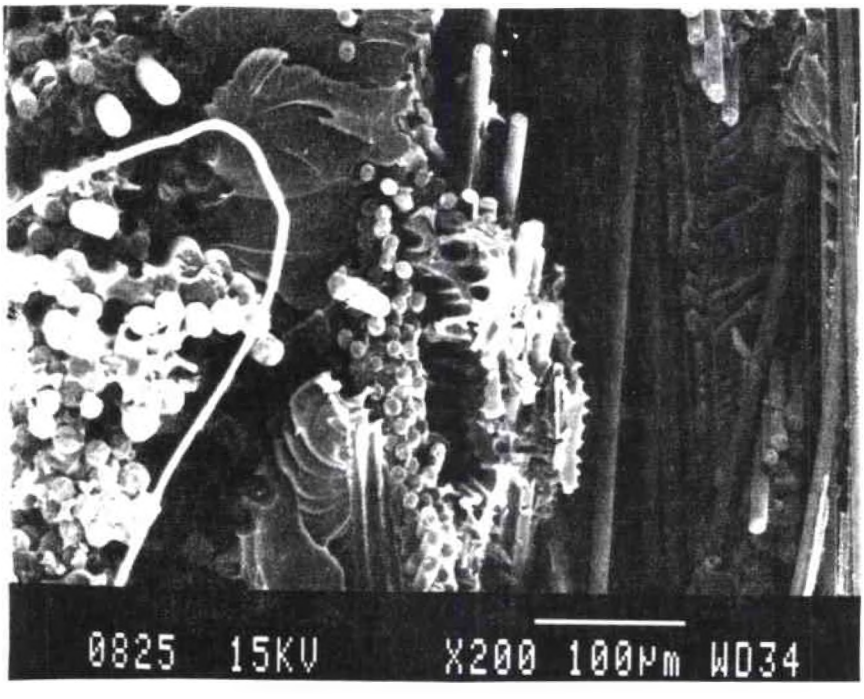

Figure 20. Smooth channels and holes from fiber pullout. RIM tension specimen, (x 200).

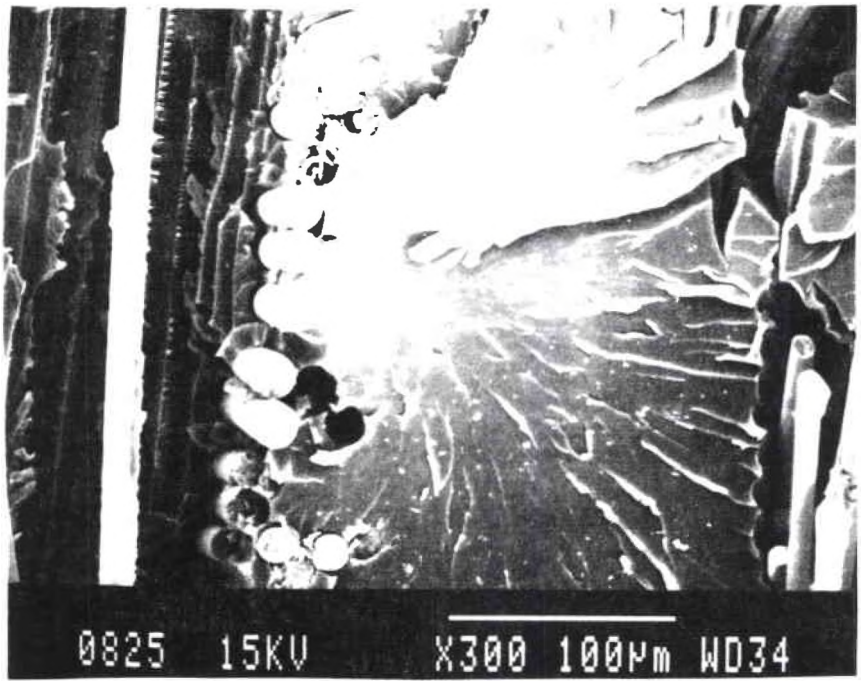

Figure 21. Matrix river patterns of RIM tension specimen (X300).

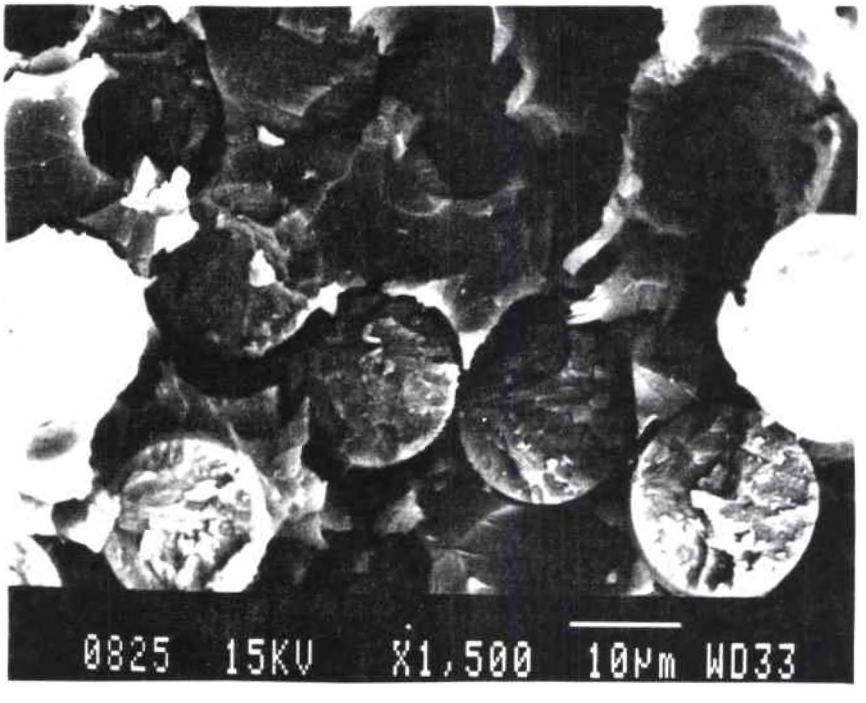

Figure 22. Radial patterns on fractured fibers of RIM tension specimen(x1500).

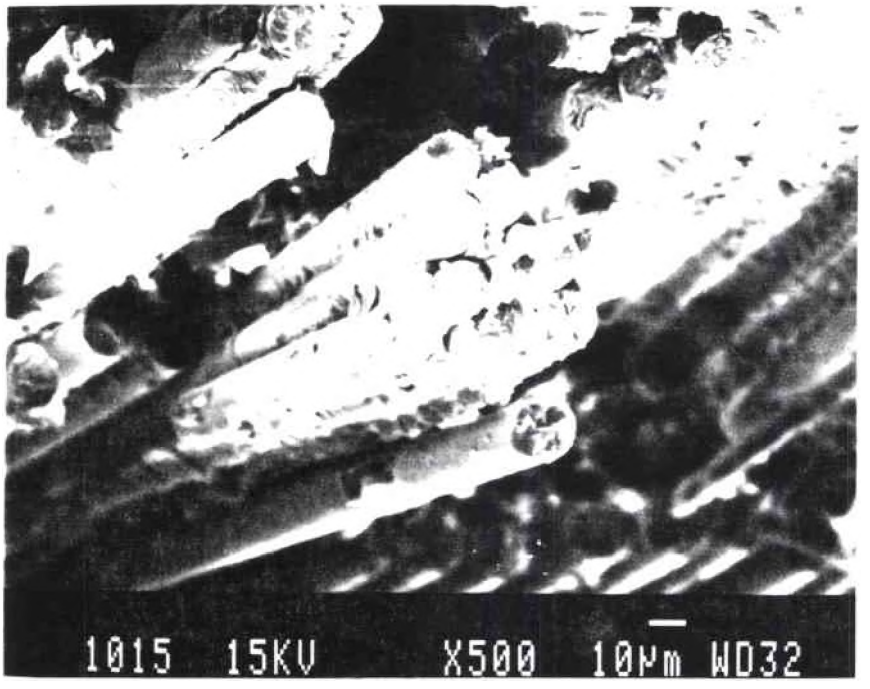

Figure 23. Matrix adhesion to fiber bundles on tension specimen (x500).

in fiber-matrix adhesion was noted. In addition, the surface where the fibers had pulled out, appeared to be much rougher as a consequence of the increase in bonding. Also, the increase in ultimate tensile strength measured from the mechanical testing of the aged specimens corresponds with the idea that better bonding was achieved in the thermally-aged specimens. River patterns on fractured matrix surfaces as well as radials on the tips occur in the aged specimens. Figures 24 and 25 illustrate these features.

In summary, the characteristics of the fracture surface observed on the thermally-aged specimens tested in tension include the following:

(1) Fiber pullout,
(2) Matrix cracking,
(3) River patterns on fracture surfaces of the matrix, and
(4) Radials on the fractured fibers.

Humidity-aged Tension

Similar characteristics were encountered on the humidity-aged fracture surfaces with respect to the unaged and thermally-aged specimens. Small amounts of debris have been observed, as well as smooth surfaces due to fiber pullout. A little more fiber-matrix adhesion has been detected on these surfaces with respect to the unaged specimens. Unlike the thermally-aged specimens, moisture seemed to play a major role in degrading the mechanical properties. Plastic deformation has been observed at some of the matrix regions shown in Figure 26, this indicates that the material is not as brittle as the unaged samples. Therefore, the plastic deformation must have been caused by increased presence of moisture. This may be due to

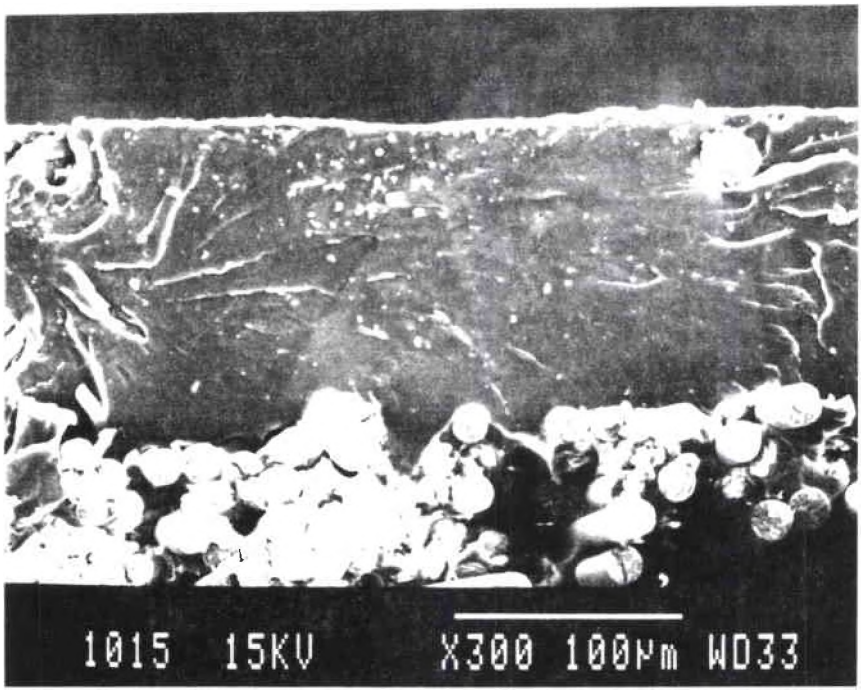

Figure 24. Radials in fiber tips as well as river patterns on matrix areas, tension specimen (x300).

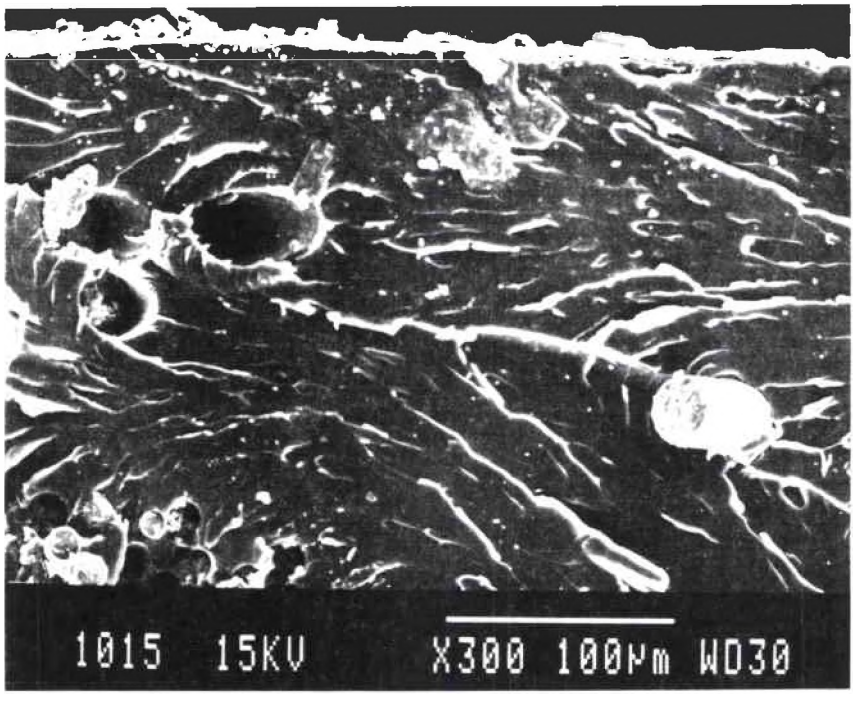

Figure 25. River patterns on matrix fracture surface and fiber pullout on tension specimen (x300).

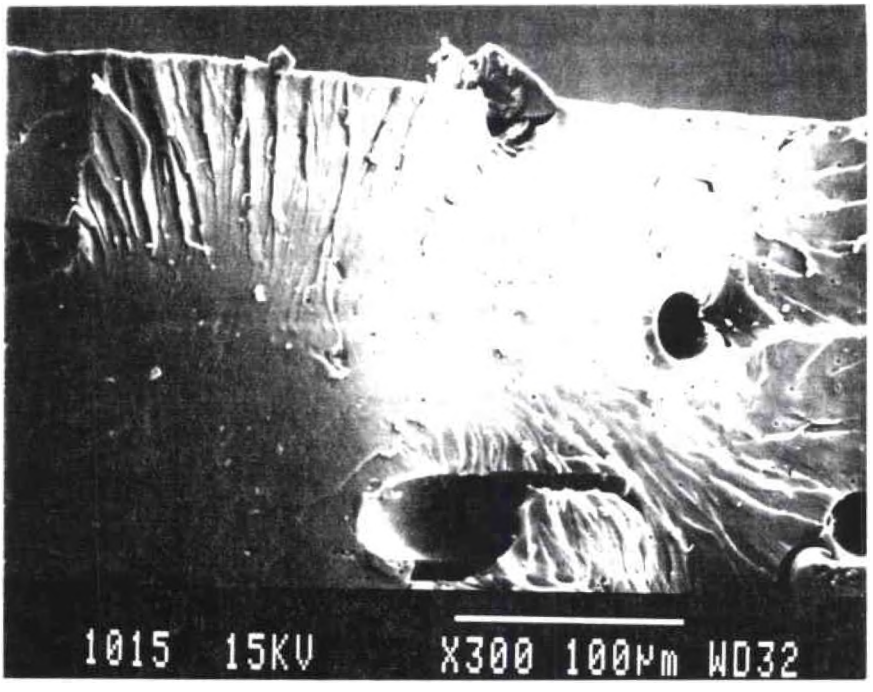

Figure 26. Fiber pullout and matrix cracking on tension specimen (x300).

increased moisture functioning as a plasticizer. Figures 27 through 29 show the various features observed on the fracture surfaces of the humidity-aged specimens.

In summary the characteristics of the fracture surface observed on the humidity-aged specimens tested in tension include the following:

(1) Fiber pullout (smooth matrix in fiber channels),
(2) Matrix cracking,
(3) Small amounts of debris,
(4) River patterns on matrix fracture surface, and
(5) Radials on fiber tips.

Unaged Compression

Typical macroscopic compressive failure locations are illustrated in Figures 30 and 31. Specimens oriented 0 and 90 degrees failed normal to the loading direction. In the 45 degrees oriented specimens failed at 45 degrees direction. In both cases, matrix cracking was observed on the fracture surface. It should be noted that delamination effects were more significant in the 45 degrees oriented specimens. For both orientations, buckling was the most significant feature on the fracture surface.

Figure 32 illustrates microbuckling of the fibers. Broken fibers and fracture debris are observed in Figure 33. Matrix cracking as well as broken fibers are noted in Figure 34. Chop marks characteristic of compression fractures and matrix cracking are shown in Figure 35. Bent fibers are illustrated in Figure 36, as well as the fiber-matrix debonding.

In summary, typical fracture surface characteristics of specimens tested in compression include:

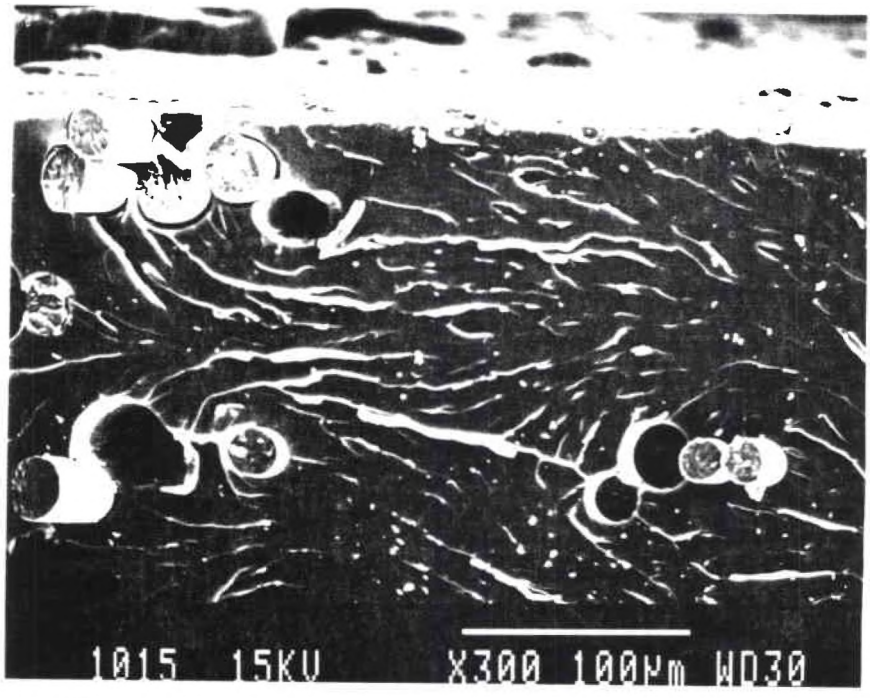

Figure 27. River patterns and fiber pullout on tension specimen (x300).

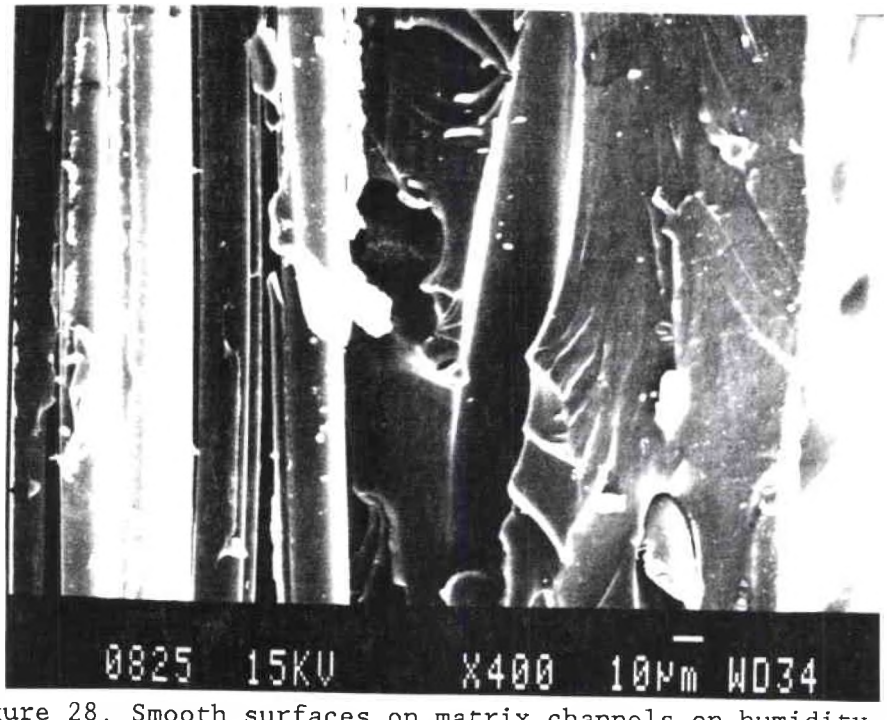

Figure 28. Smooth surfaces on matrix channels on humidity-aged tension specimen (x400).

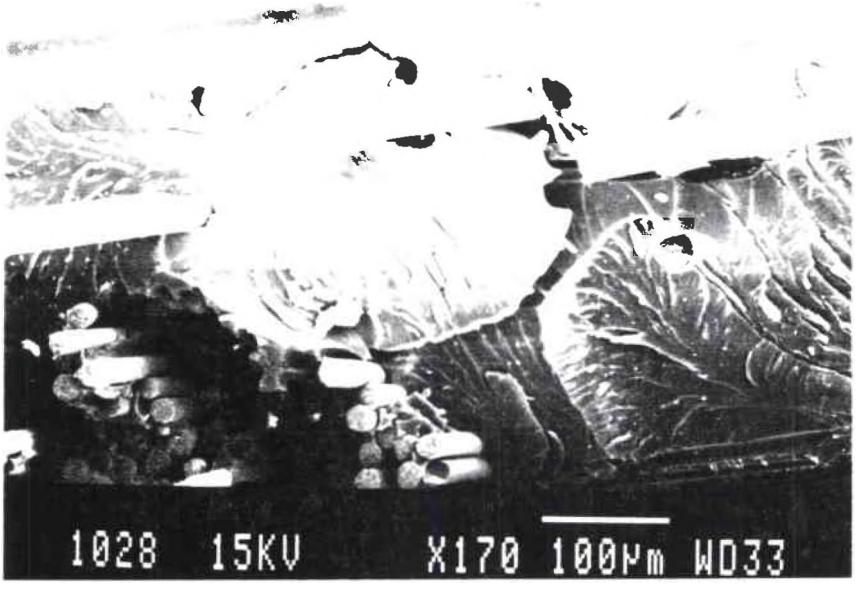

Figure 29. Matrix cracking and debris, tension humidity-aged specimen (x170).

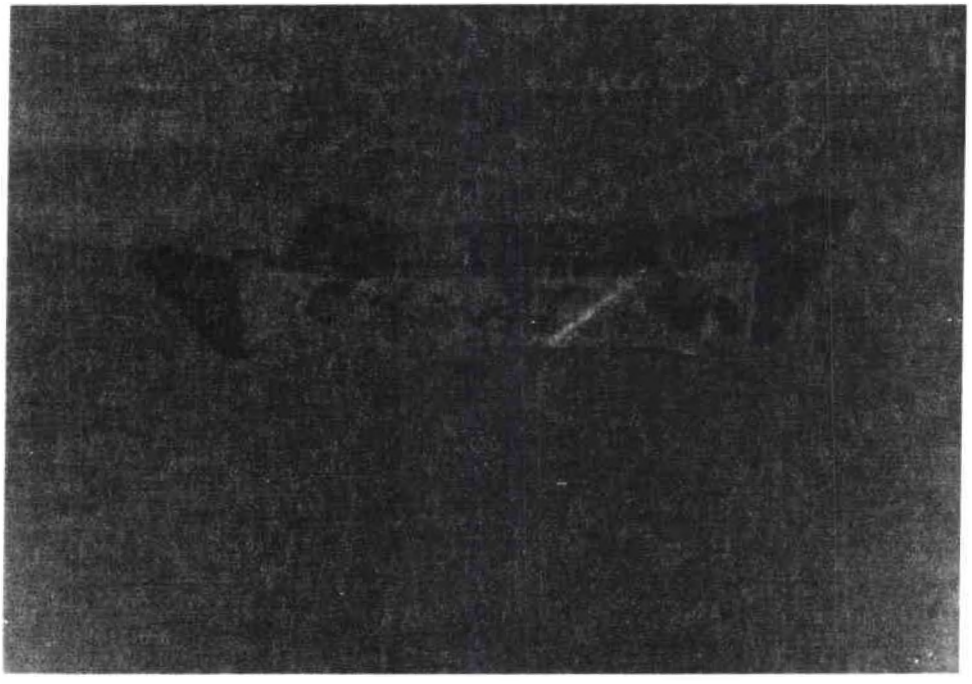

Figure 30. Fractured compression specimen, (45°layout orientation).

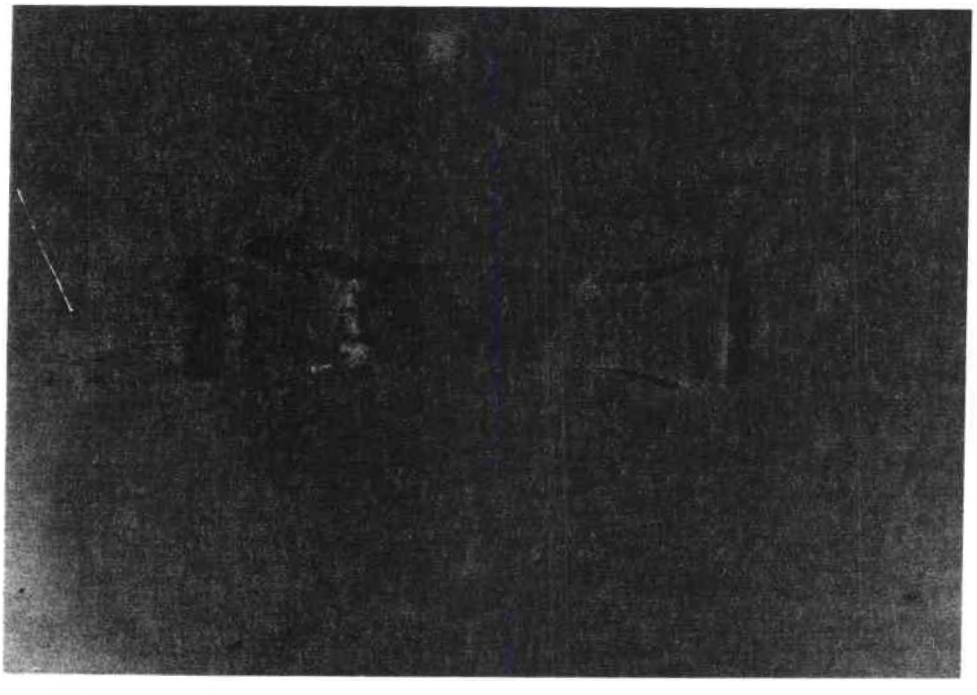

Figure 31. Fractured compression specimen, (0°-90°layout orientation).

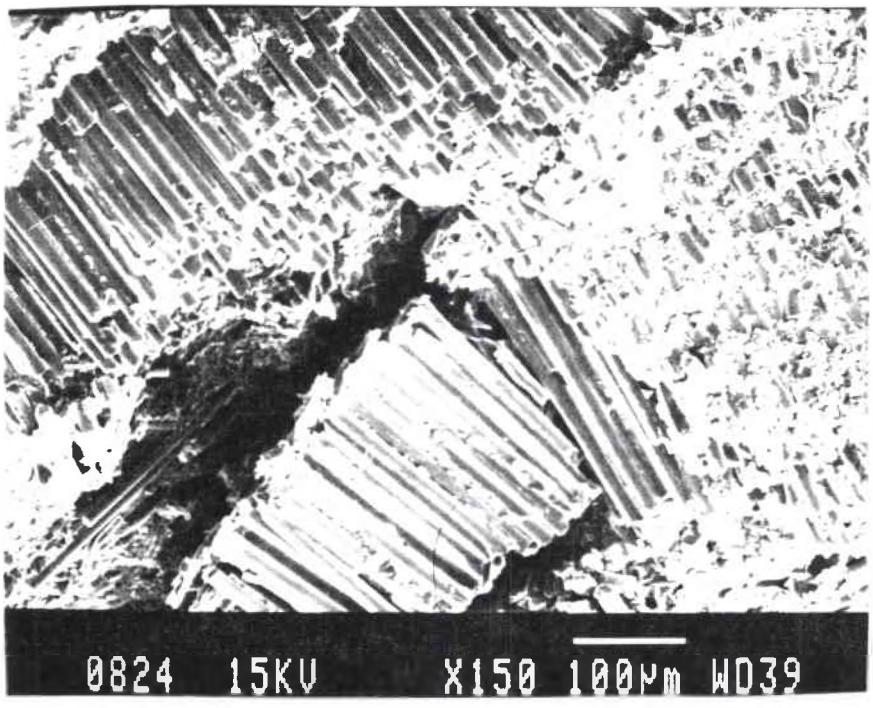

Figure 32. Microbuckling of fibers, unaged compression specimen.

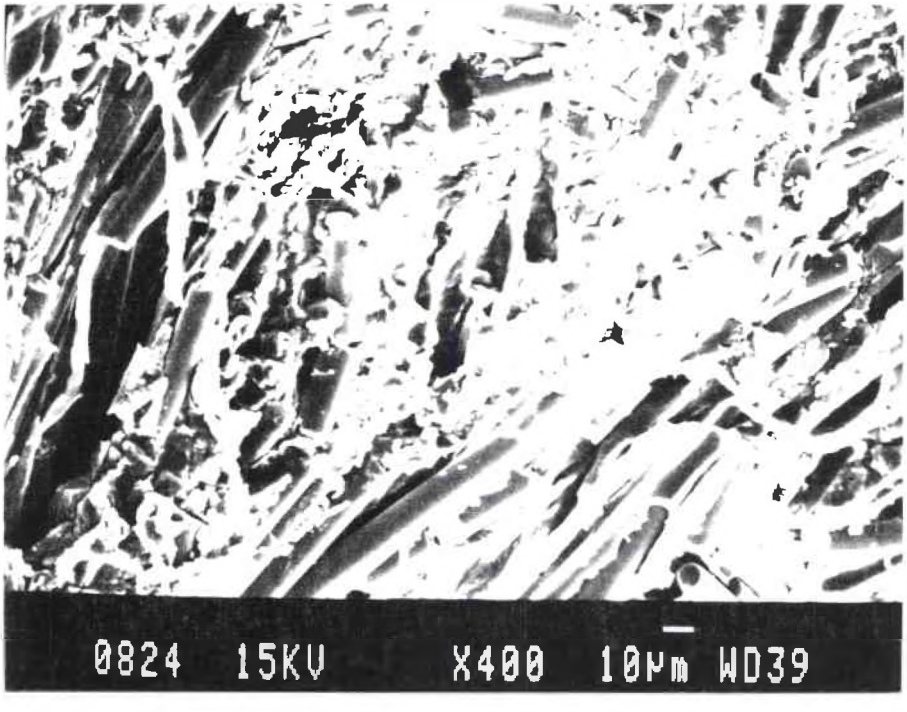

Figure 33. Broken fibers and fracture debris, unaged compression specimen.

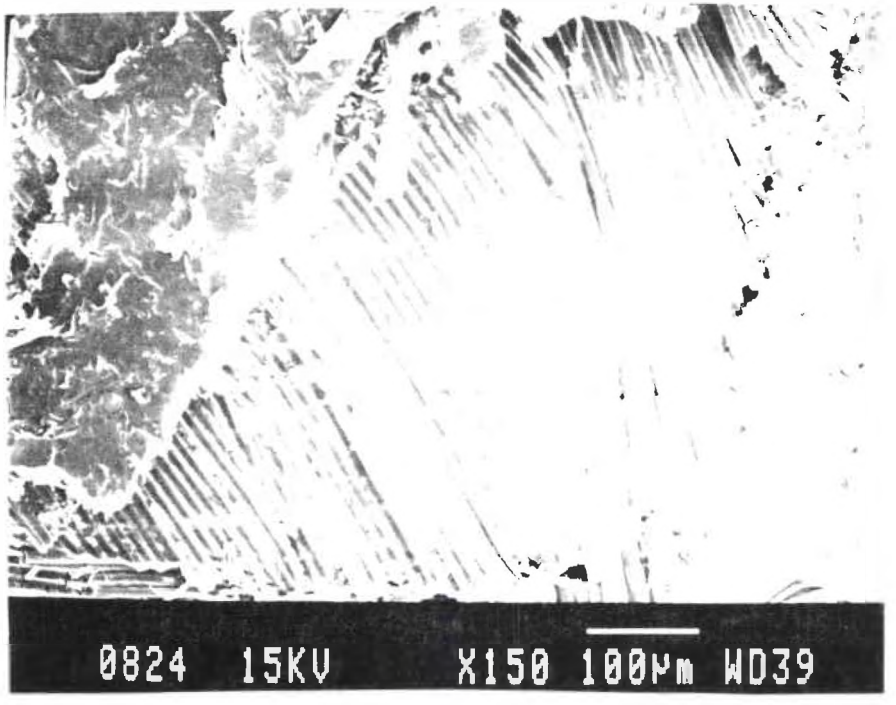

Figure 34. Matrix cracking and broken fibers on an unaged compression soecimen (x150).

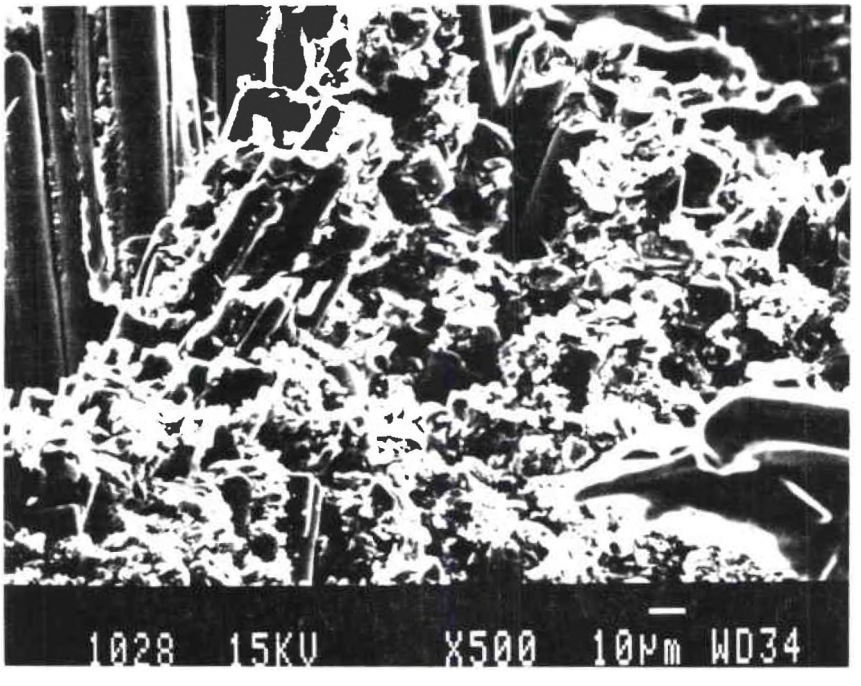

Figure 35. Matrix cracking and debris as well as fiber cracking, unaged compression specimen (x500).

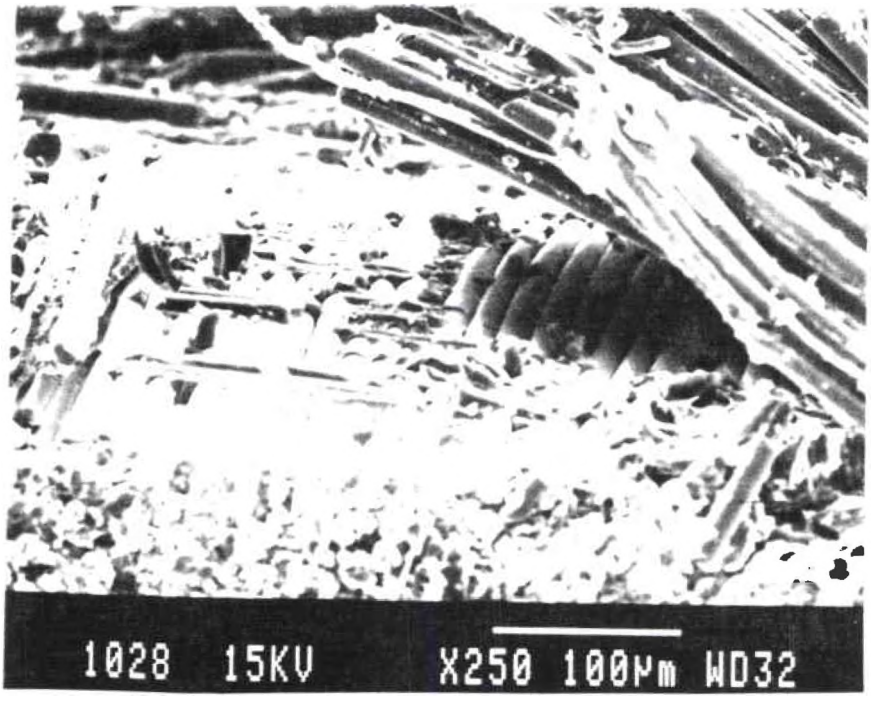

Figure 36. Bent fibers and severe fiber and matrix cracking, unaged compression specimen (x250).

(1) Microbuckling of fibers,
(2) Broken fibers,
(3) Matrix cracking,
(4) Debris on fracture surface,
(5) Chop marks on fiber fracture surface, and
(6) Bent fibers.

Thermally-Aged Compression

Figures 37 and 38 illustrate most of the characteristics of the fracture surfaces of the thermally-aged specimens. No major differences between these specimens and the unaged samples are noted, which correlates with the data obtained from mechanical testing that indicated no changes in compressive strength. Chop marks on specific fractured fibers are illustrated in Figure 38.

In summary fracture surface characteristics of thermally-aged specimens include the following:

(1) Microbuckling of fibers,
(2) Broken fibers,
(3) Debris on fracture surface,
(4) Chop marks on fiber fracture surface, and
(5) Matrix cracking.

Humidity-Aged Compression

Very similar characteristics have been noted for the compression humidity-aged fracture surfaces with respect to the unaged and thermally-aged samples. However larger amounts of matrix debris and matrix cracking, which is an indication of matrix degradation probably due to moisture, were observed. Figure 39 illustrates this effect, as well as some of the other characteristics.

In summary, typical fracture surface characteristics of humidity-aged specimens tested in compression include:

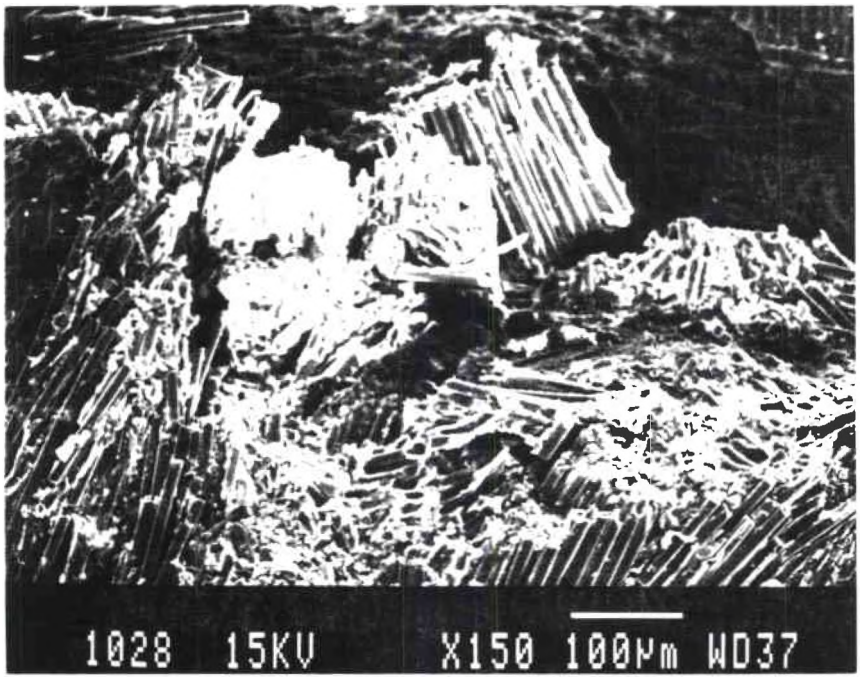

Figure 37. General overview of a thermally-aged compression specimen (x150).

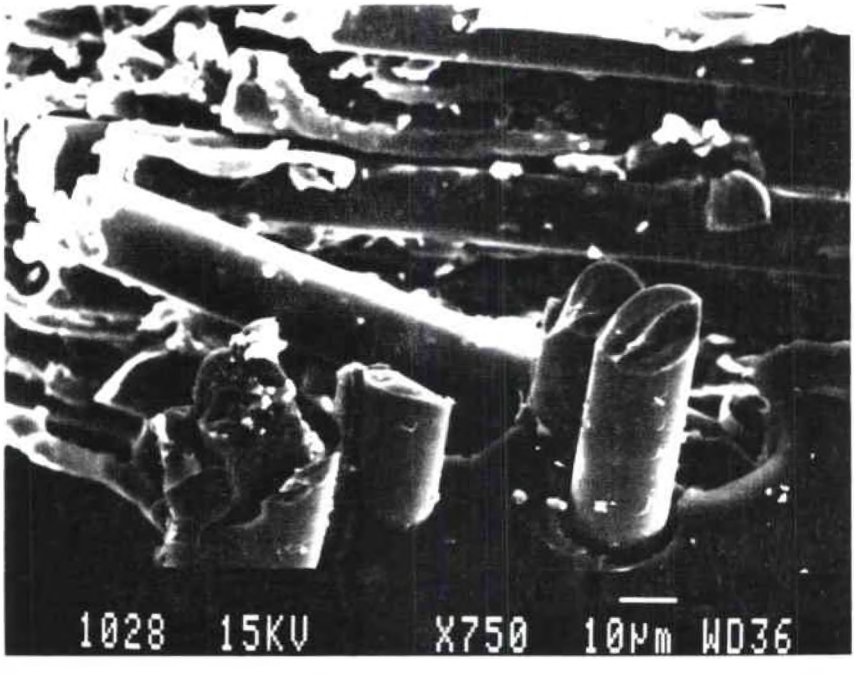

Figure 38. Fiber tip chop marks and matrix cracking debris, compression thermally-aged specimen (x750).

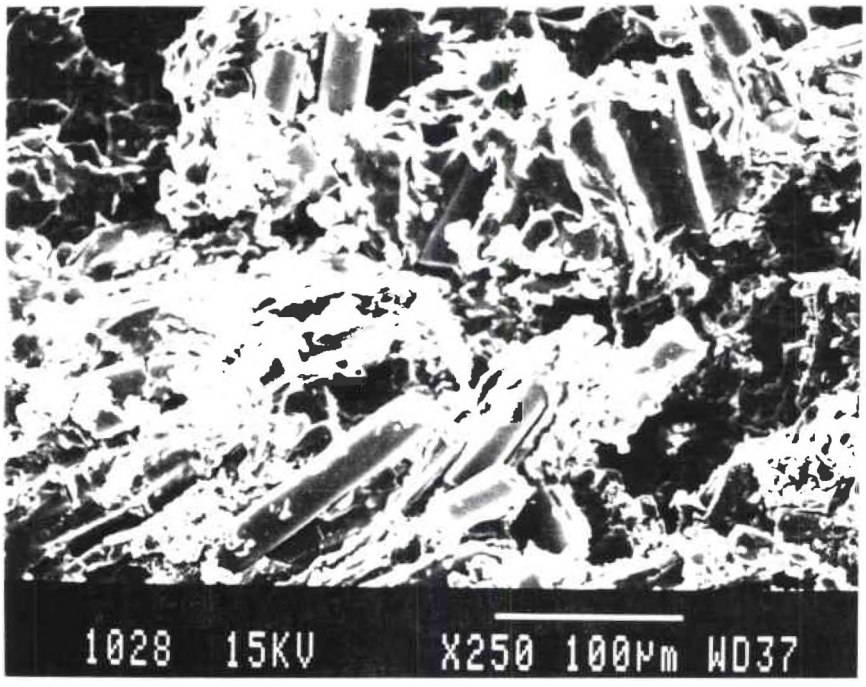

Figure 39. Severe matrix cracking and broken fibers on a humidity-aged compression specimen (x250).

(1) Microbuckling of fibers,
(2) Broken fibers,
(3) Matrix cracking,
(4) Debris on fracture surface, and
(5) Chop marks on fiber fracture surfaces.

Unaged Flexure

Typical failure locations for the flexure specimens are illustrated in Figures 40 and 41. Different fracture characteristics were observed for 0 or 90 and 45 degrees oriented specimens. The failure path for the 0 or 90 degrees oriented specimens followed a straight path normal to the length of the specimen. In contrast, in the 45 degrees oriented specimens the crack initiates as a straight line at a 45 degree angle with respect to the length, continues perpendicular to the length for approximately 0.3 in., and then runs at a -45 degree angle until it reaches the side of the specimen.

Fiber pullout indicating fiber-matrix debonding, and matrix cracking are both observed in Figure 42. Although the matrix channels left by the fibers which have been pulled out are fairly clean a small amount of debris has been observed. Figure 43 shows a fiber bundle from the compression side of the specimen, and a large area of matrix where cleavage is observed. The fiber radials are illustrated in Figure 44. Figures 45 and 46 illustrate the difference in morphology of the compression and tension sides of a flexure specimen. On the compression side, larger amounts of debris are noted as well as matrix cracking. More fiber-matrix adhesion is also observed.

In summary, characteristics of the fracture surface of specimens tested in flexure include the following:

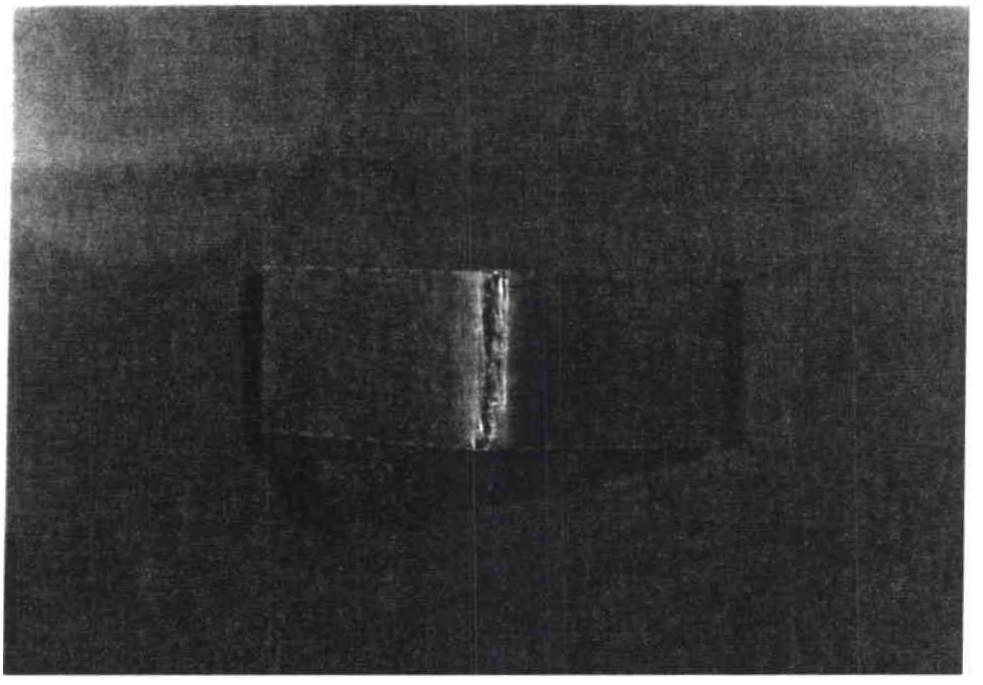

Figure 40. Fractured flexural specimen, (0°-90° layout orientation).

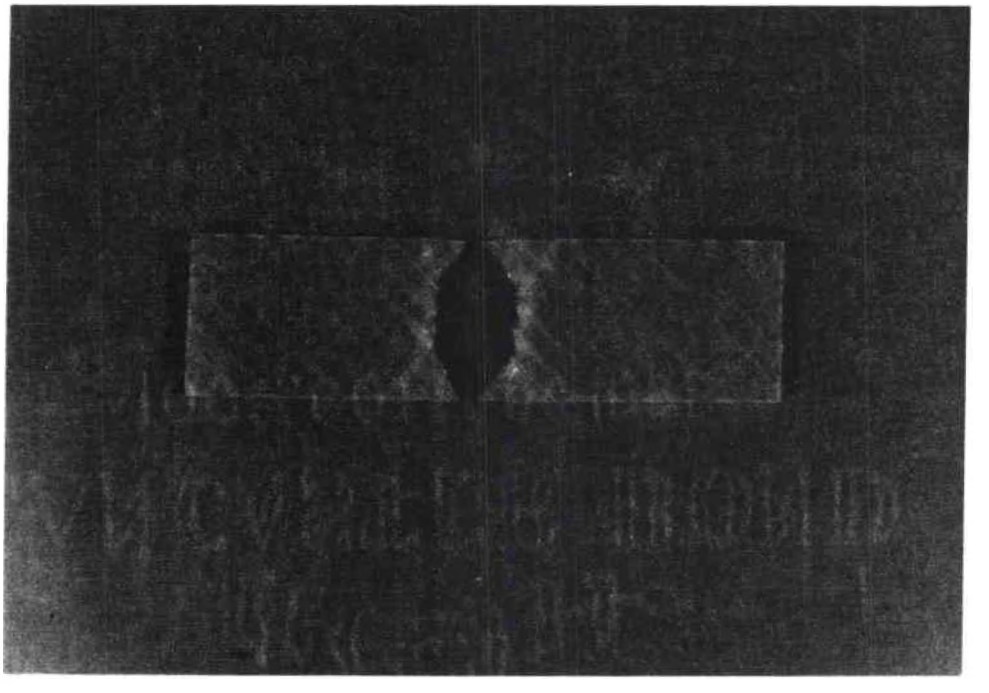

Figure 41. Fractured flexural specimen, (45 degree layout orientation).

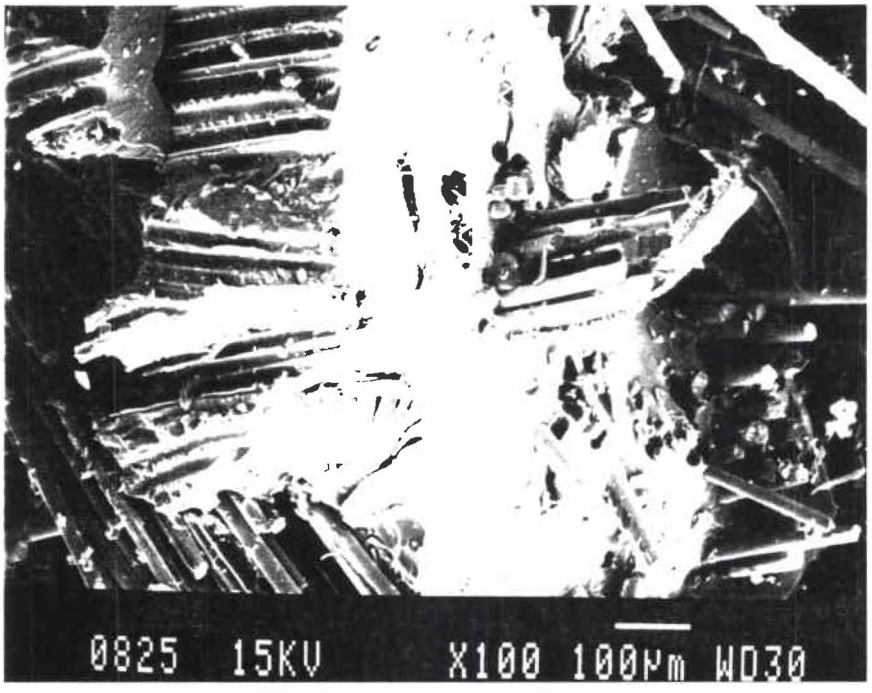

Figure 42. Fiber pullout, matrix cracking and matrix-fiber debonding (x100).

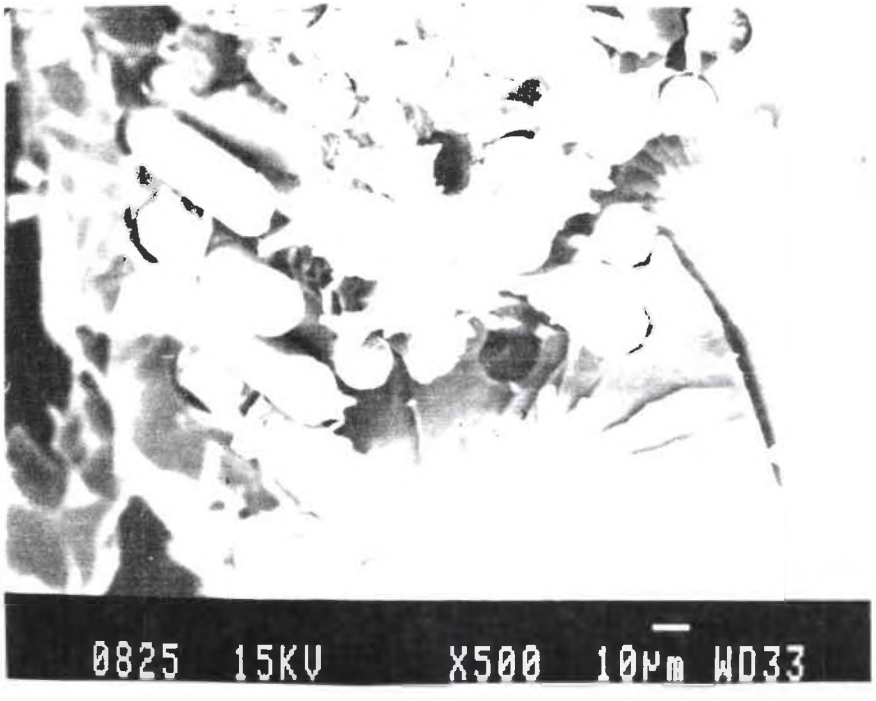

Figure 43. Fiber bundle on the compressive side of a flexure specimen (x500).

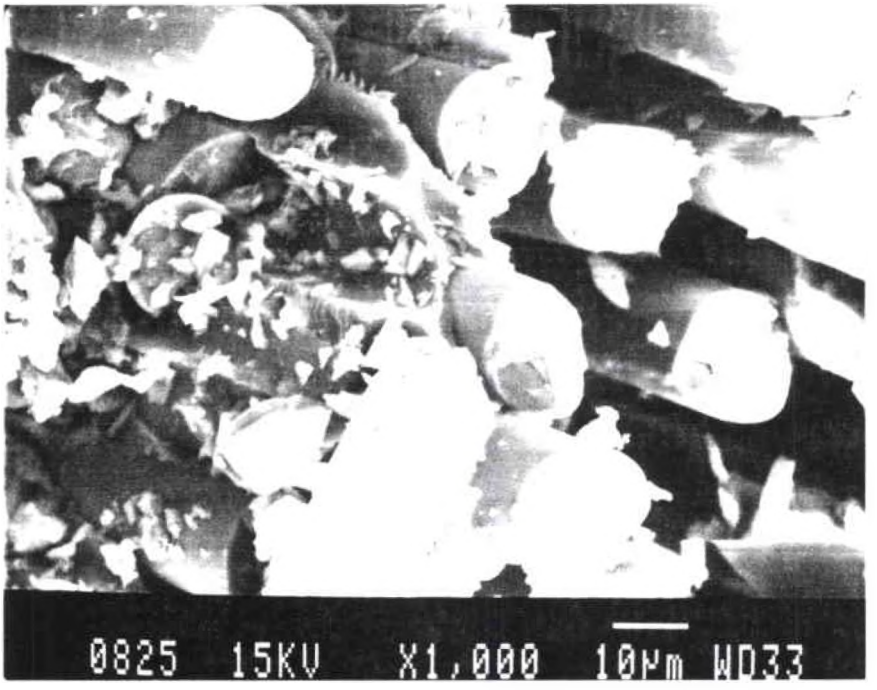

Figure 44. Debris and fiber on the tensile side of a flexure specimen (x1000).

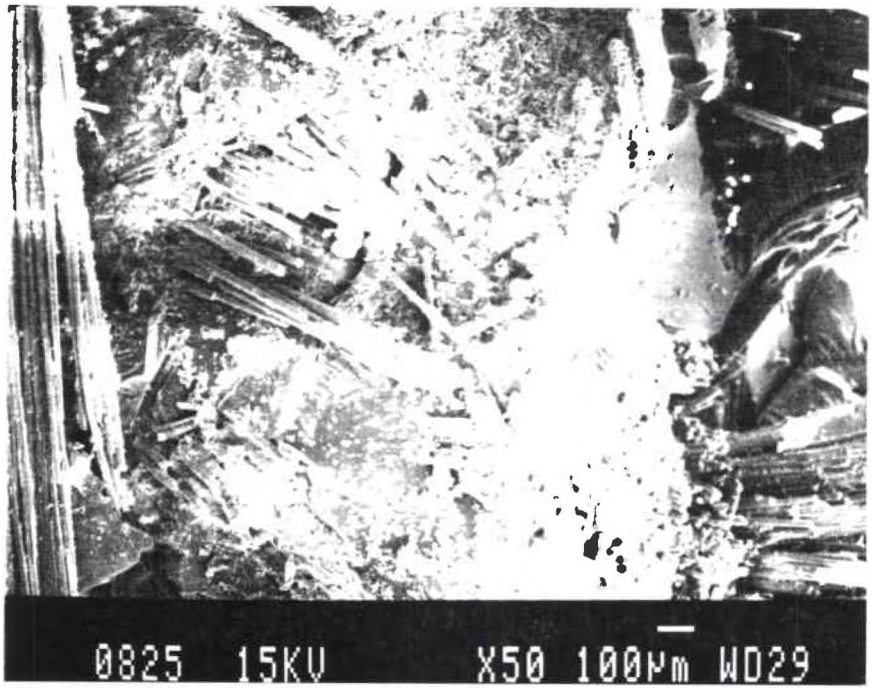

Figure 45. Compressive side of flexure specimen (x50).

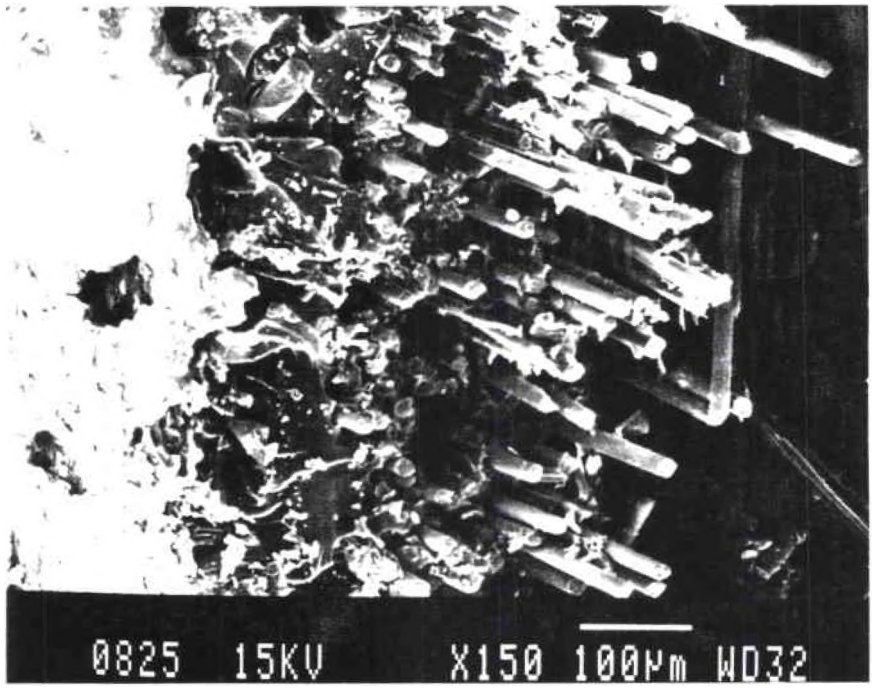

Figure 46. Tensile side of a flexure specimen (x150).

(1) Fiber pullout,
(2) Matrix cracking (cleavage),
(3) Broken fibers,
(4) Radial patterns on the fractured fiber surface,
(5) River patterns in matrix fracture surfaces, and
(6) Debris.

Thermally-aged Flexure

An increase in the fiber-matrix adhesion is a characteristic of the flexure specimens. Figure 47 shows the radials on the fracture surface of a fiber on the tension side of a flexure specimen aged at 180 °F for on week. Figure 48 illustrates a fiber from the compression side of the same flexure specimen, where chop marks appeared to be characteristic of the fiber fracture surface. River patterns on the matrix fracture surface and some void areas are shown in Figure 49. Some bent fibers with a small amount of fiber-matrix adhesion are seen in Figure 50 at the center area of the aged flexure specimen. Hackles normal to the fiber direction as seen in Figure 51 have been observed in the compression side of an aged specimen. In Figure 52 the large amount of matrix adhering to the fiber indicates the increase in fiber-matrix adhesion when the specimen has been aged for 1 month at 250 °F. Chop marks characteristic of compression failures were seen on the fractured fibers on the compression side of a flexure specimen (Figures 53 and 54). Debris in the center area of a flexure specimen aged at 250 °F for one week and is documented in Figure 55. Bent fibers, matrix cracking and debris are illustrated in Figures 56 and 57, both taken from the compression sides of specimens aged at 250 °F and 180 °F for 1 week, respectively. No major differences have been noted between specimens aged for a week or

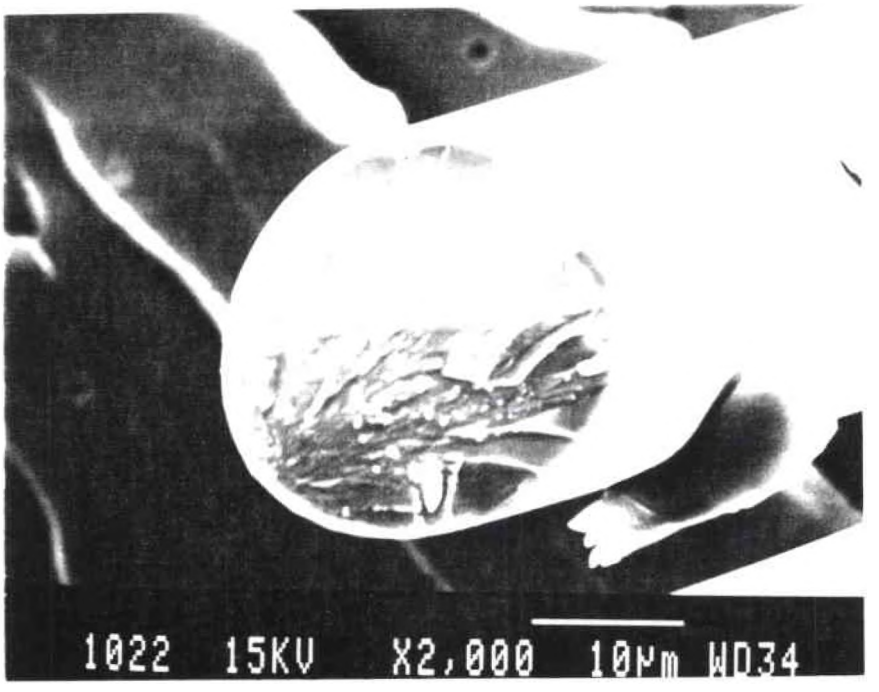

Figure 47. Radials on the tensile side fiber of a thermally-aged flexure specimen (x2000).

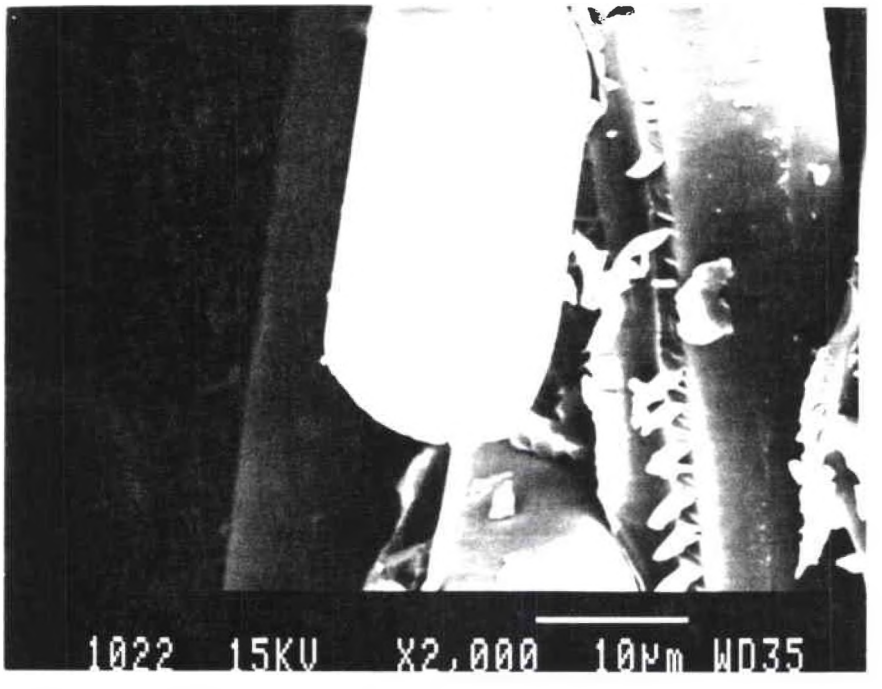

Figure 48. Compressive side of a thermally-aged flexure specimen (x2000).

Figure 49. Tensile side of a thermally-aged flexure specimen (x500).

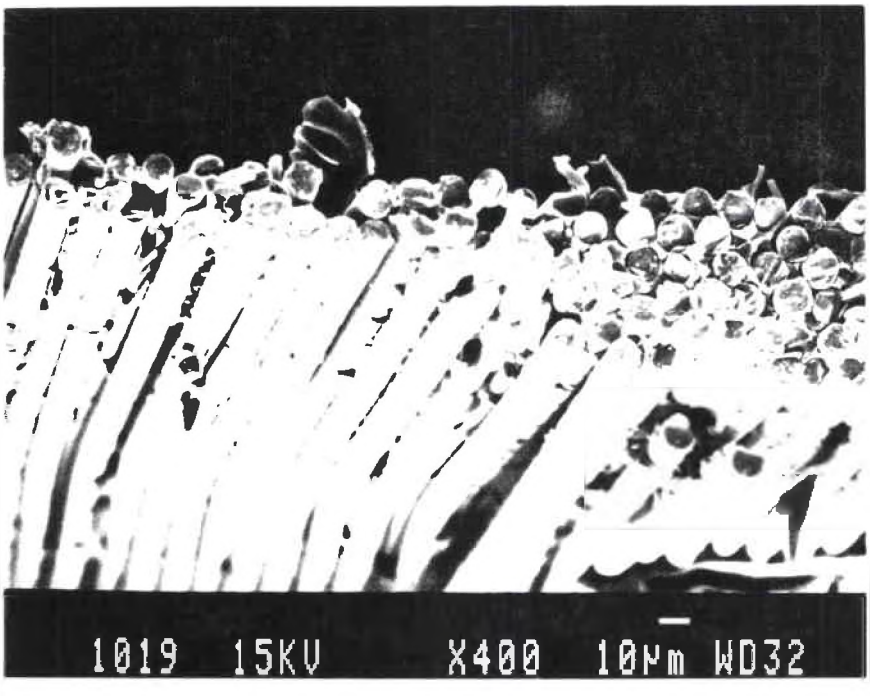

Figure 50. Compressive side of thermally-aged flexure specimen (x400).

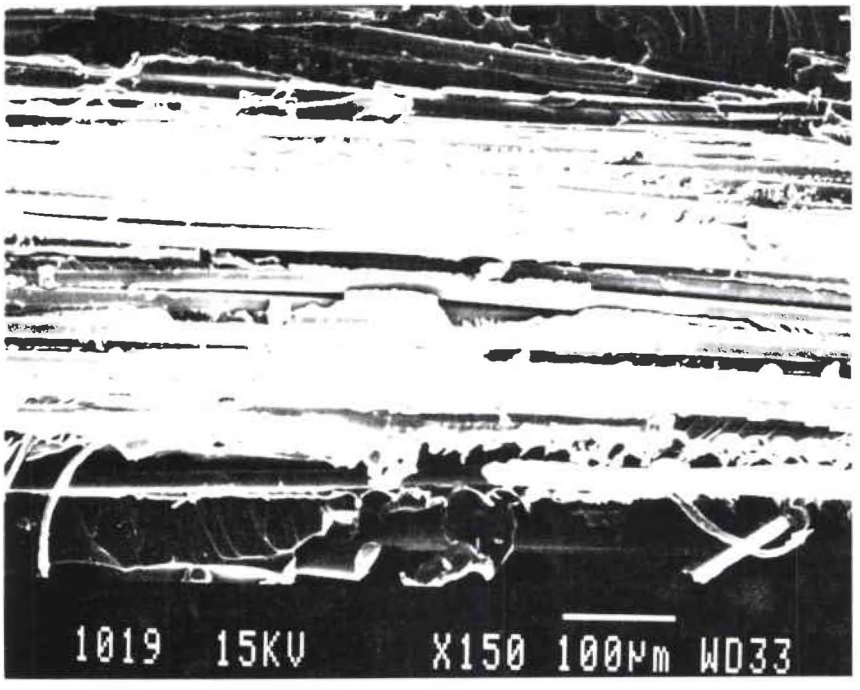

Figure 51. Hackles appeared in the matrix between fibers at the compressive side of a thermally-aged flexure specimen (x150).

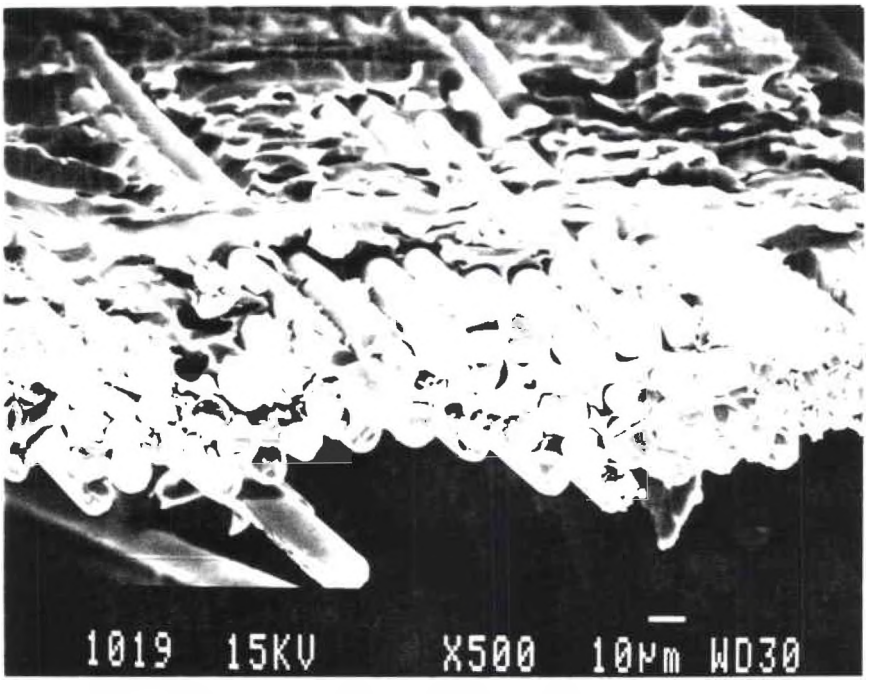

Figure 52. Chop marks on fiber tips and fiber-matrix adhesions on a thermally-aged flexure specimen compressive side (x500).

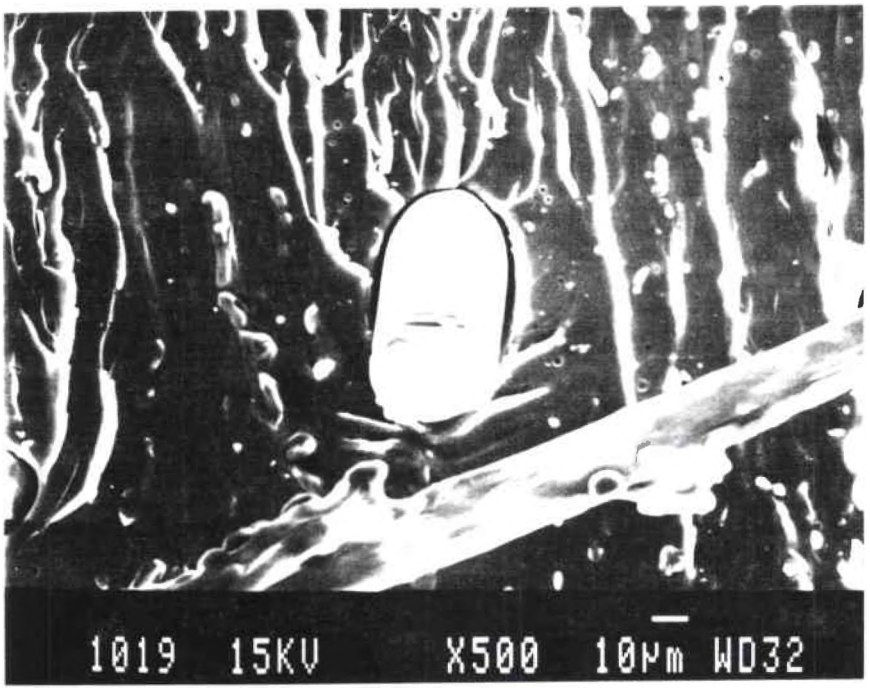

Figure 53. Chop marks on the fiber tip of thermally-aged flexure specimen compressive side (x500).

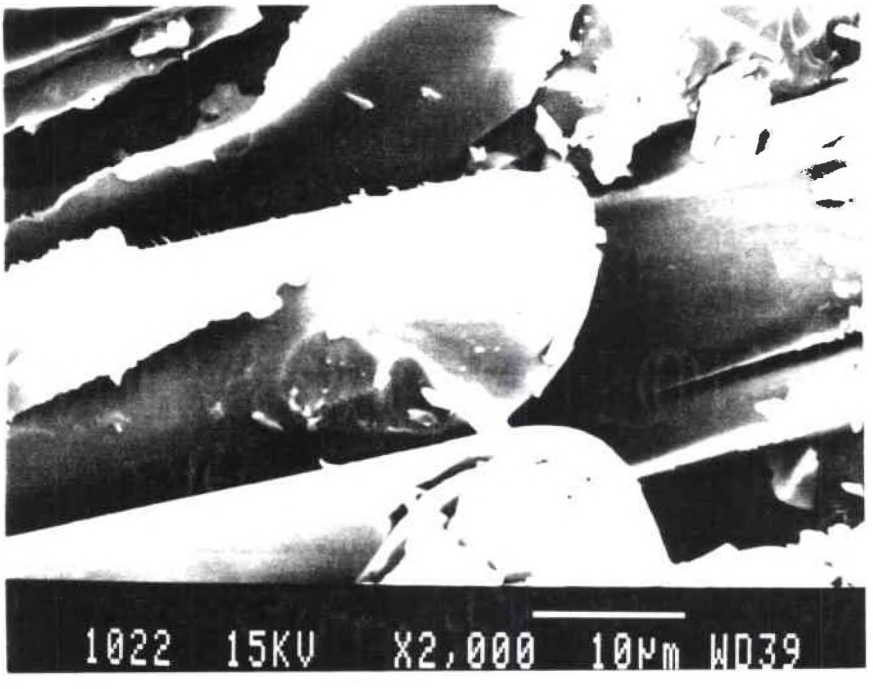

Figure 54. Characteristic chop marks on compressive side of a thermally-aged flexure specimen (x2000).

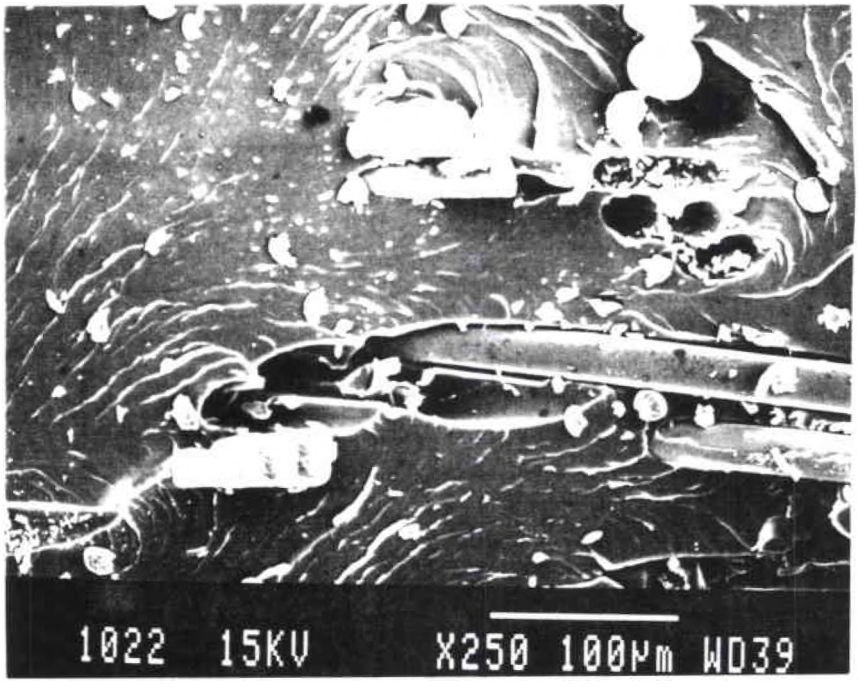

Figure 55. Matrix debris, center area of thermally-aged flexure specimen (x250).

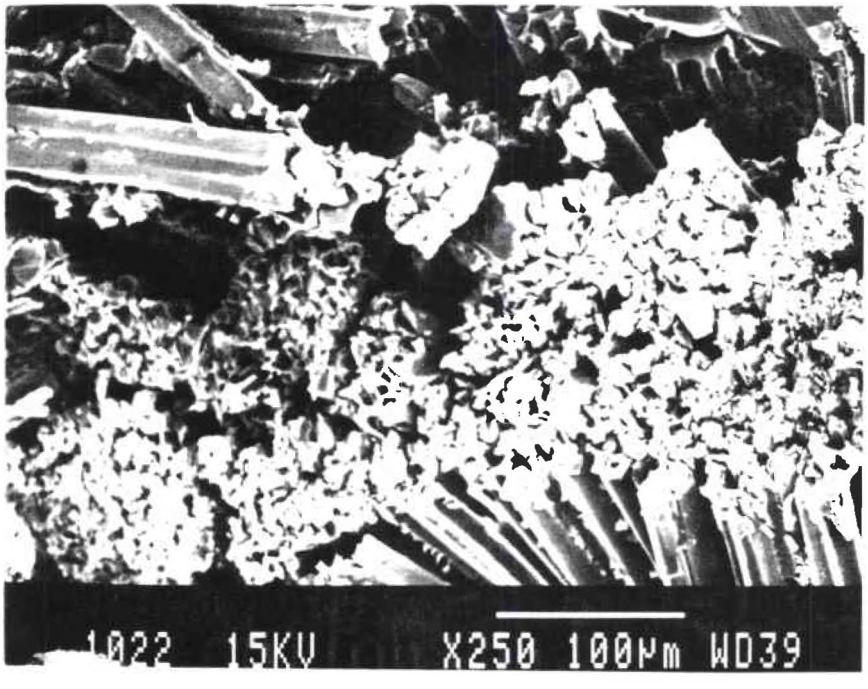

Figure 56. Bent fibers, matrix cracking, and debris on compressive side of thermally-aged flexure specimen (x250).

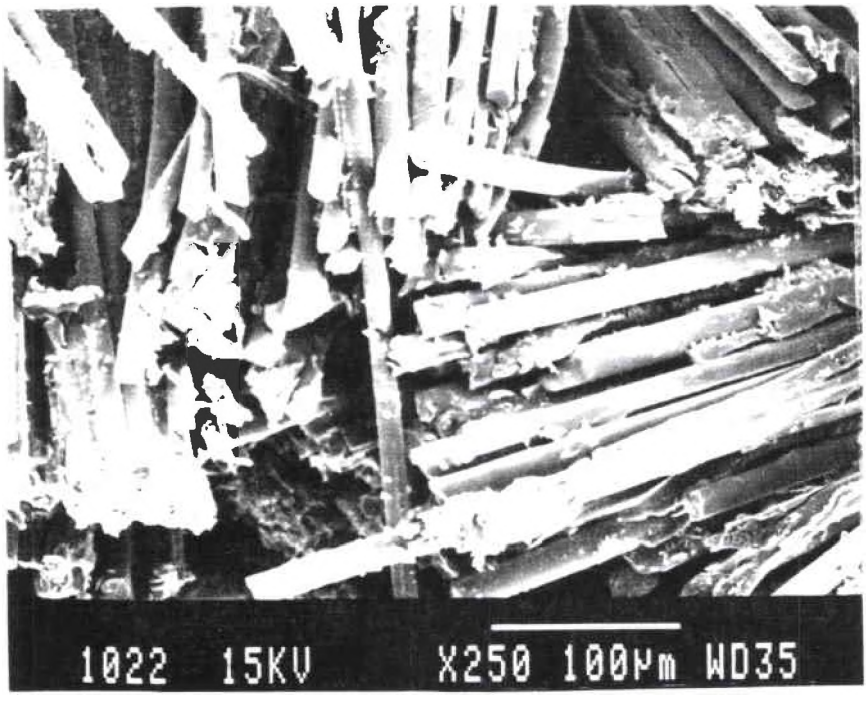

Figure 57. Compressive side of thermally-aged flexure specimen (x250).

longer at either temperatures of 180° or 250 °F. Also, specimens aged for only one day do not show any differences in morphology with respect to the unaged specimens.

In summary, the characteristics of the fracture surface observed on the aged flexure specimens include the following:

(1) Fiber pullout,
(2) Matrix cracking,
(3) Broken fibers,
(4) Debris,
(5) Radial patterns on the fiber fracture surface on the tensile side.
(6) River patterns on matrix fracture surfaces, and
(7) Chop marks on the fiber tips on the compression side.

Humidity-Aged Flexure

Figure 58 illustrates river patterns on matrix areas located at the outer surfaces on the compression side of the specimen. In addition, a small amount of fiber pullout was observed, but the majority of the fibers were severely fractured. Characteristic fiber fracture surfaces of the tension side and compression side are shown in Figures 59 and 60, respectively. Large amounts of debris and chop marks are illustrated in Figure 59, while radials were seen in Figure 60.

In summary, the characteristics of the fracture surface observed on the humidity-aged flexure specimens include:

(1) Broken fibers,
(2) Fiber pullout,
(3) Radials on fiber surface on the tension side,
(4) Chop marks on fiber tips of the compression side,
(5) Debris on fracture surface, and
(6) River patterns on matrix fracture surfaces.

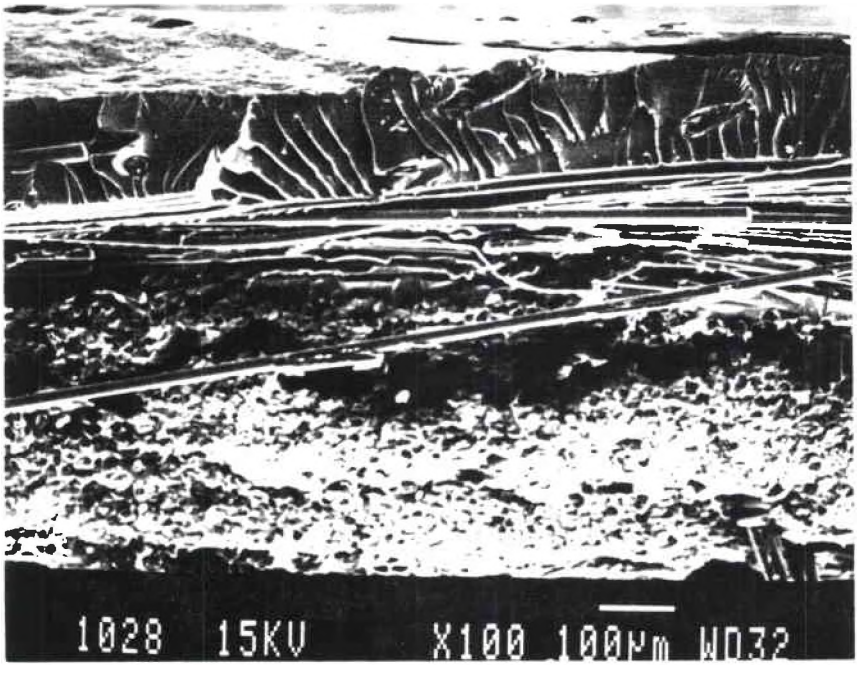

Figure 58. Compressive side of a humidity-aged flexure specimen (x100).

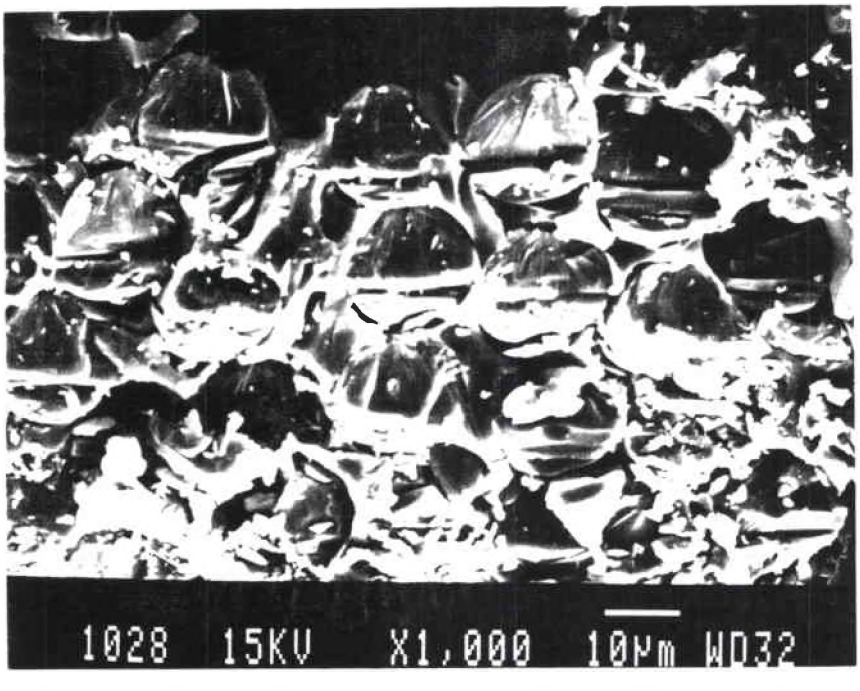

Figure 59. Compressive side of a humidity-aged flexure specimen (x1000).

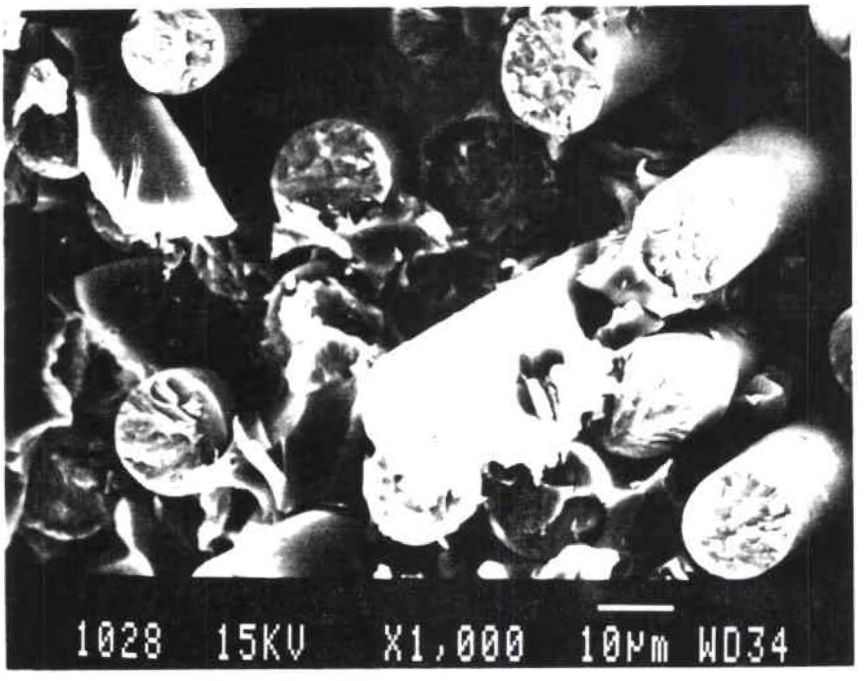

Figure 60. Radials on the fiber tips of a humidity-aged flexure specimen tensile side (x1000).

Unaged In-plane Shear

Typical failure locations for the in-plane shear specimens are shown in Figures 61 and 62. Similar crack propagation characteristics were noted for both the 45 degree oriented specimens, as well as the 0 and 90 degree oriented specimens. The crack propagated along the notch.

Figure 63 illustrates a general low magnification overview of the fracture surface, where fiber bundles running in random directions are observed. Fiber pullout and matrix cracking are illustrated in Figure 64. Hackles occurring in the matrix areas between fibers pulled out in the load direction are illustrated in Figure 65. It has been noted that the shear fractures left very smooth matrix channels resulting from fiber pullout.

In summary, typical fracture surface characteristics of specimens tested in shear include:

(1) Fiber pullout,
(2) Fiber-matrix debonding, and
(3) Matrix cracking.

Thermally-Aged In-plane Shear

No major changes in morphology have been found in the aged in-plane shear specimens with respect to the unaged specimens. Figure 66 illustrates similar characteristics as those observed for the unaged samples. This correlates with the data obtained from mechanical testing, which indicated no major changes in strength.

In summary, fracture surface characteristics of the thermally-aged in-plane shear specimens include:

(1) Fiber pullout,

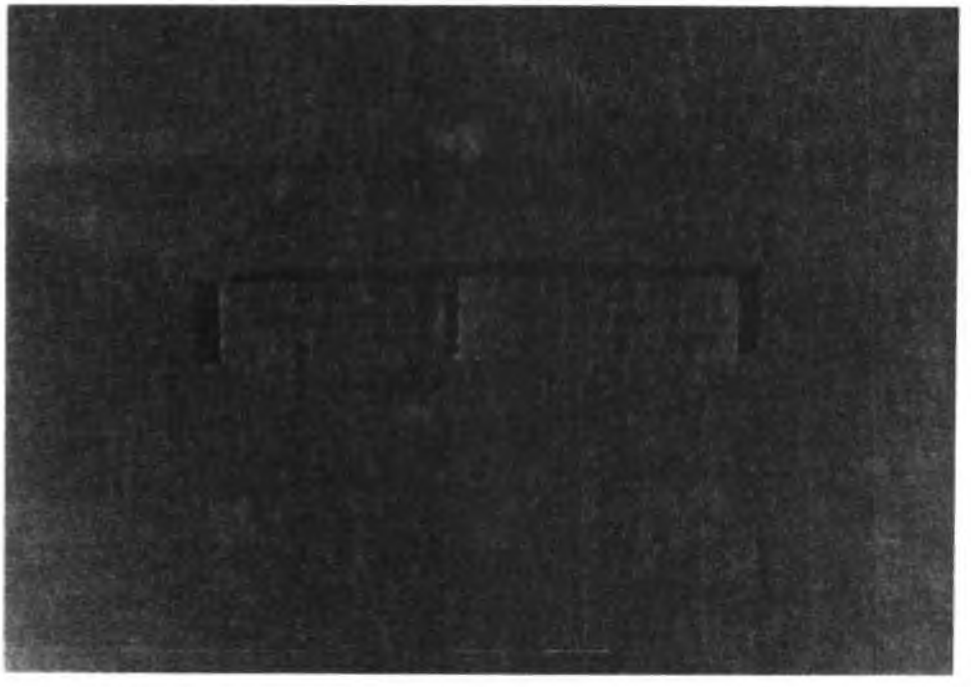

Figure 61. Top view of a fracture in-plane shear specimen.

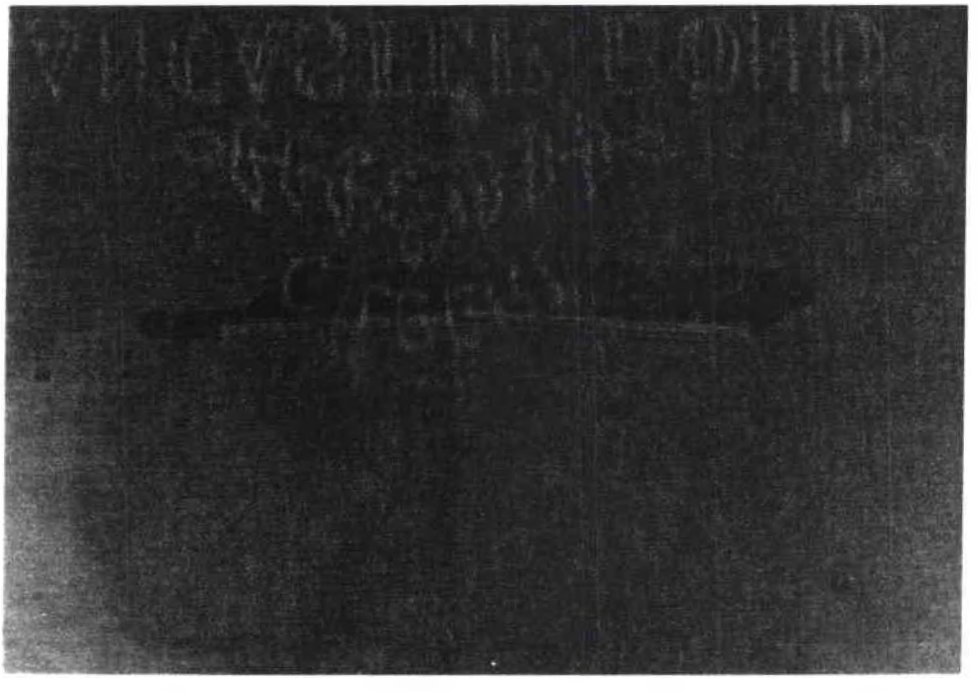

Figure 62. Side view of a fractured in-plane shear specimen.

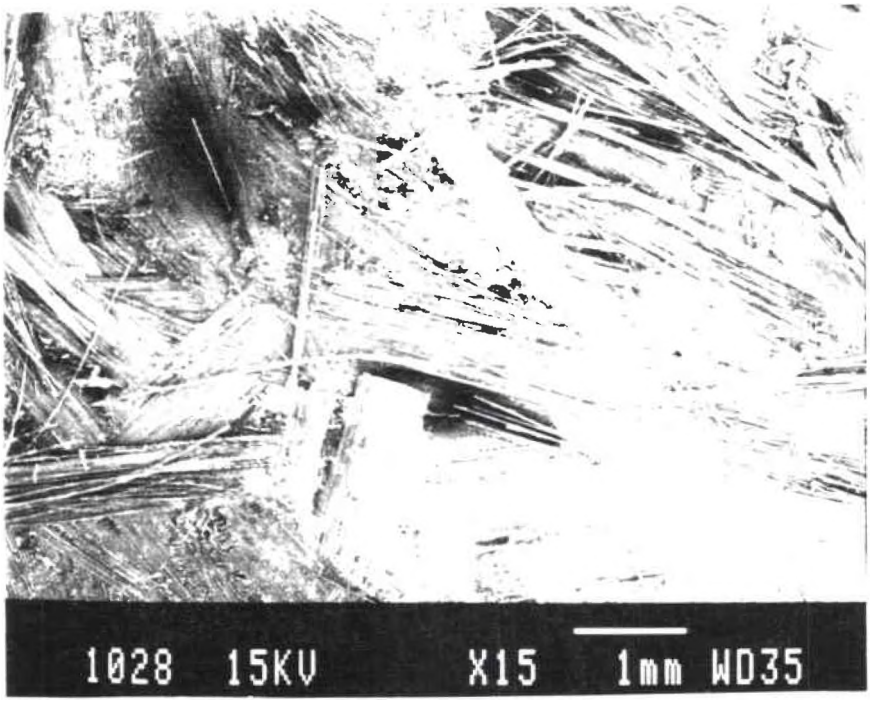

Figure 63. Overview of the fracture surface of an unaged shear specimen (x15).

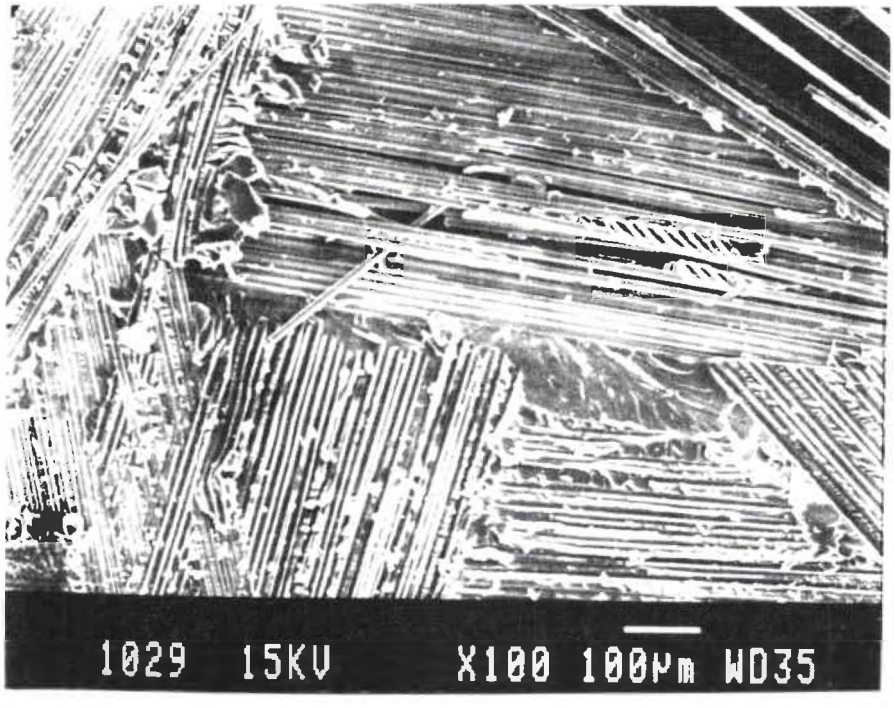

Figure 64. Matrix cracking and fiber pullout on an unaged shear specimen (x100).

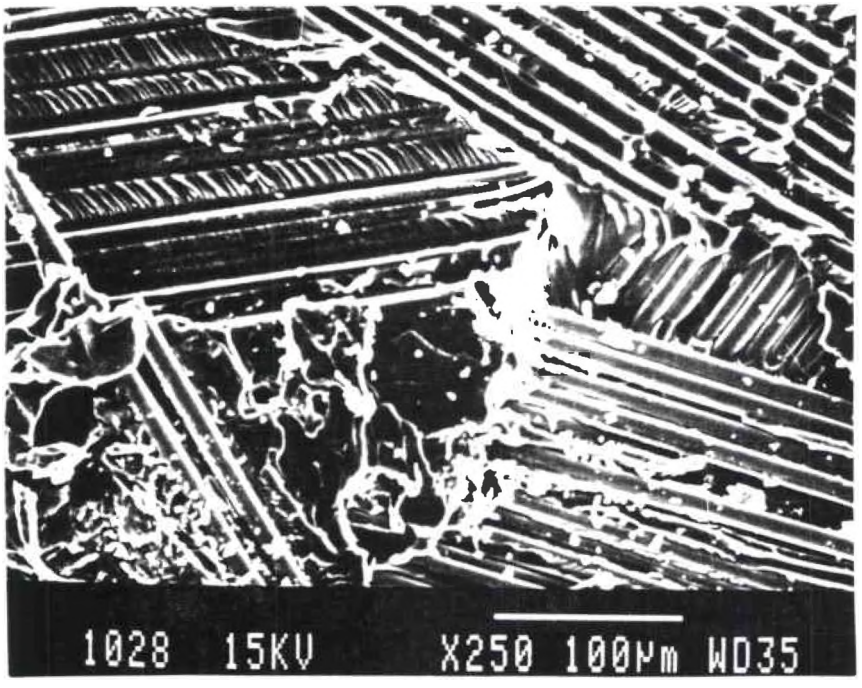

Figure 65. Hackles and matrix cracking, unaged shear specimen (x250).

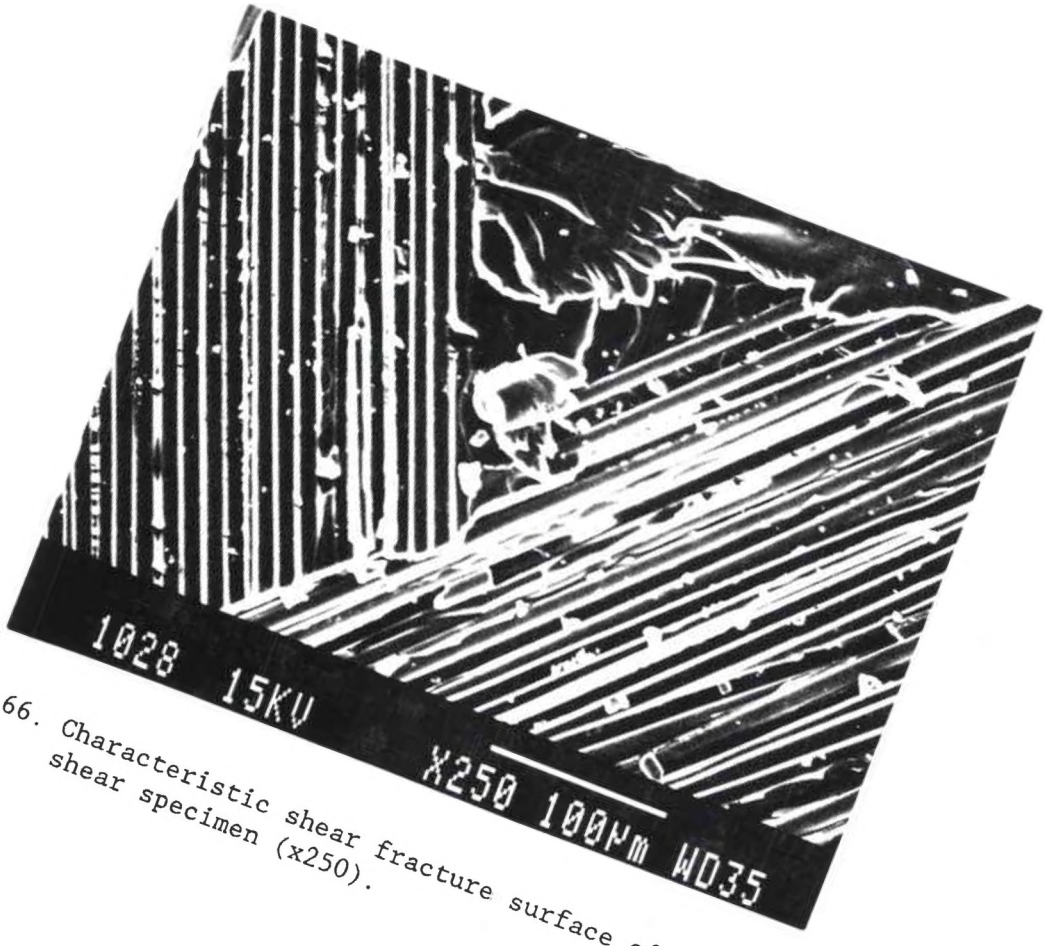

Figure 66. Characteristic shear fracture surface of thermally-aged shear specimen (x250).

(2) Matrix cracking, and
(3) Fiber-matrix debonding.

Humidity-Aged In-Plane Shear

A low magnification photograph of the fracture surface is shown in Figure 67, where loose fibers are observed. Figure 68 illustrates that the specimen failed in the 0° and 90° woven layer. Fiber pullout, as well as fiber-matrix debonding are illustrated in Figures 68 and 69. Notice the smoothness of the matrix channels in Figure 69, which indicates a very poor fiber-matrix interface, probably due to the degrading effect of humidity.

In summary, typical fracture characteristics of humidity-aged specimens tested in shear include:

(1) Fiber pullout,
(2) Matrix cracking, and
(3) Fiber-matrix debonding.

Tension-Compression Fatigue

A typical failure location can be observed in Figure 70. The crack propagated normal to the load direction. In addition, fiber pullout can also be observed.

Straight-sided tension-compression fatigue specimens were tested at room temperature for the sole purpose of providing fracture surfaces. No aging studies were conducted on these specimens.

A general overview of the fatigue fracture surface is presented in Figure 71. Already at low magnification matrix debris can be observed. Figure 72 illustrates the presence of river patterns in the matrix surrounding holes resulting from fiber pullout. Unusually high concentrations of porosity are illustrated in Figure 73, as well as

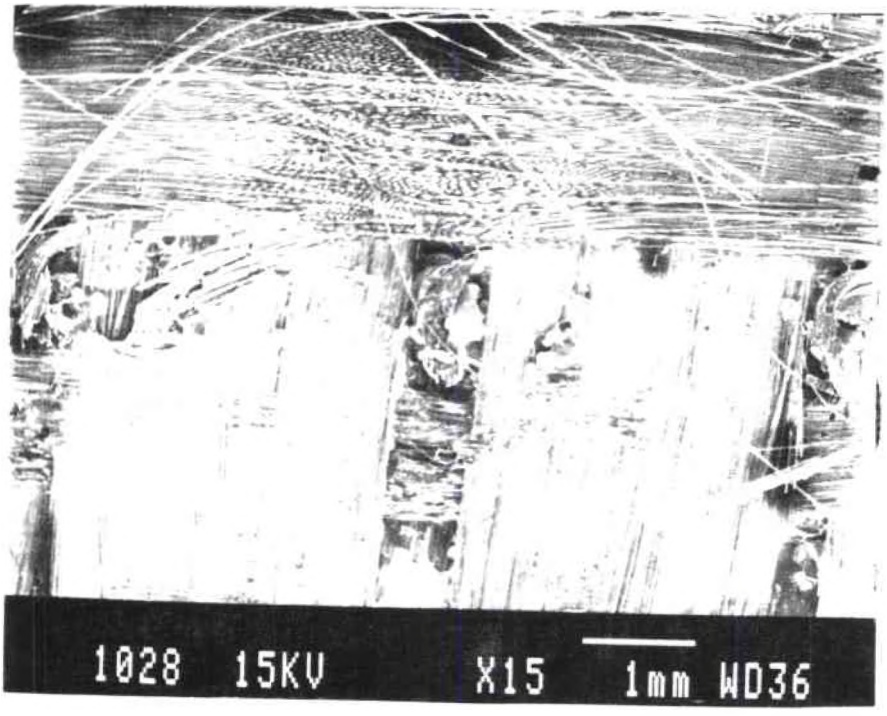

Figure 67. Fracture surface overview at low magnification of a humidity-aged shear specimen (x15).

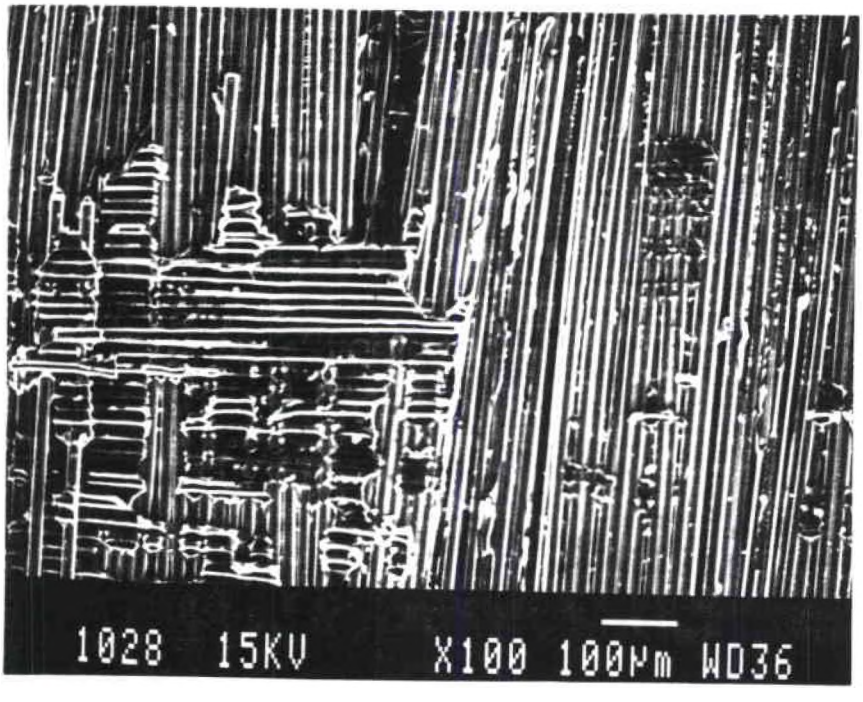

Figure 68. Fiber pullout, hackles, and fiber-matrix debonding (x100).

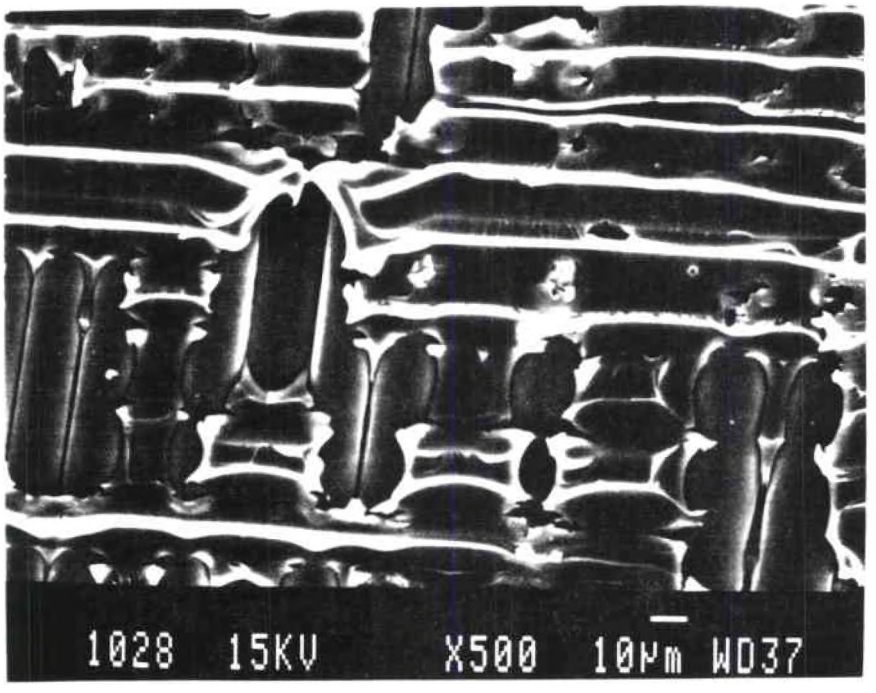

Figure 69. Smooth matrix channels, humidity-aged shear specimen (x500).

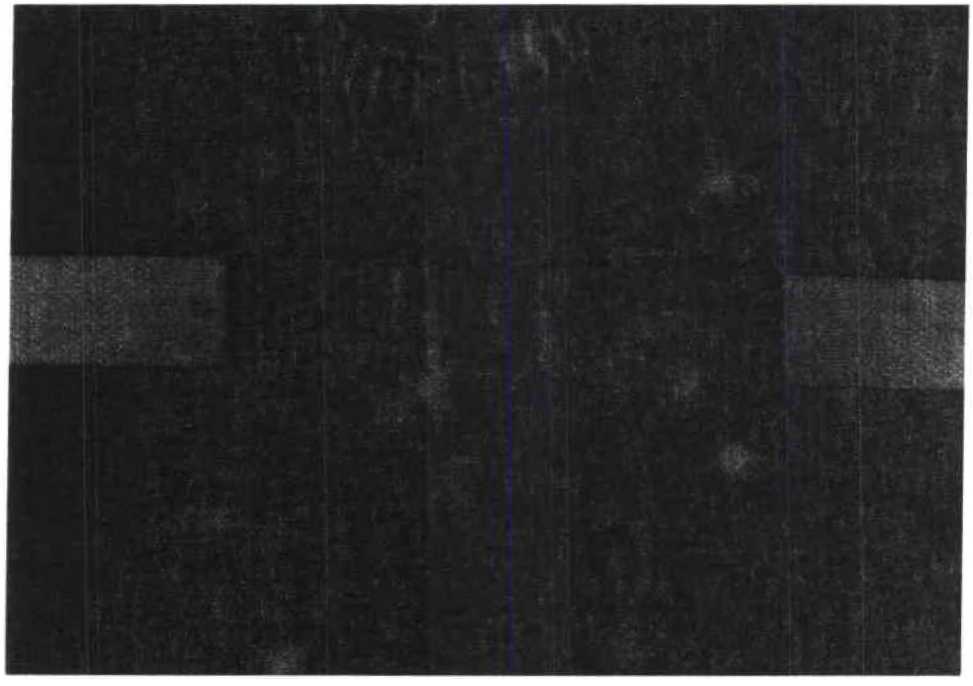

Figure 70. Tension-compression fatigue fractured specimen.

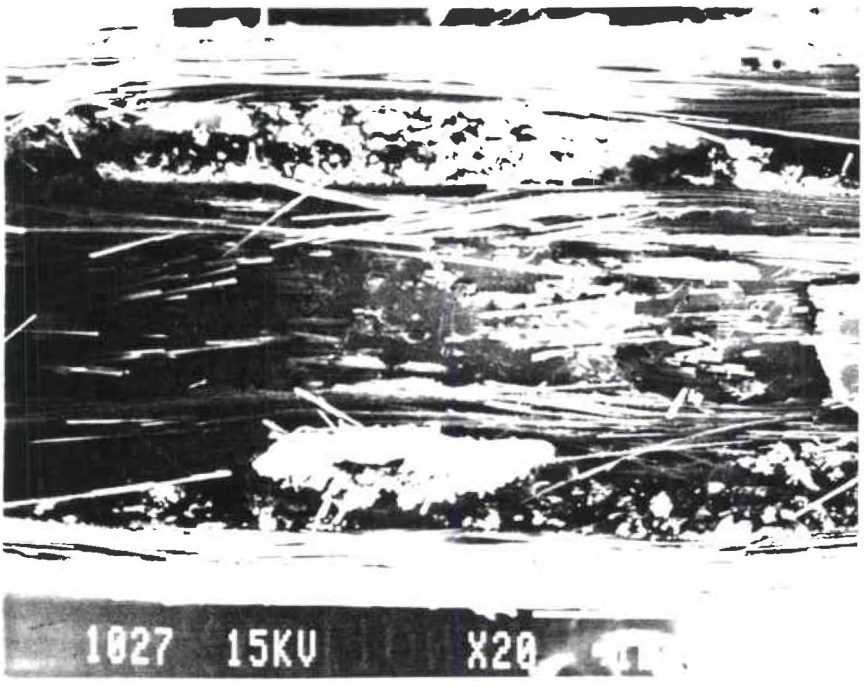

Figure 71. Tension-compression fatigue specimen (x20).

Figure 72. Tension-compression fatigue specimen (x200).

Figure 73. Tension-compression fatigue specimen (x1000).

matrix cracking and debris. Hackles in the matrix are illustrated in Figure 74.

In summary, fracture surface characteristics of the tension-compression fatigue specimens include:

(1) Fiber pullout,
(2) Fiber matrix debonding,
(3) Matrix cracking,
(4) Debris,
(5) Hackles in matrix areas between fibers, and
(6) River patterns in the matrix.

Flexural Fatigue

Figure 75 shows a photograph of the fracture surface of a flexural fatigue sample. Fiber pullout is illustrated in Figures 76 and 77 for both the compression and tension sides, respectively. Notice that the matrix channels appear to be smoother in the tension side. River patterns and hackles are illustrated in Figure 78, showing the poor ductility of the matrix. Debris can be observed in the three latter photographs.

In summary, fracture surface characteristics of the flexural fatigue specimens include:

(1) Fiber pullout,
(2) River patterns in matrix fracture surface,
(3) Hackles, and
(4) Debris.

Impact

Fracture surfaces of the specimens impacted underwent macroscopic examination. The specimens impacted at -40 °F showed a larger internal damage area, while specimens impacted at room temperature

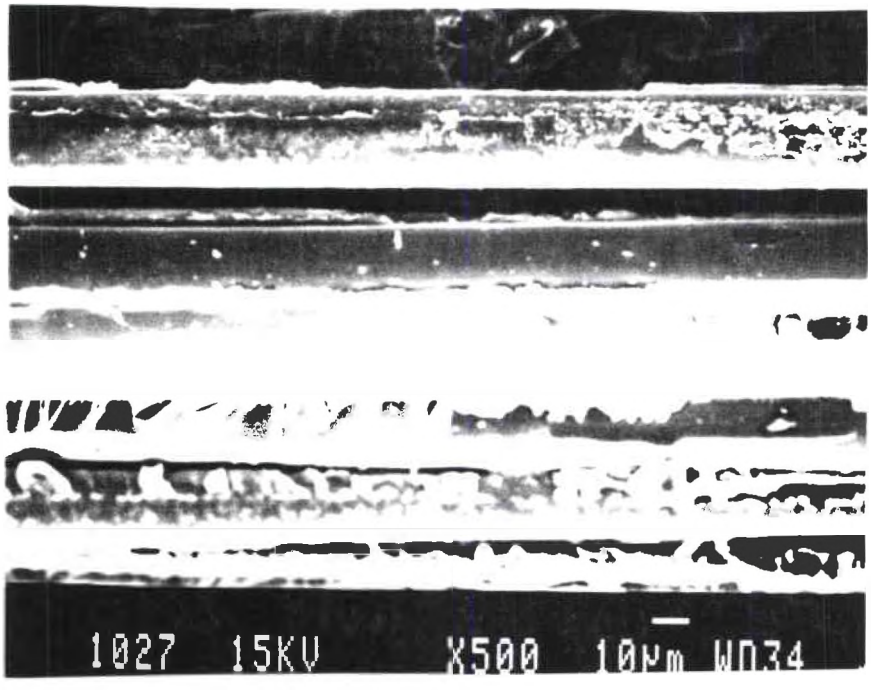

Figure 74. Tension-compression fatigue specimen (x500).

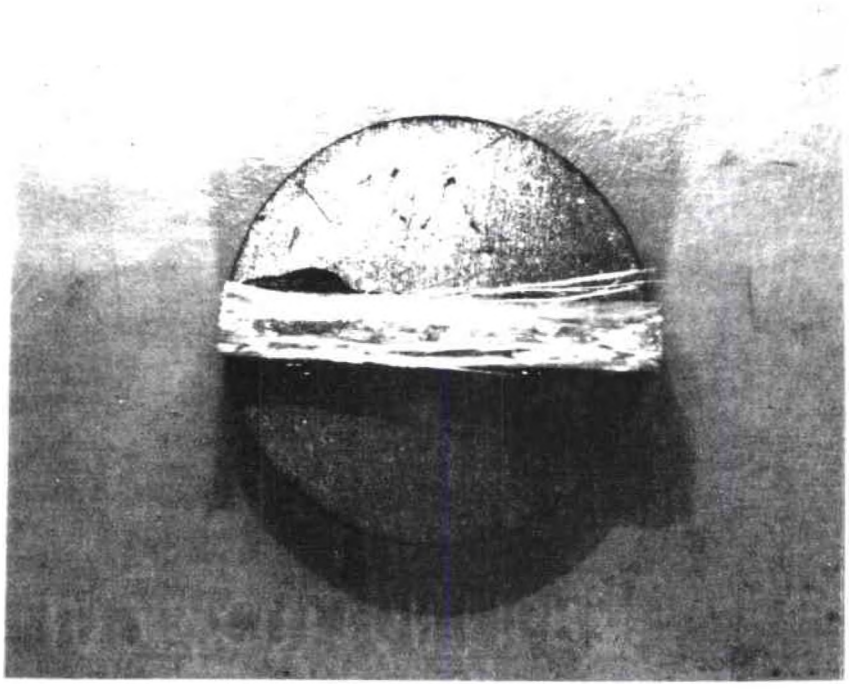

Figure 75. Flexural-fatigue fracture surface overview.

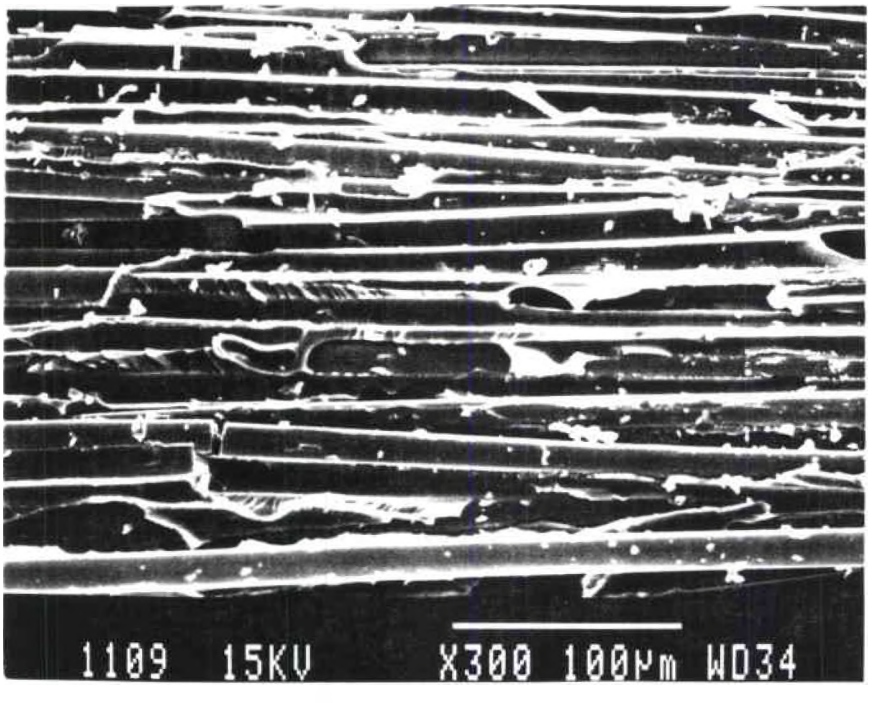

Figure 76. Flexural-fatigue specimen, compresion side (x300).

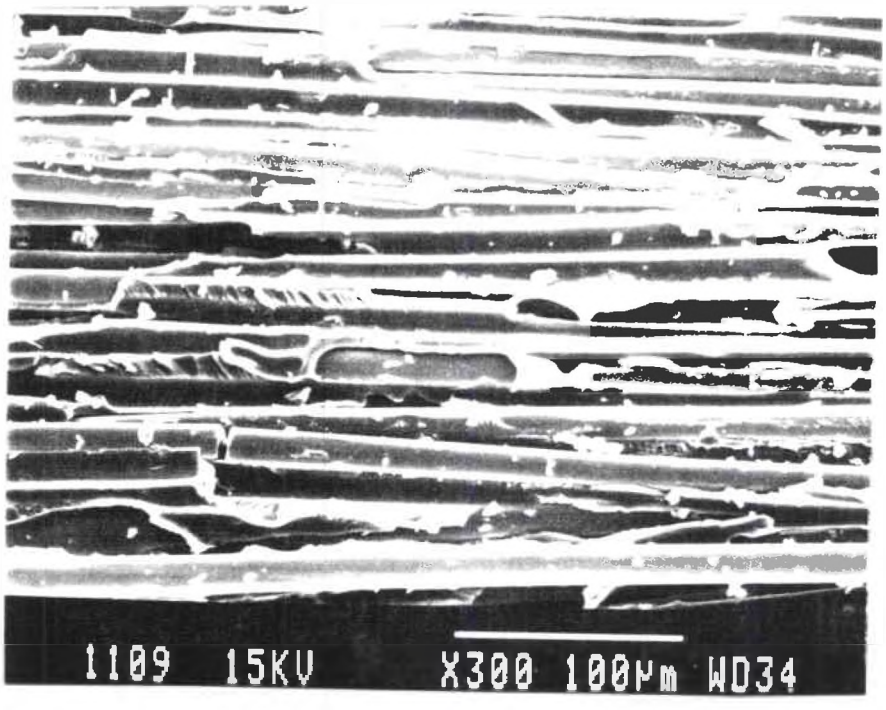

Figure 77. flexural-fatigue specimen, tensile side (x300).

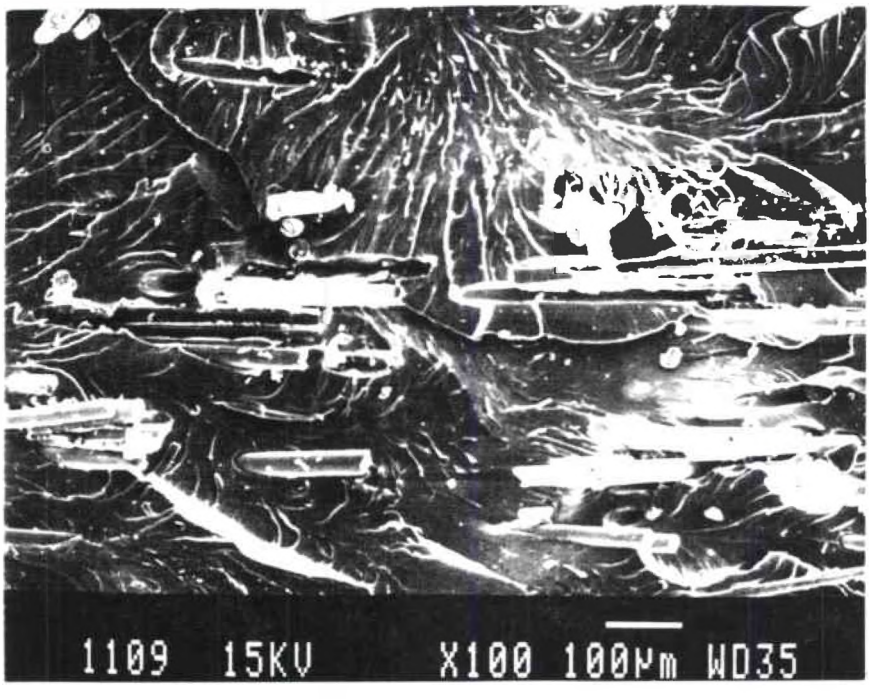

Figure 78. Flexural-fatigue specimen, center area (x300)

showed a smaller internal damage but more surface delamination and cracking. C-scans were taken of specimens see if the use of ultrasonic scanning would reveal any other damage not noted under visual inspection. The results of the C-scans showed the same type of damage as observed before. Figures 79 and 80 illustrate the C-scans, while Figures 81 through 84 illustrate the front and backs of the impacted specimens. Notice that specimens impacted from six feet presented larger amounts of debris and matrix cracking than the ones impacted from three feet.

X-Ray Photoelectron Spectroscopy (XPS)

X-ray photoelectron spectroscopy was considered to be a well developed technique to provide information about the chemical structure and binding energies of the different elements of the composite material under investigation. It was understood that some knowledge of the mechanisms that bind the different elements of the material were required. It was found that the coupling agent used to manufacture the RIM material was made by DOW Chemical and corresponds exactly to DOW Z-6040, a typical silane coupling agent commonly used in industry. Samples of the silane coupling agent were obtained to proceed with the investigation.

A flat glass sample was prepared by melting the glass fibers and polishing the surface of the resulting piece. The flat glass sample was soaked in a 1 % solution of the DOW Z-6040 silane at 60 °C three different times. Prior to each silane treatment, the sample was polished with diamond paste and ultrasonically cleaned in acetone. On two of the runs, data was collected at both 30° and 60° emission

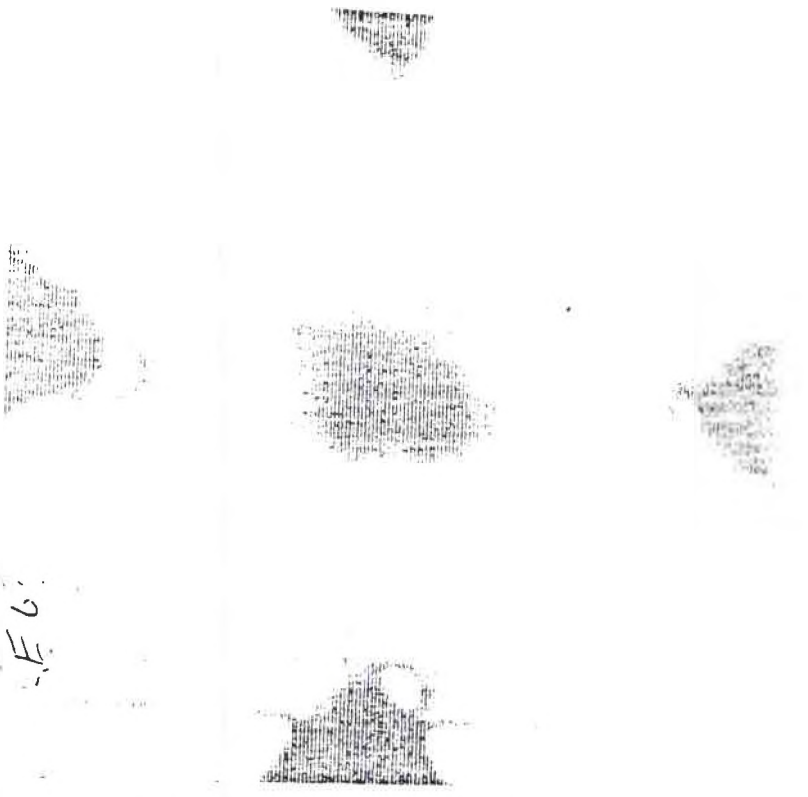

Figure 79. Ultrasonic C-scan.

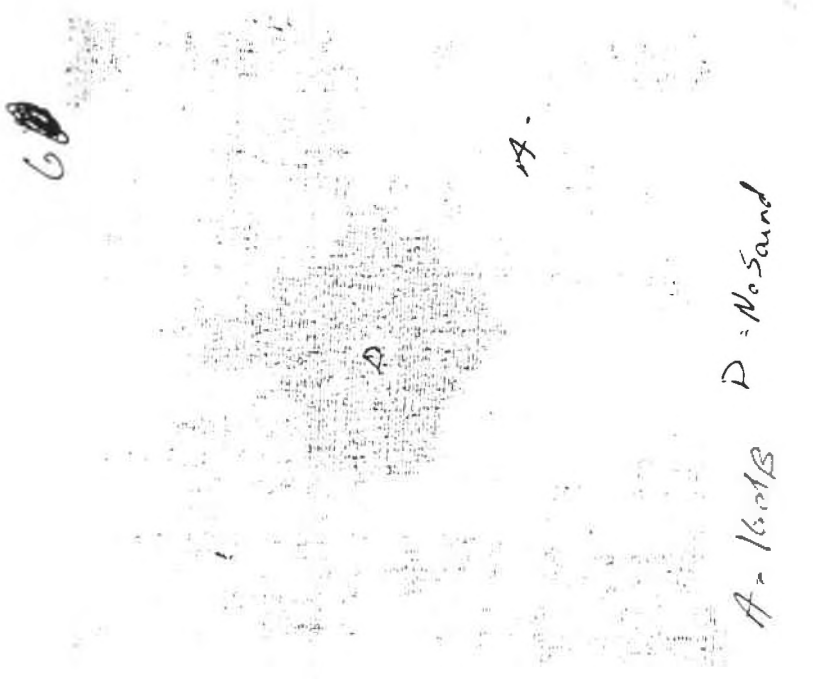

Figure 80. Ultrasonic C-scan.

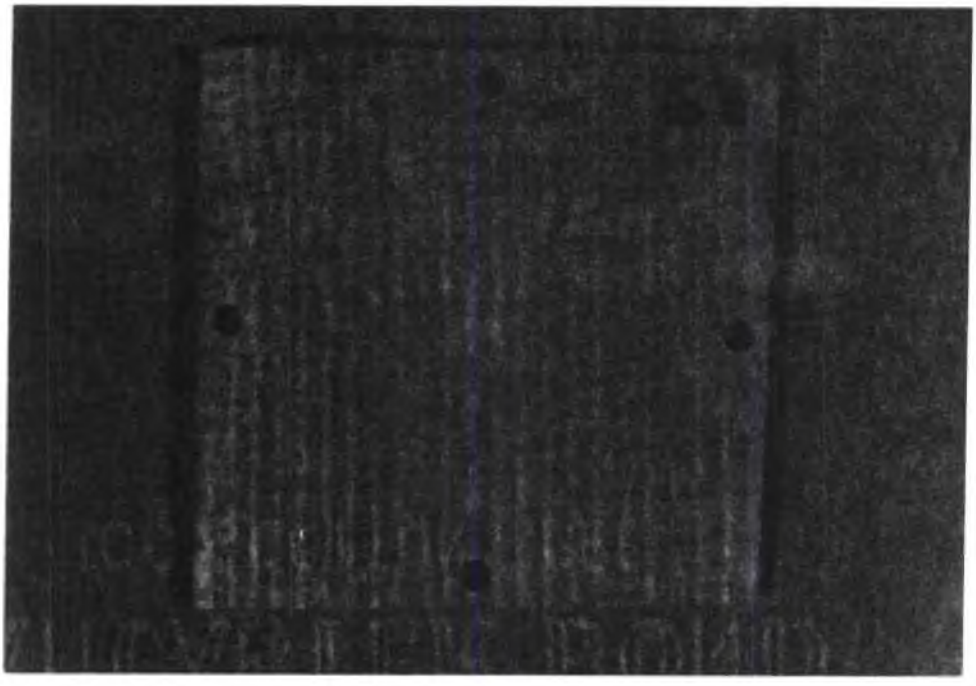

Figure 81. Impact specimen, (Front, -40 °F).

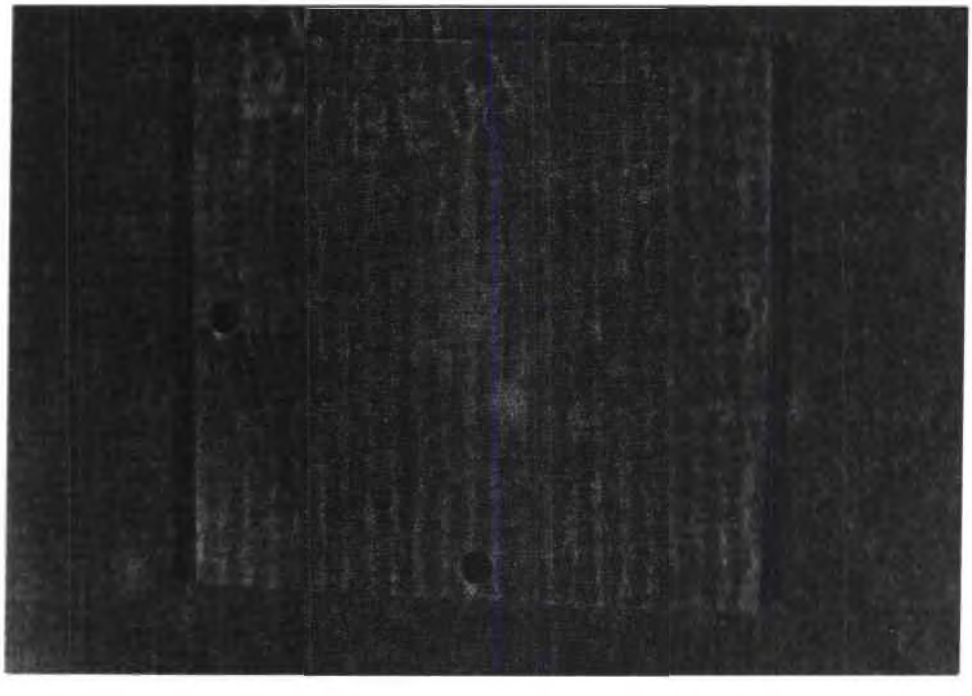

Figure 82. Impact specimen, (Back, -40 °F).

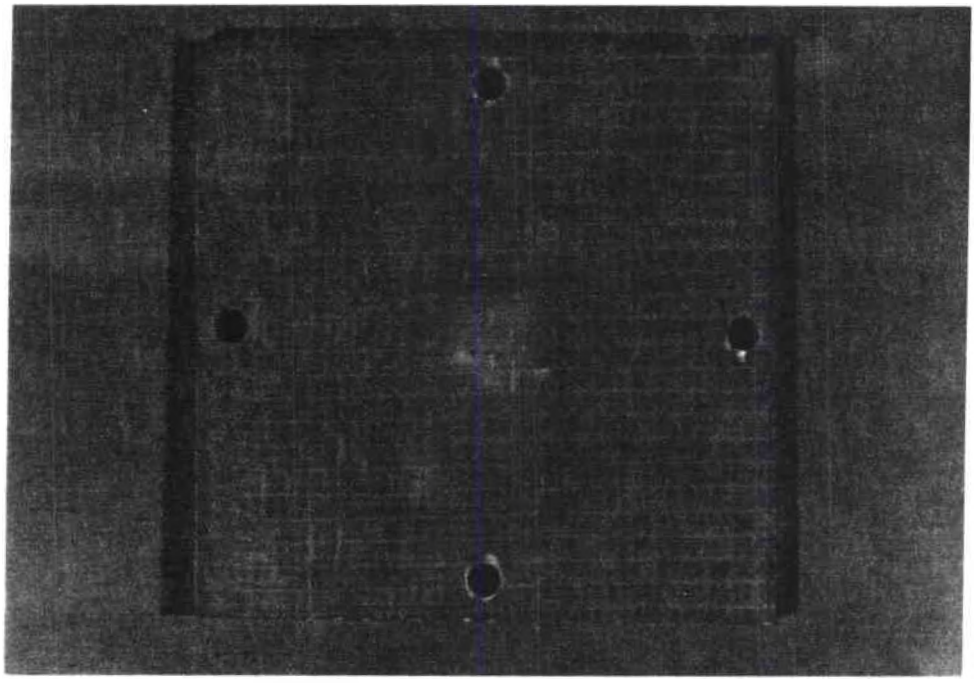

Figure 83. Impact specimen, (Front, RT).

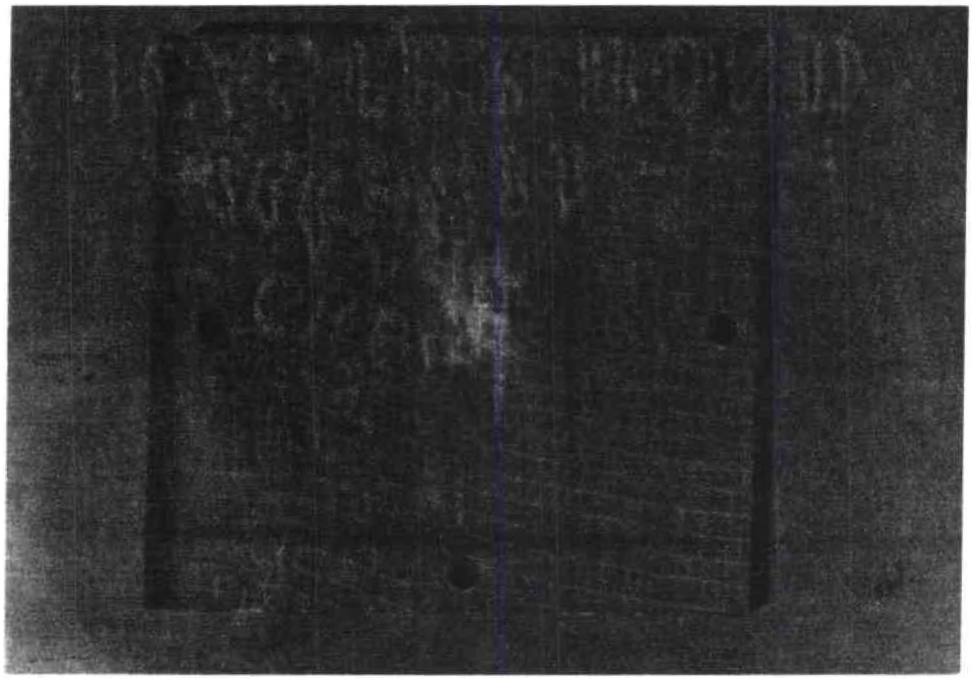

Figure 84. Impact specimen, (Back, RT).

angles. The data collected at 60° is 1.7 times more surface sensitive than the data at 30°. In other words, if the data collected at 30° comes from the top 34 A, the data collected at 60° comes from the top 20 A. Other samples of the neat DOW Z-6040 silane, as well as samples of the silane reacted overnight with water, were also analyzed. Table 21 shows that the carbon level is lower and the oxygen and silicon levels are higher on the samples reacted with water. This may indicate that some or all the methoxy groups on the silicon were replaced with hydroxyl groups. The data on the fiber glass composite shows that the expected components of polyisocyanurate are detected, but also a small amount of silicon is also detected. This may be a surface contaminant due to a silicone mold release or it may actually be exposed glass fibers [24], [27].

A summary of results collected by the XPS technique are presented in Table 7. The data presented shows that the calcium, aluminum, and sodium from the glass are attenuated after the silane treatments, while the carbon level has increased. In both the second and third runs, the carbon level is higher, while the silicon, aluminum, and calcium levels are lower on the 60° data compared to the 30° data. This may indicate that the epoxide end of the silane molecule is sticking out from the surface of the glass. Therefore, it would be the most probable agent to provide the binding with the polycarbamate matrix material. Appendix B shows some of the original data sheets for one of the XPS runs.

Table 7.
Approximate Atom % Surface Compositions of Silane Samples and Silane Treated Glass Samples.

	C			O	N	Si	Ca	Al	Na
sample	C=O	C-O	CH						
Dow Z-6040 (neat on Au foil)	4.3	37.3	15.5	35.3	--	7.2	--	--	--
Dow Z-6040; reacted overnight with water #1	3.4	35.0	14.9	38.9	--	7.7	--	--	--
Dow Z-6040; reacted overnight with water #2	2.0	36.4	14.8	39.2	--	7.7	--	--	--
Glass flat; polished and rinsed in acetone		(20.1)		54.5	--	14.6	2.5	6.1	2.3
Glass flat; 5 m. in 1% Dow Z-6040 (30° emission angle) 1st run	3.2	11.4	25.2	42.3	--	12.5	1.0	3.9	0.4
Glass flat; 5 m. in 1% Dow Z-6040 (30° emission angle) 2nd run	2.9	10.2	31.4	38.6	--	12.2	0.9	3.6	0.2
Glass flat; 5 m. in 1% Dow Z-6040 (60° emission angle) 2nd run	2.6	9.2	35.1	38.7	--	10.5	0.7	3.1	0.1
Glass flat; 5 m. in 1% Dow Z-6040 (30° emission angle) 3rd run	2.2	9.0	18.7	49.2	--	15.4	1.1	4.1	0.3
Glass flat; 5 m. in 1% Dow Z-6040 (60° emission angle) 3rd run	2.5	11.4	30.5	40.0	--	12.3	0.4	2.6	0.2
Fiberglass composite	4.5	14.8	66.1	10.2	3.0	1.3	--	--	--

CHAPTER IV

SUMMARY AND CONCLUSIONS

Physical and Thermal Properties

Examination of the physical properties of the material revealed, that the composite underwent proper manufacturing process. No superficial or internal damage was found in the received panels. At areas where ultrasonic examination (C-scan) was used, no signs of internal delamination or unusual concentrations of porosity were found. Specific gravity, resin, and fiber content values were found to correspond with the values provided by the manufacturer. Computation of the void content showed relatively low void contents. The glass transition temperature increased for thermally-aged specimens. This indicated that some crosslinking had taken place.

Mechanical Properties

The RIM fiber glass reinforced polycarbamate seemed to have relatively good structural mechanical properties. Data collected in this investigation resulted in improved mechanical properties when compared with the results reported in literature on the same material. Ultimate strengths have been found to be competitive for certain applications to those of aluminum and low grade steels. A relatively high modulus of elasticity and good impact behavior make this composite a suitable replacement for other

structural materials, in specific applications such as automotive structural parts. Data collected for thermally-aged coupons showed an increase in ultimate strength values, particularly in the tension and flexure modes. This indicates that some postcuring may be beneficial by increasing mechanical strengths of the material. Humidity-aged results indicated an appreciable decrease in strength (30 % to 50 %) for flexure and compression coupons. This fact may indicate that moisture has a fairly significant detrimental effect on the composite. Moisture resistant coatings or paints may be necessary to reduce degradation of the material
for high moisture usage.

Fractography

Unaged

Optical examination utilizing the stereo microscope, and further examination of the SEM photographs, from each loading mode, indicated the following. The level of fiber-matrix debonding was higher in the tension and interlaminar shear coupons, than in the compression and flexure specimens. A summary of the fracture surface features corresponding to specific loading modes, is listed in Table 8. Many of the fracture surface characteristics are similar for some of the failure modes considered. However, there are some topographical features unique to each failure mode, which can be used as finger prints to determine the mode of failure.

Thermally-Aged

Low magnification examination of fracture surfaces, and SEM

Table 8.

FRACTURE FEATURES IN RIM PANELS

Failure Mode	Macro Features	Micro Features
Tension	Fiber pullout Matrix cracking	Fiber pullout Matrix cracking Fiber breakage River patterns in the matrix Radial patterns on fracture fiber surface
Flexure	Fiber pullout Matrix cracking Broken fibers	Fiber pullout (tension side) Matrix cracking (cleavage) Broken fibers Radial patterns on the fractured fiber surface (tension side) Microbuckling of fibers (comp. side) River patterns in matrix fracture surfaces Debris
Compression	Microbuckling of fibers Matrix cracking Debris Bent fibers	Microbuckling of fibers* Broken fibers Matrix cracking Debris on fracture surface Chop marks on fiber surface Bent fibers
Interlaminar Shear	Fiber pullout Fiber-matrix debonding	Fiber pullout (smooth matrix in fiber channels) Fiber-matrix debonding Matrix cracking Hackles in the matrix
Tension-Compression Fatigue	Fiber pullout Matrix cracking	Fiber pullout Fiber-matrix debonding Matrix cracking Debris Hackles River patterns in matrix
Flexural Fatigue	Fiber pullout Matrix cracking	Fiber pullout River patterns in matrix fracture surface Hackles Debris
Impact	Matrix cracking Debris on fracture surface	

* Distinctive features unique to that specific loading mode.

photomicrographs from each loading mode illustrates that, in general, the same characteristics were observed in both unaged and thermally-aged coupons. A summary of the fracture features of both unaged and thermally-aged specimens, corresponding to specific loading modes is listed in Table 9.

An increase in the adhesion between the fiber and the matrix of the thermally-aged specimens when compared with the unaged specimens was the most significant difference observed. It should be noted that this conclusion was based on the analysis of many SEM photographs in addition to those included in this report. An increase in the fiber-matrix adhesion was noticed in specimens subjected to tensile, flexure, and shear loading conditions. No significant effect on the fracture surface was observed when the aging temperature was increased to 180 °F. However, there was a fairly noticeable increase for those specimens subjected to aging temperatures of 250 °F. In addition, specimens subjected to 180 °F, experienced slight changes for aging times of one month or longer. Differences in fiber-matrix adhesion became evident in specimens aged at 250 °F for at least one week.

Exposure of the RIM material to elevated temperatures is postulated to serve as a post-cure for the polycarbamate resin and, therefore, increases the fiber-matrix adhesion. Based on the mechanical properties reported for each loading mode, exposure to elevated temperatures strengthens this interface and further crosslinked the resin to significantly increase the mechanical strength of the material.

Table 9.

FRACTURE FEATURES IN RIM PANELS

Failure Mode	Unaged		Thermally-Aged	
	Macro Feature	Micro Feature	Macro Feature	Micro Feature
Tension	Fiber pullout Matrix cracking	Fiber pullout Matrix cracking Fiber breakage* River patterns in matrix Radial patterns on fiber tips	Fiber pullout Matrix cracking	Fiber pullout Matrix cracking River patterns on fractured fiber surface[1] Radials on fiber tips
Flexure	Fiber pullout (tension side) Matrix cracking Broken fibers	Fiber pullout (tension side) Matrix cracking & debris River patterns on matrix Broken fibers Radial patterns on the fractured fiber surface (tension side) Microbuckling of fibers (comp. side)	Fiber pullout (tension side) Matrix cracking Broken fibers	Fiber pullout (tension side) Matrix cracking Broken fibers River patterns in matrix fracture surface Debris Hackles in matrix Radials on fiber tips (tension side) Chop marks on fiber tips (comp. side)
Compression	Microbuckling of fibers Matrix cracking Debris on fracture surface Bent fibers	Microbuckling of fibers* Broken fibers Matrix cracking Debris on fracture surface Chop marks on fiber surface Bent fibers	Microbuckling of fibers Matrix cracking Debris on fracture surface	Microbuckling of fibers Matrix cracking Broken fibers Debris on fracture surface Chop marks on fiber surface
Interlaminar Shear	Fiber pullout Fiber-matrix debonding	Fiber pullout (smooth matrix in fiber channels) Fiber-matrix debonding Matrix cracking Hackles in the matrix	Fiber pullout	Fiber pullout Matrix cracking Fiber-matrix debonding
Impact	Matrix cracking Debris on fracture surface			

[1]This feature did not result from the elevated temperature aging. Due to the randomly oriented chopped fibers, the selected unaged specimens did not have fibers oriented so that fractured fibers could be photographed end-on.

*Distinctive features unique to that specific loading mode.

Humidity-Aged

Examination of the SEM photomicrographs from each loading mode shows that in general, similar characteristics were observed in both unaged and humidity-aged specimens. A summary of the fracture features in unaged, thermally-aged, and humidity-aged specimens is listed in Table 10.

Overall observations revealed that, more fiber pullout existed in the majority of the specimens examined for each loading condition than in the unaged and thermally-aged specimens. Severe amounts of matrix cracking are observed in the compression specimens as well as the flexure specimens. The matrix was not as badly damaged on the unaged specimens as in the humidity-aged specimens. In addition, very smooth matrix channels were observed in the tension and shear humidity-aged specimens, indicating very poor fiber-matrix bonding. Based on the decrease in mechanical properties for each loading mode, and the fracture features noted, the exposure of this material to humidity could be very detrimental to the composite strength. It was therefore, assumed that moisture produces a decrease in the fiber-matrix adhesion on RIM fiber glass reinforced polycarbamate.

X-ray Photoelectron Spectroscopy

The data provided by the various XPS analyses indicates that, calcium, aluminum, and sodium from the glass were attenuated after silane treatments, while carbon levels had increased considerably. In both second and third runs, the carbon levels were higher, while silicon, aluminum, and calcium levels were lower on the 60 degrees

Table 10.

FRACTURE FEATURES IN RIM MATERIAL

Failure Mode	Unaged		Thermally-Aged		Humidity-Aged	
	Macro Feature	Micro Feature	Macro Feature	Micro Feature	Macro Feature	Micro Feature
Tension	Fiber pullout Matrix cracking	Fiber pullout Matrix cracking Fiber breakage* River patterns in matrix Radials on fiber tips	Same as unaged	Same as unaged More fiber-matrix adhesions Rough fiber surfaces Rough matrix channels Brittle matrix No fiber stretching	Same as unaged	Same as unaged Debris Very smooth matrix channels Very smooth fiber surfaces More ductile matrix No fiber stretching
Compression	Microbuckling of fibers* Kink bands Matrix cracking Debris	Microbuckling of fibers* Broken fibers* Matrix cracking Debris Chop marks on fiber tips Bent fibers	Same as unaged	Same as unaged More fiber-matrix adhesions Rougher matrix & fiber surfaces	Same as unaged	Same as unaged More ductile matrix Very severe matrix cracking and debris Very poor fiber-matrix interfac
Flexure	Fiber pullout (tensile side) Matrix cracking Broken fibers	Fiber pullout (tensile side) Matrix cracking Debris Broken fibers River patterns in matrix Radials in fiber tips (tensile side) Secondary cracking Microbuckling in matrix (comp. side)	Same as unaged	Same as unaged Hackles in matrix More fiber-matrix adhesions Rougher matrix & fiber surfaces	Same as unaged Bent fibers	Same as unaged Very severe matrix cracking and debris Very smooth fiber-matrix surfaces
In-plane Shear	Fiber pullout Fiber-matrix debonding	Fiber pullout Fiber-matrix debonding Matrix cracking Hackles in the matrix	Same as unaged	Same as unaged Rougher fiber-matrix surfaces	Same as unaged	Same as unaged Very smooth matrix channels Very smooth fiber surfaces More ductile matrix

* Distinctive features unique to that loading mode.

data compared to the 30 degrees data. This may indicate that the epoxide end of the silane molecule is sticking out from the surface of the glass. Therefore, it would be the most probable agent to provide the binding with the polycarbamate matrix material. In general, XPS analyses indicates that a larger number of covalent bonds involving carbon were taking place on samples of glass treated with the coupling agent silane Z-6040. However, it has been estimated that the fiber-matrix interface had not reached its most optimun condition as the fractography analysis indicated. In addition, samples of the silane reacted overnight with water, showed lower carbon levels and higher levels of oxygen and silicon. This may indicate that some or all of the methoxy groups on the silicon were replaced with hydroxyl groups. In this case, the number of covalent bonds has been reduced. This corresponds with the poorer fiber-matrix interface found on the humidity-aged coupons. The slight increase in temperature (120 °F), creates a moderate expansion of the internal and external boundaries of the material. Moisture tends to deposit itself in the fiber-matrix interfaces with a corresponding detrimental effect.

Recommendations

It is recomended, that more fatigue testing on specimens submited to environmental conditioning may be of importance for a more complete characterization of the fatigue fracture surfaces. In addition, more impact testing also should be pursued, to determine the toughness and the effect of humidity and thermal aging. The use of automotive fluids to condition specimens prior to testing in the different modes may show new characteristics not observed in the other conditionings.

REFERENCES

1. Saliba, S. S., Askins, D. R., and Snide, J. A. ", Failure Mode in Fiber Reinforced Plastic Composite Materials, " UDR-TR-87-112, University of Dayton, August 1987.

2. Jones, R. M. ", Mechanics of Composite Materials," McGraw-Hill Book Company, 1975.

3. Metals Handbook, Ninth Edition, Vol. 12 Fractography, ASM International, Metals Park, Ohio, 1987.

4. Stumpff, P. and Snide, J.A.", Fractography of Composites," AFWAL-TR-86-4044, Wright Patterson Air Force Base, Dayton, Ohio.

5. Klein, A. J. ", Reaction Injection Molding: Getting Faster, " Advanced Materials and Processes incorporating Metal Progress, vol. 130, n 6, p. 52-56, Dec 1986.

6. Kropscott, E. L., Jones, E.E., and Cook, P.H. ", Instant Set Polymer - A New Dimension In Plastics, " The Dow Chemical Company.

7. Nelson, D. ", Reaction Molded Glass Reinforced Structural Polymers- What Are They?, " International SAMPE Symposium and Exhibition, 31st, Los Angeles, CA, April 7-10, 1986, p. 1049-1068.

8. Whitney, J. M., and Browning, C. E. ", On Short-Beam Shear Tests for Composite Materials, " Experimental Mechanics, Vol. 25, No. 3, pp. 294-300, September 1985.

9. Whitney, J. A. and Short, R. S. , 2nd Symposium ASC, September 24- 26, 1987.

10. Wang, S.S., Goetz, D.P., and Corten, H. T. ", Fracture of Random Short- Fiber SMC Composite Under Shear Loading," International Journal of Fracture, Vol. 26, pp. 215-227, 1984.

11. Wang, S.S., Suemasu, H., and Zahlan, N. M. ", Interlaminar Fracture of Random Short-Fiber SMC Composite," Journal of Composite Materials. Vol 18, p. 574-594, Nov. 1984.

12. Hahn, T. H., Sohi, M., and Suresh, M. ", Compression Failure Mechanisms of Composite Structures," NASA Contractor Report 3988, GRANT NAG1-295, June 1986.

13. Wang, S.S., Chim, S.-M., and Zahlan, N. M. ", Fatigue Crack Propagation in Random Short-Fiber SMC Composite," Journal of Composite Materials, Vol. 17, pp. 250-267, May 1983.

14. Owen, M.J.", Fatigue Processes in Fibre Reinforced Plastics," Phil. Trans. R. Soc. Lond., Vol. 294, pp. 535-543, 1980.

15. Newman, S. and Fresko, D.G. ", Recent Developments in Sheet Molding Compound Technology ," Polymer Composites, Vol.5, No. 1, January 1984.

16. Wang, S.S. and Chim, E.S.-M. ", Fatigue Damage and Degradation in Random Short-Fiber SMC Composite," Journal of Composite Materials, Vol. 17, pp. 114-134, March 1983.

17. Jefferey, M. R., Sourouri, J. A., and Schultz, J. M. ", Fatigue Behavoir of Thermosetting-Polyester Matrix Sheet-Molding Compounds," Polymer Composites, Vol. 3, No.1, pp. 18-28, 1982.

18. Khetan, R.P., and Chang, D. C. ", Surface Damage of Sheet Molding Compound Panels Subject to a Point Impact Loading," Journal of Composite Materials, Vol. 17, p. 182-194, March 1983.

19. Springer, G. S.", Environmental Effects On Composite Materials," Technonic Publishing Co., Inc., 1981, pp. 51-62, 126-144.

20. Plueddemann, E. P. ", State-of-the-Art of Silane Coupling Agents, " Dow Corning Corporation.

21. Kubel, E.J. ", A Composites 'Wish List', " Advanced Materials and Processes, pp. 47-54, Oct. 1987.

22. Whitaker, R. B., Attalla, A., Sullenger, D. B., Wang, P. S., Dichiaro, J. V., and Kenyon, A. S. ", Characterization and Adhesive Bonding of Poly (etheretherketone) Resins and Composites, " (Monsanto Co., St. Louis), 16th National SAMPE Technical Conference on Material and Processes, Albequerque, N. M., 1984.

23. Annual Book of ASTM Standards, American Society for Testing and Materials, 1983.

24. Wolsky, S. P. and Cxanderna, E. ", Methods of Surface Analysis, " Elsevier Scientific Publishing Company, New York, 1975.

25. Murayama, T. ", Dynamic Mechanical Analysis of Polymeric Material," Elsevier North-Holland, Inc., New York, N.Y., 1978.

26. Billmeyer, F. W. ", Textbook of Polymer Science," John Wiley & Sons, Inc., 1984.

27. Lange, F. F., and Hirlinger, M.M. ", Phase Distribution Studies Using Energy Dispersive X-ray Spectral Analysis, " Journal of Materials Science Letters (ISSN 0261-8028), Vol. 4, Dec. 1985, p. 1437-1441.

APPENDIX A

Graphite/epoxy composite fracture surface characteristics have been identified and are summarized below according to the loading condition.

Tension - 0° Orientation

Macroscopically:
(1) Transverse cracking across the 0° fibers - flat or brushlike surface appearance
(2) May have splitting along the 0° fibers

Microscopically:
(1) On transverse fracture surface
    (1) spire-like fiber bundles and fiber pullout
    (2) tensile fiber radials
    (3) river patterns in matrix
(2) Along 0° fiber matrix
    (1) hackles
    (2) debonding
    (3) matrix cracking

Tension - 90° Orientation

Macroscopically: Splitting nearly perpendicular to the applied load

Microscopically:
(1) matrix cracking including matrix cleavage
(2) Broken Fibers - some intact
                  - some out of alignment and/or pulled away from the surface (fiber bridging)
(3) Debonding

Tension - 45° Orientation

Macroscopically:
(1) 45° splitting
(2) Edge delamination at splits
(3) Some 45° fiber breakage

Microscopically:
(1) Tensile radials on some 45° fiber breaks
(2) Hackles, debonding, and matrix cracking on 45° splits

Compression - 0 Orientation

Macroscopically:
(1) 0° fiber breakage and splitting
(2) Secondary cracking
(3) Ply delamination and buckling

Microscopically:
(1) May have rows of "chop marks" indicating macrobuckling
(2) Angled fiber breakage
(3) Smeared areas or broken bits of fiber/matrix on surface
(4) Layered surfaces indicative of "shear crippling"
(5) cracking through matrix rich areas

Compression - 90° Orientation

Macroscopically:
(1) Fracture surface at 45° to load orientation
(2) Relatively flat fracture surface

Microscopically:
(1) Extensive fiber breakage
(2) Matrix cracking and debonding
(3) May have some parallel cracking of fibers
(4) Broken fibers remain intact and aligned with fractured surface

Flexure - 0° Orientation

Macroscopically:
(1) Fiber breakage on tensile side at top load points
(2) 0° fiber splitting on tensile side between two top loading points

Microscopically:
(1) Tensile radials on broken 0° fibers on

tensile side
(2) River patterns in matrix
(3) Some debonding

Flexure - 90° Orientation

Macroscopically: (1) Splitting through the 90° fibers approximately parallel to load - may have "shear lip"

Microscopically: (1) Similar to 90° tensile failure - may have dual-natured surface morphology, which may be due to abrasive action

Tension - Tension Fatigue - 0° Orientation

Macroscopically: (1) Transverse fracture of specimen

(2) Some 0° fiber splitting and some edge delamination

Microscopically: (1) Tensile radials on fractured fibers (non-distinct)
(2) Broken hackles and holes along 0° fiber splits near fracture

Tension - Tension Fatigue - 90° Orientation

Macroscopically: (1) 90° split approximately perpendicular to load direction

Microscopically: (1) Almost indistinguishable from 90° tension failure - may have slightly rougher surface

Tension - Tension Fatigue - 45° Orientation

Macroscopically: (1) 45° fiber splitting and some fiber breakage
(2) Some 45° ply delamination

Microscopically: (1) Tensile radials on fractured fibers (non-distinct)
(2) Broken lots/pieces of fiber/matrix on 45° splits
(3) Fatigue striations along 45° splits

Interlaminar Shear - 0° Orientation

Macroscopically: (1) Delamination either midplane or closer to the top of the shear specimen
(2) At midplane, one may get debonding and upright 45° hackles between fibers or

imprints

(3) On surfaces closer to loading noses, get a complex stress state and bits and pieces of fiber/matrix on surface

GLOSSARY OF TERMS

A. Macroscopic Failure Features

1. Transverse Cracking - Fracture perpendicular to load direction
   a. Brittle - minimal fiber pullout
      - fibers approximately same length
   b. Ductile - significant amount of fiber pullout
      - fiber lengths vary widely
   c. Mixed - areas of both ductile and brittle fracture

2. Interlaminar Cracking or Delamination - Fracture between plys

3. Macrobuckling - Delamination and subsequent bending of surface plys out of original plane

4. Edge Delamination - Cracking between two plys, occurring at or near the edge of the specimen only

5. Post Failure Damage - Damage to the fracture surface after failure; i.e., crushing and smearing in compressive failures

6. Splitting- Cracking parallel to the fibers

7. 45° Fracture Mode - Debonding or matrix failure in the 45° orientation

8. Shear Lip - The failure of a 90° oriented specimen at a 45° angle near the specimen edges

9. Secondary Cracking - Cracking within the specimen in addition to the main fracture surface

10. Joggle Type Failure - Fiber failure along 45° angle through part of the laminate

11. Fiber Bundle - A cluster of fibers

12. Kinking - The breaking of a series of fibers along the fiber lengths in two locations at a specific angle to the load

13. Fiber Pullout - Debonding of fiber/matrix interface with subsequent fiber failure resulting in holes in one half of specimen and fibers longer than average length on the other half of specimen

14. Extension Mode Failure - Out of phase fiber buckling

15. Shear Mode Failure - In-phase fiber buckling

16. Delamination - Cracking between two plys across the entire width of the specimen

B. Microscopic Fracture Features

1. Fiber Wetting - Matrix adhesion to the fibers

2. Bare Fibers - Fibers exhibiting no matrix adhesion

3. Fiber Pullaway - Interfacial cracking - i.e., cracking between the fiber and matrix

4. Debonding - Complete cracking around the fiber between the fiber and matrix

5. Fiber Radials - Radiating lines on a broken fiber surface emanating either from an edge or an inclusion

6. Microbuckling - Buckling of individual fibers resulting in a dual natured broken fiber surface also known as "chop marks"

7. Compressive Fracture - Clean, smooth, angled fractured fiber surfaces

8. River Patterns - Branched markings in matrix material indicating local crack propagation direction

9. Matrix Cracking - Cracking in the matrix between the fibers

10. Chevron Markings - V-shaped markings in matrix (similar to metals) indicating crack direction

11. Cleavage - Brittle matrix failures evidenced be markings in matrix between fibers

12. Hackles - Overlapping platelets of matrix found between fiber lengths and thought to be due to shear stresses - also known as "serrations". "lacerations", and "cusps"

13. S-shaped cracking - cracking thought to be caused by shear stresses and to initiate "hackles"

14. Striations - Repetitive markings found in the matrix indicative of fatigue

15. Matrix Rich Regions - Localized areas of high resin content in composite

16. Voids - Localized areas of entrapped air in matrix

17. Inclusions - Particles such as hardener, dust, chips, etc. in the specimen that are not part of the fiber/resin system

18. Flow Lines - Light markings in the resin indicative of the direction of movement of the material - also known as "feathering"

19. Globular Matrix - Bits and pieces of matrix broken into small spherical-like particles on specimen surface

20. Microcracking - Small cracks developing ahead of the crack tip in matrix

21. Fiber Bridging - The pulling of fibers away from the surface intact and then subsequent breaking of these fibers as the crack advances

22. Fiber Nesting - Broken fibers remaining intact with the rest of the surface

APPENDIX B

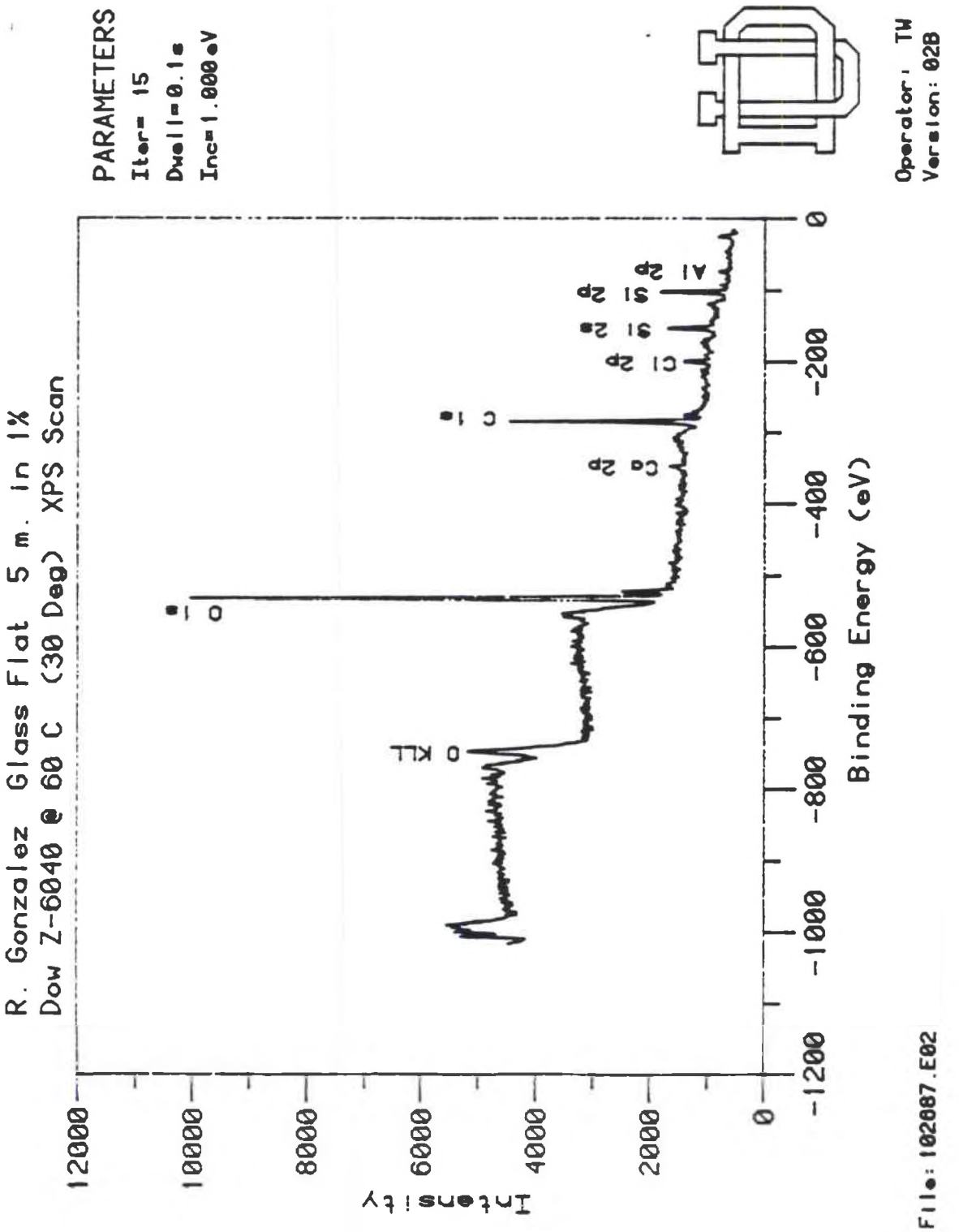
R. Gonzalez Glass Flat 5 m. in 1%
Dow Z-6040 @ 60 C (30 Deg) XPS Scan
PARAMETERS
Iter= 15
Dwell=0.1s
Inc=1.000eV
Operator: TW
Version: 02B
File: 102087.E02
Intensity
Binding Energy (eV)
O 1s
O KLL
C 1s
Ca 2p
Cl 2p
Si 2s
Si 2p
Al 2p

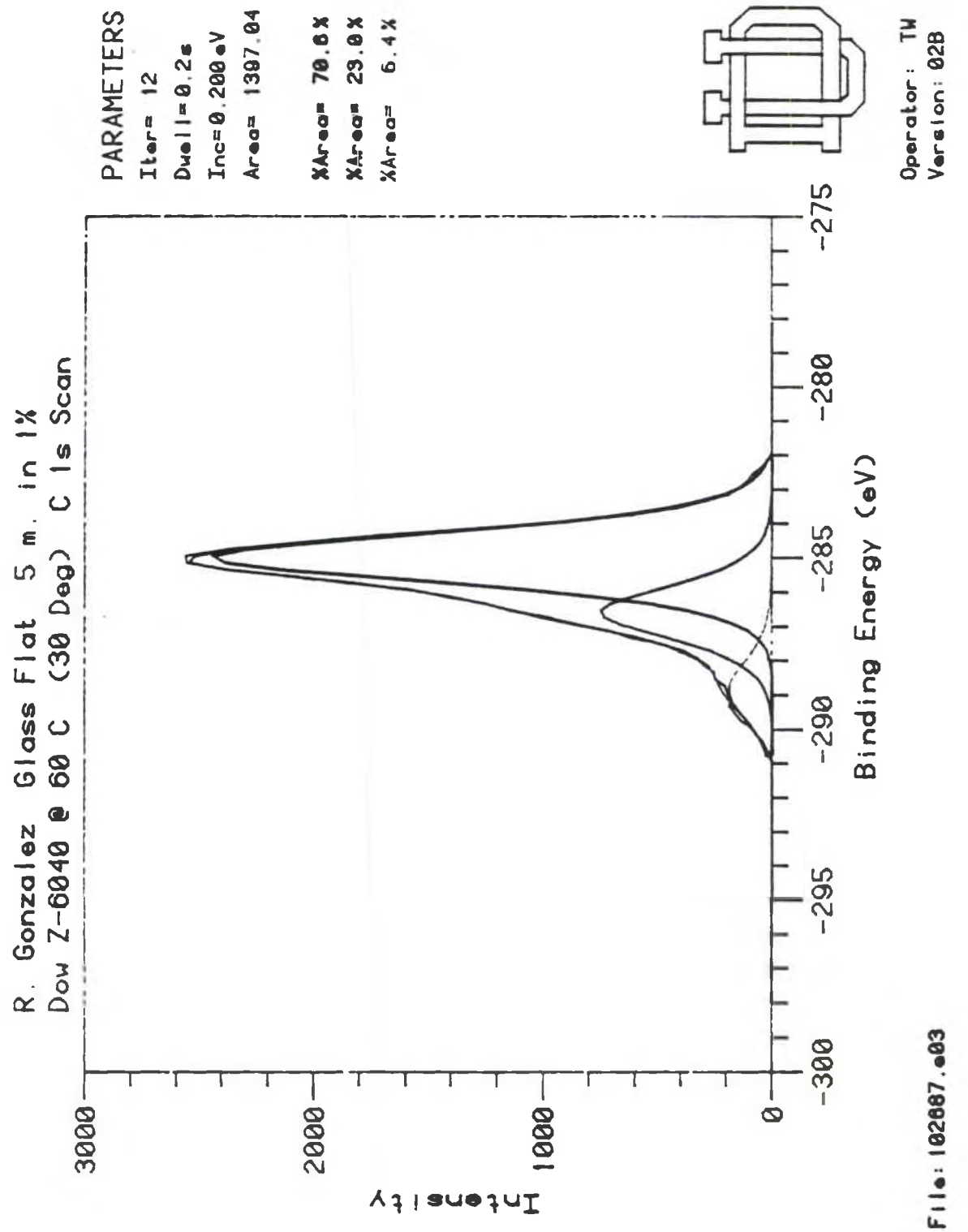
R. Gonzalez Glass Flat 5 m. in 1%
Dow Z-6040 @ 60 C (30 Deg) C 1s Scan
PARAMETERS
Iter= 12
Dwell=0.2s
Inc=0.200eV
Area= 1307.04
%Area= 70.6%
%Area= 29.0%
%Area= 6.4%
Intensity
3000
2000
1000
0
-300
-295
-290
-285
-280
-275
Binding Energy (eV)
Operator: TW
Version: 02B
File: 102887.e03

APPENDIX C

Mechanical Properties

Tension

The as-received, unaged RIM specimens were tested in tension using the D638 dogbone specimens. Results of these tests are presented in Table C1. It has been noted that the ultimate tensile strength is lower for the 45° oriented specimens than the 0° or 90° oriented coupons, while no significant differences were encountered for the 0° or 90° specimens. The fact that the 45° oriented coupons have lower mechanical properties is due to the fiber orientation in the material, since the material was pulled in tension in the axial direction, and the reinforcement was not aligned in the direction of the load. Note that these orientations correspond to the direction of the specimens layout on the panel, not to fiber direction in the material. The average values of ultimate tensile strength for unaged specimens was found to be 44.2 KSI and the average tensile modulus of elasticity was 1.8×10^6 psi [29].

Results of the coupons exposed to 180 °F and 250 °F for periods of time ranging from 1 day to 1 month, are shown in Tables C2 and C3. An increase in ultimate tensile strength of about 7 % was observed with respect to the as received unaged specimens. The average strength value for thermally-aged specimens was 47.7×10^3 psi. It is assumed that the increase in strength is due to postcuring effects.

Humidity-aged specimens test results revealed a decrease in tensile strengths of about 12 % with respect to the unaged specimens. Specimens have been exposed to 120 °F and 100 % relative humidity (RH) until saturation was reached. This seemed to degrade the mechanical

properties of the material. The average value for ultimate tensile strength under these conditions was 39.2 X 10^3 psi. Tensile properties of the humidity-aged specimens are listed in Table C4.

Flexure

The as-received, unaged RIM specimens were tested at room temperature using the ASTM D790 three-point loading method. The flexural properties were lower for the 45 degree oriented specimens, where their average value for ultimate flexural strength was found to be 38.5 X 10^3 psi. A value of 61.6 X 10^3 psi was found for the 0° and 90° oriented specimens.

No appreciable change in mechanical properties was noted in the thermally-aged specimens, with respect to the unaged specimens, although there is a slight increase in properties.

Humidity-aged specimens showed a noticeable decrease (30%) in their mechanical properties. The average value for the ultimate flexural strength of the humidity-aged samples was 44 X 10^3 psi. The flexural mechanical are listed in Tables C5 through C8 for the various orientations and treatments.

Compression

As-received, unaged RIM specimens were tested at room temperature. Results of the compression tests are presented in Table C9. The overall average of the 0° and 90° oriented specimens was found to be 52.1 X 10^3 psi. In addition, all the specimens failed in the gage area while exhibiting a typical compression failure mode. An average value of 2.57 X 10^6 psi for the compressive modulus of

elasticity was determined.

The compressive strengths for the thermally-aged specimens are listed in Table C10. The average compressive strength is 52.0 X 10^3 psi, therefore, thermal aging had a minimal effect on the compressive properties of this material.

Humidity-aged specimens showed a major reduction (50%) in their compressive strength, which indicates this material's compressive properties degrade considerable in high humidity environments. Table C11 lists these compressive properties.

In-Plane Shear

The unaged RIM specimens were tested in shear using the ASTM D3846 method. The results of these tests are presented in Table C12, where an average value of 6.5 X 10^3 psi was computed for the ultimate shear strength of the RIM material. All the specimens failed in the notch area. A 20 % reduction in strength for the 45 degrees oriented specimens (S = 5.0 X 10^3 psi) was observed when compared to the 0° and 90° oriented specimens.

Thermally-aged specimens showed some change in their ultimate mechanical strength, where the average value was 5.5 X 10^3 psi for 0° and 90° oriented specimens. Results are presented in tables C13 and C14. Specimens cut at a 45° angle and thermally-aged do not present any major changes in mechanical properties.

The mechanical properties reported in Table C15 for the humidity-aged specimens are not useful for comparison with the previously tested coupons because they were inadvertently tested in a different mode.

Table C1. Tensile Properties of RIM Polycarbamate Material

Specimen I.D.	Orientation[1]	Test Temp(°F)	Pre-Test Aging	Ultimate Tensile Strength ($psi \times 10^3$)	Tensile Modulus of Elasticity ($psi \times 10^6$)	Failure Location
T1AP	0°	72	None	42.2	2.10	Gage Section
T2AP	0°	72	None	47.3	2.02	"
T3AP	0°	72	None	44.4	1.91	"
T4AP	0°	72	None	44.9	1.75	"
T5AP	0°	72	None	47.2	1.76	"
			Average	45.2	1.90	
			Std. Dev.	2.1	0.15	
T6AP	90°	72	None	39.9	1.67	Fillet Radius
T7AP	90°	72	None	42.7	1.87	Gage Section
T8AP	90°	72	None	45.7	1.53	
T9AP	90°	72	None	43.9	1.60	
T10AP	90°	72	None	44.9	1.87	
			Average	43.2	1.70	
			Std. Dev.	2.7	0.15	

[1] The orientation corresponds to the direction of specimen layout on the panel, not to fiber direction.

Table C2. Tensile Properties of RIM Polycarbamate Material

Specimen I.D.	Orientation[1]	Test Temp(°F)	Pre-Test Aging	Ultimate Tensile Strength ($psi \times 10^3$)	Failure Location
T11AP	0°	74	180°F- 1 day	47.9	Gage Section
T12AP	0°	74	180°F- 1 week	48.1	"
T13AP	0°	74	180°F- 1 month	47.7	"
T14AP	90°	74	250°F- 1 day	55.2	"
T15AP	90°	74	250°F- 1 week	40.1	"
T16AP	90°	74	250°F- 1 month	46.6	"

[1] The orientation corresponds to the direction of specimen layout on the panel, not to fiber direction.

Table C3. Tensile Properties of RIM Polycarbamate Material

Specimen I.D.	Orientation[1]	Test Temp(°F)	Pre-Test Aging	Ultimate Tensile Strength ($psi \times 10^3$)	Failure Location
T43AP	45°	74	None	16.5	Gage Section
T44AP	45°	74	None	17.1	"
			Average	16.8	
			Std. Dev.	0.42	
T46APA	45°	74	180°F- 1 day	17.8	"
T47APA	45°	74	250°F- 1 week	18.6	"
T48APA	45°	74	250°F- 1 month	17.1	"

[1] The orientation corresponds to the direction of specimen layout on the panel, not to fiber direction.

Table C4. Tensile Properties of RIM Polycarbamate Material

Specimen I.D.	Orientation[1]	Test Temp(°F)	Pre-Test Aging	Ultimate Tensile Strength ($psi \times 10^3$)	Failure Location
T21APE	0°	74	Humidity Aged at 120°F	37.1	Gage Section
T27APE	90°	74	"	40.2	"
T28APE	90°	74	"	38.3	"
T29APE	90°	74	"	41.4	"
			Average	39.2	
			Std. Dev.	1.92	

[1] The orientation corresponds to the direction of specimen layout on the panel, not to fiber direction.

Table C5. Flexural Properties of RIM Polycarbamate Material

Specimen I.D.	Orientation[1]	Test Temp(°F)	Pre-Test Aging	Ultimate Flexural Strength (psi X10^3)	Flexural Modulus of Elasticity (psi X10^6)	Failure Mode
F1AP	0°	74	None	54.5	1.99	Tensile
F2AP	0°	74	None	60.0	2.02	"
F3AP	0°	74	None	58.9	2.01	"
F4AP	0°	74	None	58.2	2.07	"
F5AP	0°	74	None	57.8	2.05	"
			Average	58.0		
			Std. Dev.	2.1		
F6AP	90°	74	None	59.0	2.32	Tensile
F7AP	90°	74	None	68.1	2.45	"
F8AP	90°	74	None	66.2	2.58	"
F9AP	90°	74	None	62.7	2.56	"
F10AP	90°	74	None	70.1	2.63	"
			Average	65.2	2.51	
			Std. Dev.	4.4	0.12	

[1] The orientation corresponds to the direction of specimen layout on the panel, not to fiber direction.

Table C6. Flexural Properties of RIM Polycarbamate Material

Specimen I.D.	Orientation[1]	Test Temp(°F)	Pre-Test Aging	Ultimate Flexural Strength (psi X10^3)	Failure Mode
F11APE	0°	74	180°F- 1 day	63.4	Tensile
F12APE	0°	74	180°F- 1 week	61.3	"
F18APE	90°	74	180°F- 1 month	67.9	"
F16APE	90°	74	250°F- 1 day	68.9	"
F17APE	90°	74	250°F- 1 week	67.5	"
F13APE	0°	74	250°F- 1 month	67.9	"

[1] The orientation corresponds to the direction of specimen layout on the panel, not to fiber direction.

Table C7. Flexural Properties of RIM Polycarbamate Material

Specimen I.D.	Orientation[1]	Test Temp(°F)	Pre-Test Aging	Ultimate Flexural Strength ($psi \times 10^3$)	Failure Mode
F41AP	45°	74	None	38.0	Tensile
F42AP	45°	74	None	39.0	"
			Average	38.5	
			Std. Dev.	0.71	
F44APA	45°	74	180°F- 1 day	46.2	"
F45APA	45°	74	250°F- 1 week	42.6	"
F46APA	45°	74	180°F- 1 month	44.2	"

[1] The orientation corresponds to the direction of specimen layout on the panel, not to fiber direction.

Table C8. Flexural Properties of RIM Polycarbamate Material

Specimen I.D.	Orientation[1]	Test Temp(°F)	Pre-Test Aging	Ultimate Flexural Strength (psi X10^3)	Failure Mode
F22APE	0°	74	Humidity Aged at 120°F	44.6	Tensile
F26APE	0°	74	"	44.1	"
F48APE	45°	74	"	34.7	"
F49APE	45°	74	"	34.2	"
			Average	39.4	
			Std. Dev.	5.7	

[1] The orientation corresponds to the direction of specimen layout on the panel, not to fiber direction.

Table C9. Compressive Properties of RIM Polycarbamate Material

Specimen I.D.	Orientation[1]	Test Temp(°F)	Pre-Test Aging	Ultimate Compressive ($psi \times 10^3$)	Compressive Modulus of ($psi \times 10^6$)
C1AP	0°	72	None	52.6	2.67
C2AP	0°	72	None	50.5	2.69
C3AP	0°	72	None	53.0	2.60
C4AP	0°	72	None	51.5	2.56
C5AP	0°	72	None	52.2	2.60
			Average	52.0	2.62
			Std. Dev.	0.99	0.05
C6AP	90°	72	None	53.3	2.58
C7AP	90°	72	None	52.6	2.49
C8AP	90°	72	None	53.1	2.53
C9AP	90°	72	None	53.4	2.47
C10AP	90°	72	None	53.8	2.51
			Average	53.2	2.52
			Std. Dev.	0.46	0.04
		Overall(0°, 90°)	Average	52.6	2.57
			Std. Dev.	0.98	0.07

[1] The orientation corresponds to the direction of specimen layout on the panel, not to fiber direction.

Table C10. Compressive Properties of RIM Polycarbamate Material

Specimen I.D.	Orientation[1]	Test Temp(°F)	Pre-Test Aging	Ultimate Compressive Strength ($psi \times 10^3$)
C16APA	90°	74	180°F- 1 day	55.0
C17APA	90°	74	180°F- 1 week	46.9
C18APA	90°	74	180°F- 1 month	52.3
C11APA	0°	74	250°F- 1 day	51.6
C12APA	0°	74	250°F- 1 week	50.9
C13APA	0°	74	250°F- 1 month	54.9
C41AP	45°	74	None	18.5
C42AP	45°	74	None	19.0
			Average	18.75
			Std. Dev.	0.35
C44APA	45°	74	180°F- 1 day	21.6
C45APA	45°	74	250°F- 1 week	22.2
C46APA	45°	74	250°F- 1 month	22.9

[1] The orientation corresponds to the direction of specimen layout on the panel, not to fiber direction.

Table C11. Compressive Properties of RIM Polycarbamate Material

Specimen I.D.	Orientation[1]	Test Temp(°F)	Pre-Test Aging	Ultimate Compressive Strength ($psi \times 10^3$)
C22APE	0°	74	Humidity Aged at 120 °F	19.3
C27APE	90°	74	"	27.5
			Average	23.4
			Std. Dev.	5.8

[1] The orientation corresponds to the direction of specimen layout on the panel, not to fiber direction.

Table C12. In-plane Shear Properties of RIM Polycarbamate Material

Specimen I.D.	Orientation[1]	Test Temp(°F)	Pre-Test Aging	Ultimate Shear Strength ($psi \times 10^3$)	Failure Location
S1AP	0°	72	None	6.8	Notch-Area
S2AP	0°	72	None	6.5	"
S3AP	0°	72	None	6.2	"
S4AP	0°	72	None	6.6	"
S5AP	0°	72	None	6.4	"
			Average	6.6	
			Std. Dev.	0.20	
S6AP	90°	72	None	6.8	Notch-Area
S7AP	90°	72	None	6.6	"
S8AP	90°	72	None	6.2	"
S9AP	90°	72	None	6.2	"
			Average	6.4	
			Std. Dev.	0.23	
		Overall(0°, 90°)	Average	6.5	
			Std. Dev.	0.23	

1. The orientation corresponds to the direction of specimen layout on the panel, not to fiber direction.

Table C13. In-plane Shear Properties of RIM Polycarbamate Material

Specimen I.D.	Orientation[1]	Test Temp(°F)	Pre-Test Aging	Ultimate Shear Strength ($psi \times 10^3$)
S11APA	0°	74	180°F- 1 day	5.4
S12APA	0°	74	180°F- 1 week	5.2
S13APA	0°	74	180°F- 1 month	5.8
S16APA	90°	74	250°F- 1 day	5.4
S17APA	90°	74	250°F- 1 week	5.3
S18APA	90°	74	250°F- 1 month	6.1

[1] The orientation corresponds to the direction of specimen layout on the panel, not to fiber direction.

Table C14. In-plane Shear Properties of RIM Polycarbamate Material

Specimen I.D.	Orientation[1]	Test Temp(°F)	Pre-Test Aging	Ultimate Shear Strength ($psi \times 10^3$)	Failure Location
S41AP	45°	74	None	5.0	Notch-Area
S42AP	45°	74	None	5.4	"
S43AP	45°	74	None	4.6	"
			Average	5.02	
			Std. Dev.	0.4	
S44APA	45°	74	180°F- 1 day	5.2	"
S45APA	45°	74	250°F- 1 week	5.2	"
S46APA	45°	74	180°F- 1 month	5.2	"

[1] The orientation corresponds to the direction of specimen layout on the panel, not to fiber direction.

Table C15. In-plane Shear Properties of RIM Polycarbamate Material

Specimen I.D.	Orientation[1]	Test Temp(°F)	Pre-Test Aging	Ultimate Shear Strength ($psi \times 10^3$)	Failure Location
S22APE	0°	74	Humidity Aged at 120 °F	0.9	Notch-Area
S26APE	90°	74	"	2.0	"
			Average	1.48	
			Std. Dev.	0.78	
S47APE	45°	74	"	1.3	"
S48APE	45°	74	"	1.7	"
			Average	1.5	
			Std. Dev.	0.28	

[1] The orientation corresponds to the direction of specimen layout on the panel, not to fiber direction.